

VŠB - Technical University of Ostrava  
Faculty of Mechanical Engineering  
Department of Applied Mechanics



Bachelor Thesis

## Stiffness Analysis of Formula Student Frame

*Analýza tuhosti rámu studentské formule*

*David Krzikalla*

Supervisor: Ing. Zdeněk Poruba, Ph.D.

Field of study: Applied Mechanics, 3901R003

Ostrava 2018

## Zadání bakalářské práce

Student: **David Krzikalla**  
Studijní program: B2341 Strojírenství  
Studijní obor: 3901R003 Aplikovaná mechanika  
Téma: **Analýza tuhosti rámu studentské formule**  
**Stiffness Analysis of Formula Student Frame**  
Jazyk vypracování: čeština

### Zásady pro vypracování:

- 1) Uveďte základní technické požadavky na vozy pro soutěž Formula SAE a blíže specifikujte a diskutujte požadavky týkající se rámu studentské formule.
- 2) Vytvořte geometrický a konečnoprvkový model rámu studentké formule dle požadavku týmu Formula SAE VŠB-TU Ostrava.
- 3) Aplikujte vhodné okrajové podmínky za účelem výpočetního ověření tuhosti rámu studentské formule.
- 4) Proveďte výpočet tuhosti rámu vozu pomocí metody konečných prvků, diskutujte nastavení konečnoprvkové analýzy a vypočtené hodnoty.
- 5) Na základě dosažených výsledků zvažte možnosti optimalizace rámu za účelem zvýšení jeho tuhosti, popř. snížení hmotnosti.

### Seznam doporučené odborné literatury:

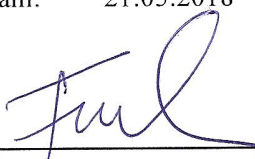
1. COOK, Robert D. *Finite element modeling for stress analysis*. Vyd. 1. Hong Kong: John Wiley, 1995, 320 s. ISBN 04-711-0774-3.
2. ANSYS® *Academic Teaching Advanced, Release 16.2, help system, ANSYS, Inc*
3. 2017 - 18 Formula SAE® Rules. *Formula SAE* [online]. SAE International [cit. 2017-12-08]. Dostupné z:  
[https://www.google.cz/url?sa=t&rct=j&q=&esrc=s&source=web&cd=1&cad=rja&uact=8&ved=0ahUKEwi-k860sfrXAhXS\\_KQKHdTNDB0QFggoMAA&url=https%3A%2F%2Fwww.fsaeonline.com%2Fcontent%2F2017-18%2520FSAE%2520Rules%25209.2.16a.pdf&usg=AOvVaw3b7L6QH-xLI2dnQOJAACo0](https://www.google.cz/url?sa=t&rct=j&q=&esrc=s&source=web&cd=1&cad=rja&uact=8&ved=0ahUKEwi-k860sfrXAhXS_KQKHdTNDB0QFggoMAA&url=https%3A%2F%2Fwww.fsaeonline.com%2Fcontent%2F2017-18%2520FSAE%2520Rules%25209.2.16a.pdf&usg=AOvVaw3b7L6QH-xLI2dnQOJAACo0)

Formální náležitosti a rozsah bakalářské práce stanoví pokyny pro vypracování zveřejněné na webových stránkách fakulty.


Vedoucí bakalářské práce: **Ing. Zdeněk Poruba, Ph.D.**

Datum zadání: 08.12.2017

Datum odevzdání: 21.05.2018

  
Ing. Martin Fusek, Ph.D.  
vedoucí katedry



  
doc. Ing. Ivo Hlavatý, Ph.D.  
děkan fakulty

## Declaration of the Student

I hereby declare that I have completed this bachelor thesis and all its appendices independently under supervision of the supervisor of the bachelor thesis and that I have listed all the literature and publications used.

Šilheřovice 14. 5. 2018

Student's signature.....

### Prohlašuji, že

- jsem si vědom, že na tuto moji závěrečnou bakalářskou práci se plně vztahuje zákon č. 121/2000 Sb. Zákon o právu autorském, o právech souvisejících s právem autorským a o změně některých zákonů (dále jen Autorský zákon), zejména §35 (Užití díla v rámci občanských či náboženských obřadů nebo v rámci úředních akcí pořádaných orgány veřejné správy, v rámci školních představení a užití díla školního) a §60 (Školní dílo),
- beru na vědomí, že Vysoká škola báňská - Technická univerzita Ostrava (dále jen „VŠB - TUO“) má právo užít tuto závěrečnou bakalářskou práci nekomerčně ke své vnitřní potřebě (§35 odst. 3 Autorského zákona),
- bude-li požadováno, jeden výtisk této bakalářské práce bude uložen u vedoucího práce,
- s VŠB - TUO, v případě zájmu u její strany, uzavřu licenční smlouvu s oprávněním užít dílo v rozsahu §12 odst. 4 Autorského zákona,
- užít toto své dílo, nebo poskytnout licenci k jejímu využití, mohu jen se souhlasem VŠB - TUO, která je oprávněna v takovém případě ode mne požadovat přiměřený příspěvek na úhradu nákladů, které byly VŠB - TUO na vytvoření díla vynaloženy (až do jejich skutečné výše),
- beru na vědomí, že - podle zákona č. 111/1998 Sb., o vysokých školách a o změně a doplnění dalších zákonů (zákon o vysokých školách), ve znění pozdějších předpisů - že tato bakalářská práce bude před obhajobou zveřejněna na pracovišti vedoucího práce, a v elektronické podobě uložena a po obhajobě zveřejněna v Ústřední knihovně VŠB - TUO, a to bez ohledu na výsledek její obhajoby.

V Šilheřovicích dne 14. května 2018



.....  
podpis

Jméno a příjmení autora práce:

David Krzikalla

Adresa trvalého pobytu autora práce:

Střední 212, 747 15 Šilheřovice

# Anotace bakalářské práce

KRZIKALLA, D. *Analýza tuhosti rámu studentské formule: bakalářská práce.* Ostrava: VŠB - Technická univerzita Ostrava, Fakulta strojní, Katedra aplikované mechaniky, 2018, 116 s. Vedoucí práce: Poruba, Z.

Bakalářská práce se zabývá analýzou torzní tuhosti rámu studentské formule Vector 04 týmu Formula TU Ostrava. V úvodu práce je představen projekt Formula SAE<sup>®</sup>, poté následuje popis technických požadavků na vozy a jejich rámy dle pravidel Formula SAE<sup>®</sup>. Práce pokračuje popisem stavby modelu pro simulaci torzní tuhosti, který je založen na tzv. metodě se dvěma nosníky, kdy rám je uchycen ke 2 nosníkům. Aplikací síly na jeden z nich je generováno zatížení rámu. Jsou popsána zjednodušení modelu a aplikovány okrajové podmínky, tak aby výsledky bylo možné porovnat s výsledky experimentu, který byl proveden ve stejném duchu pro verifikaci a nalazení simulace. Výsledky simulací a experimentu jsou porovnány mezi sebou, a také se zkrutnou tuhostí náprav. Z porovnání vyplývá, že analýza je přijatelně nalazena vzhledem k experimentu a torzní tuhost rámu vzhledem ke zkrutné tuhosti náprav je dostatečná. Nakonec jsou diskutovány možnosti optimalizace rámu z pohledu zvýšení tuhosti (popř. snížení hmotnosti) a je zde uveden příklad takové optimalizace.

# Annotation of Bachelor Thesis

KRZIKALLA, D. *Stiffness Analysis of Formula Student Frame: Bachelor Thesis.* Ostrava: VŠB - Technical University of Ostrava, Faculty of Mechanical Engineering, Department of Applied Mechanics, 2018, 116 p. Thesis head: Poruba, Z.

Bachelor thesis is dealing with analysis of torsion stiffness of the frame of Formula TU Ostrava team vehicle Vector 04. Firstly, the project Formula SAE<sup>®</sup> is introduced followed by a description of technical requirements for Formula SAE<sup>®</sup> vehicles and for frames of such vehicles. The thesis continues with description of simulation model for torsion stiffness analysis based on so called two-beams method. The method is based on attachment of the frame to two beams. Application of a force on one of beams causes torsion loading of the frame. Simplifications of the model are discussed and boundary conditions are applied in such manner to allow comparison of result with the experiment which is also carried out for verification and tuning of the simulation. The results from simulations and from experiment are compared together and with roll stiffness of suspension. From comparisons follows that the simulation is acceptably tuned with respect to experiment and the frame is sufficiently stiff with respect to roll stiffness of the suspension. The thesis is concluded by possibilities of optimization of the frame to increase torsion stiffness (and possibly reduce mass of the frame) and one example of such an optimization is introduced.

# Contents

<b>List of Abbreviations and Symbols</b>	<b>8</b>
<b>Introduction</b>	<b>11</b>
<b>1 Technical Requirements for Formula SAE<sup>®</sup> Vehicles</b>	<b>17</b>
1.1 Fundamental Requirements for Formula SAE <sup>®</sup> Vehicles . . . . .	17
1.1.1 Vehicle Configuration . . . . .	17
1.1.2 Bodywork . . . . .	18
1.1.3 Wheelbase . . . . .	18
1.1.4 Visible Access . . . . .	18
1.1.5 General Chassis Rules . . . . .	18
1.1.6 Brake System . . . . .	19
1.1.7 Power-train . . . . .	19
1.1.8 Aerodynamic Devices . . . . .	19
1.1.9 Compressed Gas Systems and High Pressure Hydraulics . . . . .	20
1.1.10 Fasteners . . . . .	20
1.2 Technical Requirements for Formula SAE <sup>®</sup> Frame Design . . . . .	20
1.2.1 Definition of the Frame Structure . . . . .	21
1.2.2 Material Requirements . . . . .	23
1.2.3 Front Bulkhead . . . . .	24
1.2.4 Main Hoop . . . . .	24
1.2.5 Main Hoop Bracing . . . . .	24
1.2.6 Front Hoop . . . . .	25
1.2.7 Front Hoop Bracing . . . . .	25
1.2.8 Side Impact Structure . . . . .	26
1.2.9 Cockpit . . . . .	26
1.2.10 95th Percentile Male Template . . . . .	27
1.2.11 Torsion Stiffness of Frame . . . . .	28
<b>2 Geometric and Finite Element Model of Frame</b>	<b>30</b>
2.1 Model of Frame . . . . .	30
2.1.1 Geometric Model of Frame . . . . .	30
2.1.2 Finite Element Model of Frame . . . . .	32
2.2 Finite Element Model . . . . .	33
2.2.1 Properties of Materials Used . . . . .	40

<b>3</b>	<b>Mesh, Boundary Conditions and Settings of Analysis</b>	<b>41</b>
3.1	Element Type and Mesh Used . . . . .	41
3.1.1	Element Type . . . . .	41
3.1.2	Mesh . . . . .	43
3.2	Boundary Conditions . . . . .	45
3.2.1	Force . . . . .	45
3.2.2	Constraints . . . . .	46
3.3	Settings of Simulation . . . . .	47
3.4	Modal Analysis of Finite Element Model . . . . .	48
<b>4</b>	<b>Evaluation of the Frame Stiffness</b>	<b>50</b>
4.1	Description of Testing and Simulation Procedure . . . . .	50
4.2	Experimental Part . . . . .	53
4.2.1	Testing Environment . . . . .	53
4.2.2	Measuring Procedure . . . . .	54
4.2.3	Evaluation of the Torsion Stiffness from Experiment . . . . .	55
4.3	Simulation Part . . . . .	63
4.3.1	Points of Interest Within the Frame . . . . .	63
4.3.2	Evaluation of the Torsion Stiffness from Simulation . . . . .	64
4.4	Comparison of the Results from the Experiment and from Simulations . . . . .	69
4.4.1	Overall Comparison of the Results . . . . .	69
4.4.2	Comparison with Roll Stiffness of the Suspension . . . . .	71
<b>5</b>	<b>Possibilities of Optimization of the Frame</b>	<b>74</b>
5.1	Examination of the Sectional Stiffness of the Frame . . . . .	75
5.2	Example of Optimization . . . . .	77
5.3	Assessment of the Optimization . . . . .	78
<b>6</b>	<b>Discussion of Results and Conclusion</b>	<b>79</b>
	<b>Acknowledgment</b>	<b>82</b>
	<b>Bibliography</b>	<b>87</b>
	<b>Table of Contents for Appendix</b>	<b>89</b>

# List of Abbreviations and Symbols

ARB	Anti-roll bar
C-S (c-s)	Cross-section
DOF	Degree of freedom
FH	Front Hoop
hp	horsepower
IA	Impact Attenuator
MH	Main Hoop
MPC	Multi point constraint
SAE <sup>®</sup>	Society of Automobile Engineers
SES	Structural Equivalency Spreadsheet
Sim.	Simulation
SIS	Side impact structure

$a$	mm	Length of edge of square cross-section
$a_F$	mm	Length of edge of square cross - section of front upright
$a_R$	mm	Length of edge of square cross - section of rear upright
$A$	mm <sup>2</sup>	Area
$c_{TR}$	—	Torsion/Roll stiffness ratio
$c_{TRexp}$	—	Torsion/Roll stiffness ratio for experiment
$C$	Nm/deg	Torsion stiffness of certain section
$C_B$	Nm/deg	Torsion stiffness of section B
$C_C$	Nm/deg	Torsion stiffness of section C
$C_l$	Nm <sup>2</sup> /deg	Torsion stiffness on unit of length
$C_R$	Nm/deg	Roll stiffness of suspension
$C_T$	Nm/deg	Torsion stiffness
$C_{lB}$	Nm <sup>2</sup> /deg	Torsion stiffness on unit of length of section B
$C_{lC}$	Nm <sup>2</sup> /deg	Torsion stiffness on unit of length of section C
$C_{Rf}$	Nm/deg	Roll stiffness of front axle
$C_{Rr}$	Nm/deg	Roll stiffness of rear axle
$C_{Texp}$	Nm/deg	Torsion stiffness from experiment
$C_{B7}$	Nm/deg	Torsion stiffness of section B of seventh line in evaluation table
$C_{C7}$	Nm/deg	Torsion stiffness of section C of seventh line in evaluation table
$C_{T3}$	Nm/deg	Torsion stiffness of the third line in evaluation table
$C_{T9}$	Nm/deg	Torsion stiffness of the ninth line in evaluation table



$C_T/m$	—	Torsion stiffness/mass ratio
$C_T/m_b$	—	Torsion stiffness/mass ratio of base frame design
$C_T/m_o$	—	Torsion stiffness/mass ratio of optimized frame design
$d_i$	mm	Inner diameter
$d_o$	mm	Outer diameter
E	MPa	Young's modulus
F	N	Force
g	m/s <sup>2</sup>	Gravity acceleration
k	N/mm	Stiffness
$k_F$	N/mm	Stiffness of front upright
$k_R$	N/mm	Stiffness of rear upright
l	m	Length of certain section
$l_B$	m	Length of section B
$l_C$	m	Length of section C
$l_n$	mm	Length between pair of nodes
L	m	Distance from point of force to point of rotation
$L_F$	mm	Length of front upright
$L_R$	mm	Length of rear upright
$L_0$	mm	Original length
$L_{12}$	mm	Distance between points 1, 2
$L_{34}$	mm	Distance between points 3, 4
$L_{56}$	mm	Distance between points 5, 6
m	kg	Mass
$m_7$	kg	Applied mass during 7th load step
n	—	Number of values
T	Nm	Torque
$T_7$	Nm	Torque within 7th line of the evaluation table
$u_l$	mm	Displacement of node at left Path
$u_r$	mm	Displacement of node at right Path
$u_1$	mm	Displacement of point 1
$u_2$	mm	Displacement of point 2
$u_3$	mm	Displacement of point 3
$u_4$	mm	Displacement of point 4
$u_5$	mm	Displacement of point 5
$u_6$	mm	Displacement of point 6
$x_i$	—	Individual value
$\bar{x}$	—	Arithmetic mean

$\alpha$	deg	Deformation angle
$\alpha_B$	deg	Deformation angle of section B
$\alpha_C$	deg	Deformation angle of section C
$\alpha_D$	deg	Deformation angle for Path
$\alpha_{B7}$	deg	Deformation angle of section B within 7th line of the evaluation table
$\alpha_{C7}$	deg	Deformation angle of section C within 7th line of the evaluation table
$\alpha_{12}$	deg	Deformation angle of section at points 1, 2
$\alpha_{34}$	deg	Deformation angle of section at points 3, 4
$\alpha_{56}$	deg	Deformation angle of section at points 5, 6
$\Delta L$	mm	Deformation
$\varepsilon$	—	Strain
$\sigma$	MPa	Stress



# Introduction

## History of Formula SAE®

Formula SAE® started in 1980 as an idea of four officers at the University of Texas. They decided to establish Formula SAE® as a successor of Mini Indy competition which was tarmac racing with small 5-hp engines. Brand new rules of Formula SAE® declared, among other, that teams could use any 4-stroke engine even modified, what was officially encouraged, but the intake was restricted to one inch (25.4 mm).

The first competition took place in 1981. Six university teams showed their interest but four of them competed in 4 dynamic and 2 static events eventually. The dynamic events were: acceleration, maneuverability, endurance and fuel economy. The statics were: Appearance award and Engineering and Design Creativity award. There was no overall winner but each event had its own winner.



Figure 1: 1982 University of Houston Formula SAE® car(2)

Since the year 1982, as the Formula SAE® became an official SAE® event and rules package included only four pages, the competition grew not only in number of participants. It grew even in improvement of rules and competition events. The significant point is that this environment encourage teams to develop new solutions to be the best when compete with each other.

The Formula SAE® spread not only in United States but internationally with numerous competitions all over the world. Because other international competitions such as Formula Student Germany or Formula Student Japan occurred, the Formula SAE® recognized them

as part of the Official Series. This allowed university teams from all over the world to compete with each other under almost the same conditions. Nowadays there are about 500 teams in the world (1).

## **Description of Formula SAE®**

Formula SAE® is engineering competition for university students under SAE® International Organization (initially as the Society of Automobile Engineers) which associates professionals from transport, automotive, aerospace and commercial vehicles industry.

During years, three categories of vehicles occurred:

- Combustion vehicles - vehicles powered by 4-stroke combustion engine
- Electric vehicles - vehicles powered by electric motors
- Driver-less vehicles - autonomous vehicles powered by both combustion or electric power-train.

## **Objectives of Formula SAE®**

The objective of Formula SAE® is to design a race car according to official rules, test the car before competition for possible issues and then race it on competition. Since an integral part of competition are static disciplines, where team must prove understanding of design of car or business thinking, the Formula SAE® is not only about racing but mainly about development, research, improvements and application of knowledge into real technical issues.

Sometimes, the race for the first position can be really intensive. To avoid dangerous situations coming from risky design of a car, each team have to design the car according to official rules which satisfy mainly safety reasons. There is no need for rules to restrict design ideas. The Formula SAE® rules nowadays consist of about 180 pages covering both design and competition part.

As I mentioned, the Formula SAE® competition aims on development and improvement of technologies and manufacturing manners. Thus, teams have to build a new car each year or made some significant changes to the last year's car. It is not allowed to use older than one year car. This way, the teams are pushed forward to perform the best.

## **Competition Event**

After successful designing and testing of a race car, team attends competition event where competes with another teams from all over the world. This event is for each team the top of the season. Since there is a lot of competitions worldwide, for example Europe has about 18, team can choose appropriate one to participate. Number of attended competitions is not limited depending only on time management and budget of team.

To get permission to start on a race a team have to submit required documents and pass registration event which is basically a test of about 15 questions from Formula SAE® rules and engineering fundamentals. Every competition has certain number of teams allowed to

participate. According to results of registration test a list of teams is established. The position of team within the list depends on number of right answers and time which the team takes to complete the test. The right answers are of greater value than the time.

It is possible to divide the competition into three parts and each part includes several events.

Parts of competition:

- Scrutineering
- Static disciplines
- Dynamic disciplines

Scrutineering is comprised of:

- Technical inspection - overall check of vehicle (accordance with Formula SAE<sup>®</sup> rules).
- Tilt test - vehicle is tilted in certain angle to check any possible spillage of fluids.
- Brake test - a test where all four wheels of a vehicle have to be blocked simultaneously once braking .
- Noise test - officials measure the noise of exhaust by certain procedure to check whether the noise level is below the value given by Formula SAE<sup>®</sup> rules.

Static disciplines are:

- Design Presentation - team defends and explains design of the car and engineering solutions to judges (professionals from usually automotive industry).
- Cost and Manufacturing presentation - team presents the cost list of all components of the car together with manufacturing processes used.
- Business Plan presentation - team presents devised business plan of production of the car to convince a fictive investor.

Dynamic disciplines are following:

- Acceleration - sprint 75 meters long with standing start.
- Skid-pad - race in eight-shaped track (see Fig. 2).
- Autocross - race on approximately one kilometer track, serves also as qualification for Endurance and Efficiency.
- Endurance and Efficiency - race approximately 22 kilometers long with change of drivers in the middle. After the discipline, the consumption of vehicle is also measured.

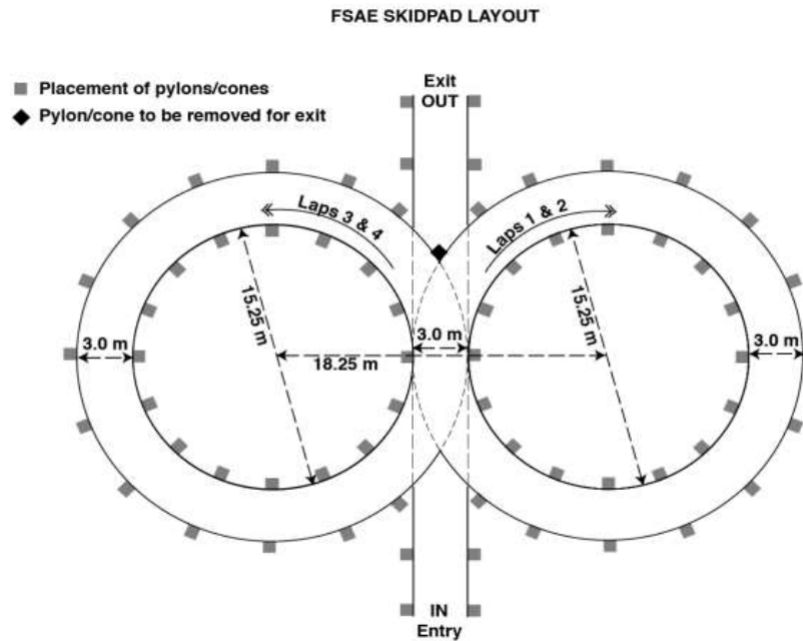


Figure 2: Skid-pad layout according to Formula SAE rules (3)

Each discipline is evaluated separately and team can achieve certain maximal amount of points for each discipline (see Tab. 1). The points are counted up thus each team ends up with certain amount of points and the ranking list of teams is established according to the amount of gathered points.

Static events		
	Business plan presentation	75
	Cost and Manufacturing presentation	100
	Design Presentation	150
Dynamic events		
	Acceleration	100
	Skid-pad	75
	Autocross	125
	Endurance	275
	Efficiency	100
Total points		1000

Table 1: Maximal available points for disciplines (3)

## Frame of Formula SAE<sup>®</sup> Vehicle

### Types of Frames Used for Formula SAE<sup>®</sup> Vehicles

- Space steel tube frame (see Fig. 3 )

Basic form of frame for Formula SAE<sup>®</sup> vehicles is made from steel tubes welded together. Such frames are widely used by beginner teams in project because of its relative easy and cheap construction (compared to other types of frames below) and possibility to change or repair it easily.

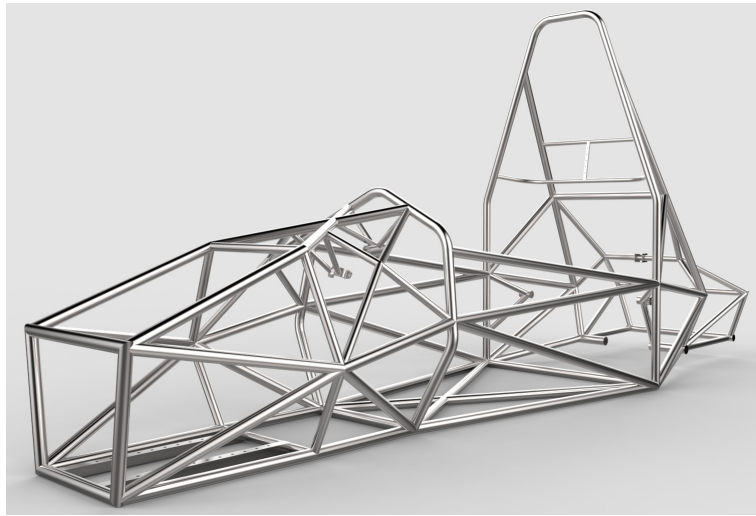


Figure 3: Steel tube frame (4)

- Aluminum monocoque

One can imagine an aluminum shell composed of aluminum honeycomb plates and panes usually connected together by rivets.

- Carbon fibre monocoque (see Fig. 4 )

Nowadays, more advanced teams are using the carbon-fibre monocoque because of its stiffness and strength compared to the steel tube frames. The drawbacks are, however, very good required knowledge of processing of carbon-fibre and great design of all further parts connected with monocoque because its tricky reparability after manufacture and high cost. Such frame structures have to be composed of carbon - fibre monocoque with steel tube parts. According to rules some parts of frame must be made of steel only, i.g. Main hoop.

- Hybrid material frame

Frame made from i.g. steel and carbon-fibre tubes properly connected together. Such frames are liable to alternative frame rules according to Formula SAE<sup>®</sup> rules to prove its quality.

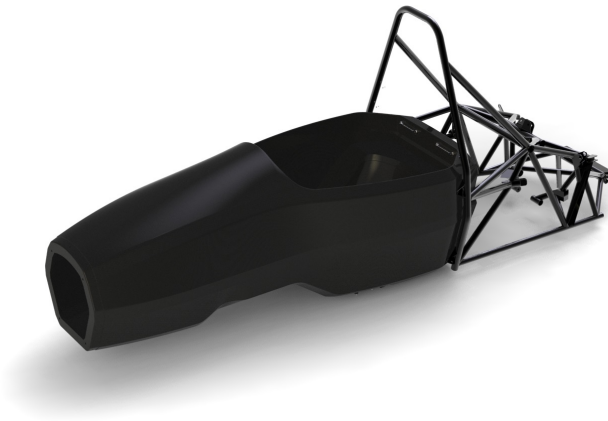


Figure 4: Carbon fibre monocoque (5)

## **Formulation of a Topic and Targets of This Thesis**

I work in Formula TU Ostrava team in Chassis and Ergonomics Group thus my task is to prepare a model of the frame for Vector 04 vehicle (season 2017-2018) and evaluate its torsional stiffness. The aim of this thesis is to prepare a simulation model for evaluation of the torsion stiffness of the frame and tune the model according to results from the experimental testing. I am going to carry out the simulation in ANSYS Workbench 18.2 software. At the end, I am going to propose possible options for optimization of the frame, make comparisons and conclude the results.



# Chapter 1

## Technical Requirements for Formula SAE<sup>®</sup> Vehicles

### 1.1 Fundamental Requirements for Formula SAE<sup>®</sup> Vehicles

#### 1.1.1 Vehicle Configuration

Formula SAE<sup>®</sup> 2017-2018 rules say that the vehicle must be open-wheeled and open-cockpit with four wheels.

Open wheel means that the top 180 degrees of the wheels/tires must be unobstructed when viewed from vertically above wheel. Also wheels/tires must be unobstructed when viewed from the side. There must be free space of 75 mm around wheel when measured from outer diameter of tire from ground to upside with tires steered straight ahead. The zones are highlighted in Fig. 1.1.

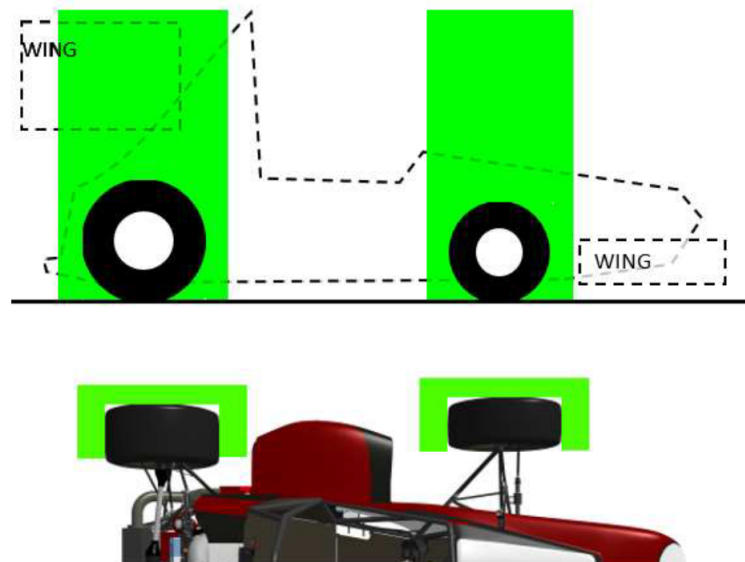


Figure 1.1: Unobstructed zones (3)

### 1.1.2 Bodywork

All openings, but other that required for cockpit opening, are prohibited through the bodywork into driver compartment from the front to the back of the vehicle, to the roll bar Main hoop or Firewall. Minimal openings are allowed around suspension components.

### 1.1.3 Wheelbase

Minimal wheelbase is 1525 mm. The wheelbase is measured from center of ground contact of front tire to the rear tire when the wheels steered straight ahead.

### 1.1.4 Visible Access

The vehicle must be designed the way that all parts during the Technical Inspection are clearly visible to the inspectors with no use of endoscopes, mirrors or such instruments. Body panels may be removed to provide desired access.

### 1.1.5 General Chassis Rules

- Suspension

The car must be equipped with fully working suspension system with front and rear shock absorbers. At Technical inspection all parts must be visible, either direct view or by removing its covers.

- Ground clearance

To prevent touching ground during dynamic events, the ground clearance must be sufficient.

- Tires

Teams are allowed to use both dry and wet tires. The dry tires must be on the vehicle during Technical inspection and may be slick or treaded. The wet tires can be any size or type of grooves with minimum of 2.4 mm depth.

- Steering

Only mechanically connected steering wheel to the front wheels is allowed. The steering wheel must be attached to the steering column with a quick release component, must be circular-shaped or oval-shaped without concave sections. No part of the steering wheel must exceed higher than horizontal level at top-most point of Front Hoop.

- Jacking point

The point (in reality a tube) which is capable to support car and is located at the rear of the car. Such point must be painted in orange, clearly visible for a person standing one meter behind the car, placed horizontally and perpendicular to the longitudinal axis of the car, 300 mm long in minimal, accessible from the rear of the car.

- Rollover stability

The design of the vehicle (track and center of gravity) must provide rollover stability which is evaluated during Technical inspection by Tilt test. The car is tilted at angle of 60 degrees around its longitudinal axis, corresponding to 1.7 G's, with driver seated. All tires must remain in contact with the tilting deck.

### 1.1.6 Brake System

The brake system of Formula SAE<sup>®</sup> vehicles must act on all four wheels and must be capable to lock all wheels while operated by a single control. Ability to lock all four wheels is checked during Brake test within Technical inspection. The brake system must be comprised of two independent hydraulic circuits each with its own fluid reserve. Prohibited are brake-by-wire systems as well as using of unarmored plastic lines.

Brake pedal is allowed to be of steel, aluminum or titanium and must be designed to withstand a force of 2 kN without any failure of pedal or pedal box. The brake pedal must be also equipped with over-travel switch, which is part of shutdown system, so in case of failure or over-travel of brake pedal the shutdown system is activated.

Formula SAE<sup>®</sup> vehicle must be also equipped with a red brake light with minimal shining surface of 15 cm<sup>2</sup> that must be clearly visible from rear even in very bright sunlight.

### 1.1.7 Power-train

Engines which have water-cooling system must use only water. Electric motors, accumulators or high voltage electronics may use water or oil to cooling. Any other additives, antifreeze or lubricants are prohibited. Cooling system must be also equipped with separate catch cans to catch any vents from cooling system or lubrication system.

There is no restriction about transmission and drive-train. High-speed drive-train equipment such as gears or pulleys must be shielded according to Formula SAE<sup>®</sup> rules for case of failure.

### 1.1.8 Aerodynamic Devices

Aerodynamic devices such as wings or splitters must be located only within certain places according to Formula SAE<sup>®</sup> rules. All horizontal wing edges pointing forward must have minimum radius of 5 mm and 3 mm for the vertical ones.

Aerodynamic devices for Formula SAE<sup>®</sup> vehicles must be also designed to provide adequate stiffness in static conditions to prevent significant movement while the vehicle is moving. In the Formula SAE<sup>®</sup> rules, there is prescribed a guidance how to determine significant move of aerodynamic devices.

### 1.1.9 Compressed Gas Systems and High Pressure Hydraulics

Systems of Formula SAE<sup>®</sup> vehicles using compressed gas must use the non-flammable one such as air, nitrogen, carbon dioxide. Gas tank must be adequately manufactured and certified, equipped with pressure regulation valve, protected from rollover or any other damage caused by failure of rotating components. The gas tank must be also attached to the frame, engine or transmission, insulated from any heat sources and the tank's axis must not point at the driver. It is prohibited to locate the gas tank and pressure regulator into cockpit.

#### 1.1.10 Fasteners

Minimal grade of fasteners used for driver's cell structure, steering, braking, driver's harness and suspension system is Metric grade 8.8. For above mentioned systems together with Impact Attenuator and Primary structure, some bolt types (e.g. button head cap, countersunk head screws or bolts) are prohibited. For the systems are permitted hexagonal socket head bolts.

Formula SAE<sup>®</sup> rules even prescribe minimal ratio between hole diameter and distance to nearest free edge for bolted joints in the Primary structure (see 1.2.1) once the brackets are used.

Joints which are critical (steering, braking, driver's harness and suspension system) must be secured with so called positive locking system. That means the joints must be secured against sudden loss of nut by mechanisms such as safety wiring, cotter pins, nylon lock nuts (except high temperature places, i.e. over 80 degrees Celsius) or prevailing torque lock nuts. From any lock nut minimum two threads must exceed.

## 1.2 Technical Requirements for Formula SAE<sup>®</sup> Frame Design

There are two options for teams how to design the frame:

- General Requirements

May be followed with no need of any structural strength analysis because the minimal material requirements are prescribed. Teams must submit the Structural Equivalency Spreadsheet (SES) document to prove the design of the frame. The SES team fills with material and cross-section of tubes used. Then macros and formulas in the document can determine if the design of the frame is sufficient or not.

- Alternate frame rules and Monocoque General Requirements

Useful once team considers to design frame from materials or cross-sections which differ from the prescribed ones in General Requirements. Then the teams can more easily design, for example, carbon-fibre monocoques or various steel tube frames. Frames designed following the Alternate frame rules must undergo structural strength analysis. Team must also prove equivalence of used materials by testing. All required procedures for analyze and testing are described within Alternate frame rules and Monocoque General Requirements.

Further on in this thesis, I am considering only General Requirements for frame.

### 1.2.1 Definition of the Frame Structure

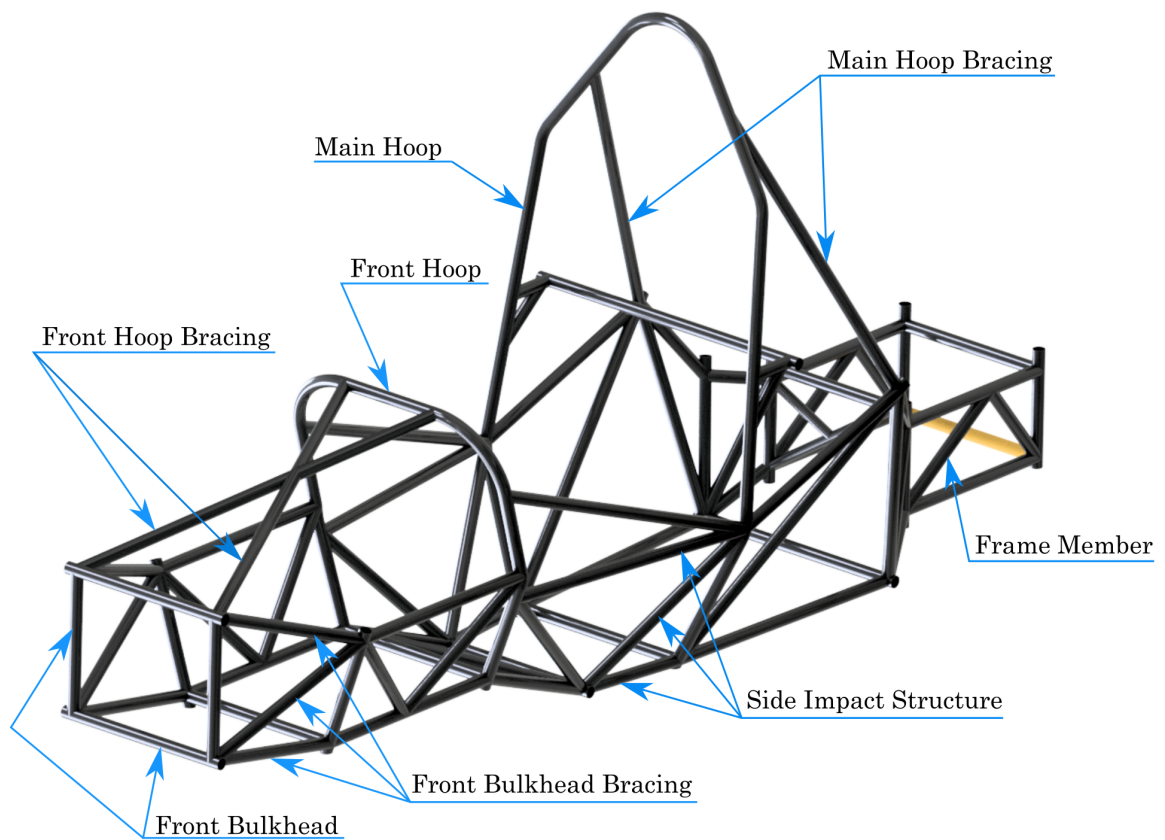


Figure 1.2: Description of frame structure of Vector 04 vehicle

- Main Hoop  
An arc-shaped tube which is right behind driver.
- Front Hoop  
An arc-shaped tube which is located above driver's legs, near to steering wheel.
- Main Hoop Bracing  
Structure which supports Main hoop.
- Front Hoop Bracing  
Structure which supports Front hoop.

- Side Impact Structure

Side area of the car extending to 350 mm above the ground and connecting the Front Hoop and the Main Hoop.

- Front Bulkhead

Structure which is defined as the most-forward one of the Major structure of the frame. To this structure is attached Impact Attenuator with Anti-Intrusion Plate. Such assembly (see Fig. 1.3) serve as deformable, energy absorbing device for case of crash.

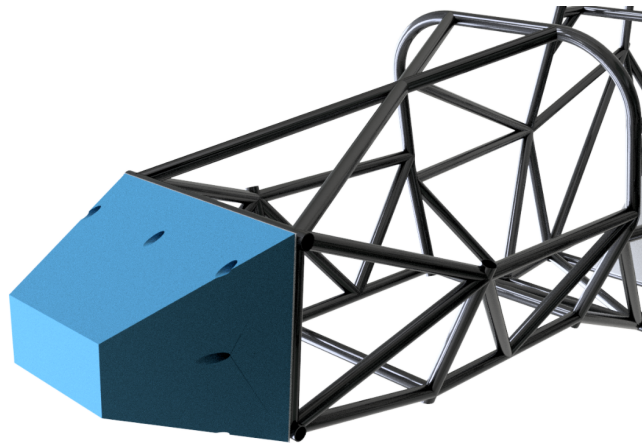


Figure 1.3: Impact Attenuator with Anti-Intrusion Plate mounted on the Front Bulkhead

- Frame Member

A single piece of tubing.

- Primary structure

Primary structure is the structure which consist of: 1) Main Hoop, 2) Front Hoop, 3) Front Hoop Bracing, 4) Main Hoop Bracing, 5) Side Impact Structure, 6) Front Bulkhead, 7) Front Bulkhead Bracing and all Frame Members that transfer loading from driver's restraint system into 1) - 7) structures.

- Major structure of the frame

The part of the frame which is within area defined by Primary structure. Main Hoop Bracing and the part of the MH above a horizontal plane which lies at the top of the upper Side Impact Structure bar is not included in Major structure of the frame.

- Node-to-node triangulation

Arrangement of tubes to be *properly triangulated*. If the frame members are projected onto a plane where a co-planar loading occurs that can results in only tension/compression loading of Frame members (see Fig. 1.4).

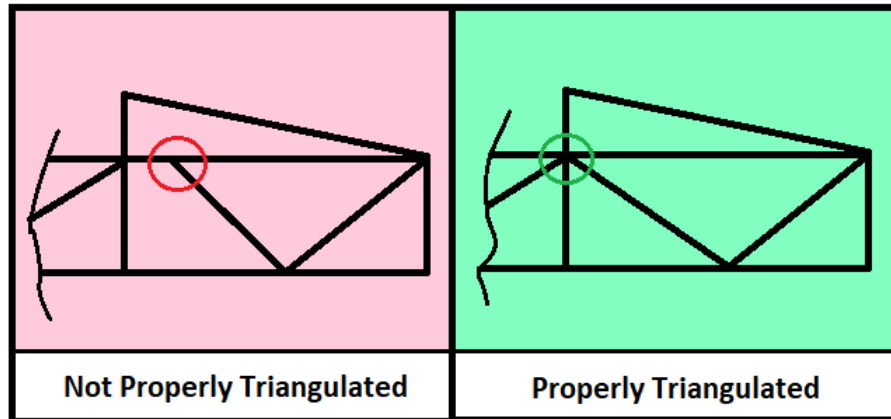


Figure 1.4: Example of triangulation (3)

### 1.2.2 Material Requirements

Material allowed for the Primary structure is mild or alloyed steel with more than 0.1 % of carbon. Minimal profile and cross-section requirements are in Tab. 1.1.

Item of usage	Profile and cross-section
Main and Front hoop, Shoulder harness bar	Round tube 1 x 0.095 inch or Round tube 25 x 2.5 mm
Side Impact Structure, Front bulkhead, Front hoop bracing, Main hoop bracing, Driver's restrain harness mounting	Round tube 1 x 0.065 inch or Round tube 25 x 1.75 mm or Round tube 25.4 x 1.6 mm or Square tube 1 x 0.047 inch or Square tube 25 x 1.2 mm
Front bulkhead bracing, Main hoop bracing support, Shoulder harness bar support	Round tube 1 x 0.047 inch or Round tube 25 x 1.5 mm or Round tube 26 x 1.2 mm
Bent upper side-impact member	Round tube 1.375 x 0.047 inch

Table 1.1: Minimal profile and C-S requirements

If the alloyed steel tube is used its wall thickness must be at least as the mild steel tube thickness. It is allowed to use tubes of outside diameter or wall thickness given by Tab. 1.1 and greater wall thickness or greater outside diameter respectively, without any approval according to Alternate frame rules.

As I have mentioned above, the SES document use set of formulas to evaluate the frame structures. Material properties used in the calculations are in Tab. 1.2 and serve as minimal material requirements.

Non-welded strength for continuous material calculation

Young's modulus (E) = 200 GPa  
Yield strength (Sy) = 305 MPa  
Ultimate strength (Su) = 365 MPa

Welded strength for discontinuous material calculation (i.e. joints)

Young's modulus (E) = 200 GPa  
Yield strength (Sy) = 180 MPa  
Ultimate strength (Su) = 300 MPa

Table 1.2: Minimal material properties

### 1.2.3 Front Bulkhead

As mentioned above in section 1.2.1, Front bulkhead is structure in front of the car to which is the Impact Attenuator assembly attached. This structure must be of closed cross-section, of material according to section 1.2.2 and situated forward of all non-crushable items such as master cylinders, hydraulic reservoirs, batteries. Front bulkhead must be securely integrated to the frame and supported by at least three tubes on each side of the vehicle and triangulated.

Impact Attenuator assembly consists of Impact Attenuator and Anti-intrusion plate. Impact Attenuator is item which must be from material which can excellently absorb deformation energy during impact. The team can choose either standard Formula SAE<sup>®</sup> Impact Attenuator which already certified or customized IA. The customized attenuators must be proven by specific procedure noted in Formula SAE<sup>®</sup> rules and the team must submit technical papers from testing of the attenuator.

Anti-intrusion plate is sheet of steel or aluminium to which the Impact Attenuator is mounted. The whole assembly is attached to the Front Bulkhead by screw joints or welded.

### 1.2.4 Main Hoop

Formula SAE<sup>®</sup> rules says that Main Hoop must be designed as single, continuous tube of closed cross-section and must go from the lowest Frame member on one side of the frame, up, over and down to the other side lowest Frame member. Prohibited material for Main hoop are aluminum alloy, titanium alloy and even composite materials. One can take a side look on the vehicle then any part above the Side Impact Structure's upper member of the Main hoop can be inclined maximum of 10 degrees from vertical. The lower part of Main Hoop underneath the upper member of Side Impact Structure can be inclined in any angle in forward direction but maximum of 10 degrees rearward from the vertical.

### 1.2.5 Main Hoop Bracing

Material requirements are according to section 1.2.2. MH Bracing must be: of closed cross-section, straight (i.e. no bends are allowed), attached maximum of 160 mm below the top surface of MH (see Fig. 1.5). Angle between MH and MH Bracing must be minimum of



30 degrees (see Fig. 1.5). MH Bracing must support MH by tubes extending in forward or rearward direction on left and right side of Main Hoop. Main Hoop Bracing must be able to transmit all loads from MH into Major Structure (see section 1.2.1) without failing thus secure integration into the frame is necessary. There is also requirement that MH Bracing must be supported back to the Main Hoop by at least two Frame Members (see section 1.2.1) on each side of the vehicle while connected by proper triangulation.

### 1.2.6 Front Hoop

As well as the Main Hoop, the Front Hoop must be designed of closed cross-section tubing and must go from the lowest Frame Member on one side of the frame, up, over and down to the other side lowest Frame Member. There is no restriction about material except that mentioned above and it is even allowed to have the Front Hoop from more than one piece of tube but with proper triangulation. Front Hoop must be inclined maximum of 20 degrees from the vertical and top surface of Front Hoop must be no higher that steering wheel in any position (see Fig. 1.5).

### 1.2.7 Front Hoop Bracing

It is only allowed to have Front Hoop Bracing of material discussed in section 1.2.2. Front Hoop Bracing must be straight (i.e. no bends are allowed) and designed in such manner that: driver's feet and legs are within Major structure of the frame (see section 1.2.1), FH braces are attached not lower than of 50.8 mm from top surface of FH (see Fig. 1.5), braces are extending forward on both right and left side of the FH. The additional bracing going rearward must occur once the FH is inclined more than of 10 degrees from vertical in rear direction.

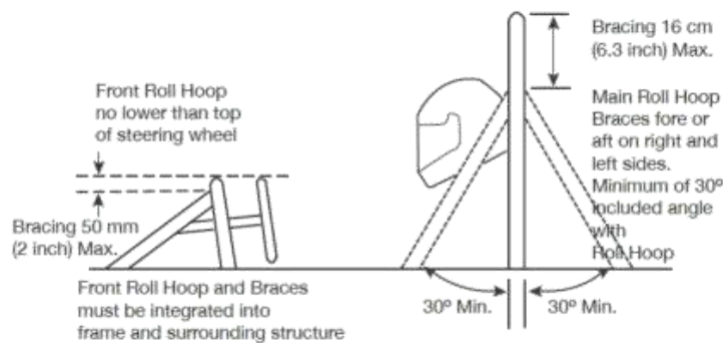


Figure 1.5: Prescribed dimensions and positions (3)

### 1.2.8 Side Impact Structure

Side Impact Structure material is subject of section 1.2.2. SIS must be comprised of at least three tubes on each side of the vehicle. Position of each member of SIS is shown in Fig. 1.6 during 77 kg driver seated in normal position in the car. It is allowed to have SIS members from more than one piece of tube but must be properly triangulated.

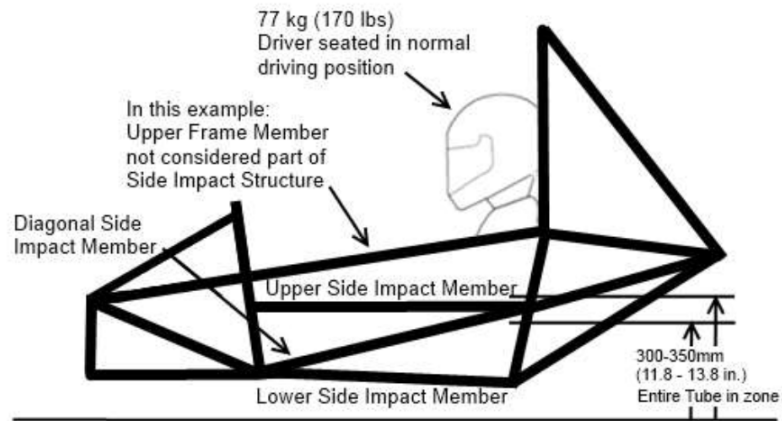


Figure 1.6: Side impact structure requirements (3)

### 1.2.9 Cockpit

Since the Cockpit must satisfy some conditions (i.e. egress of driver within 5 seconds, sufficient space for equipment and driver) there are established two templates (see Fig. 1.7), one for cockpit opening and second for cockpit internal cross-section. The two templates must be able to go through cockpit opening and cockpit internal cross-section respectively.

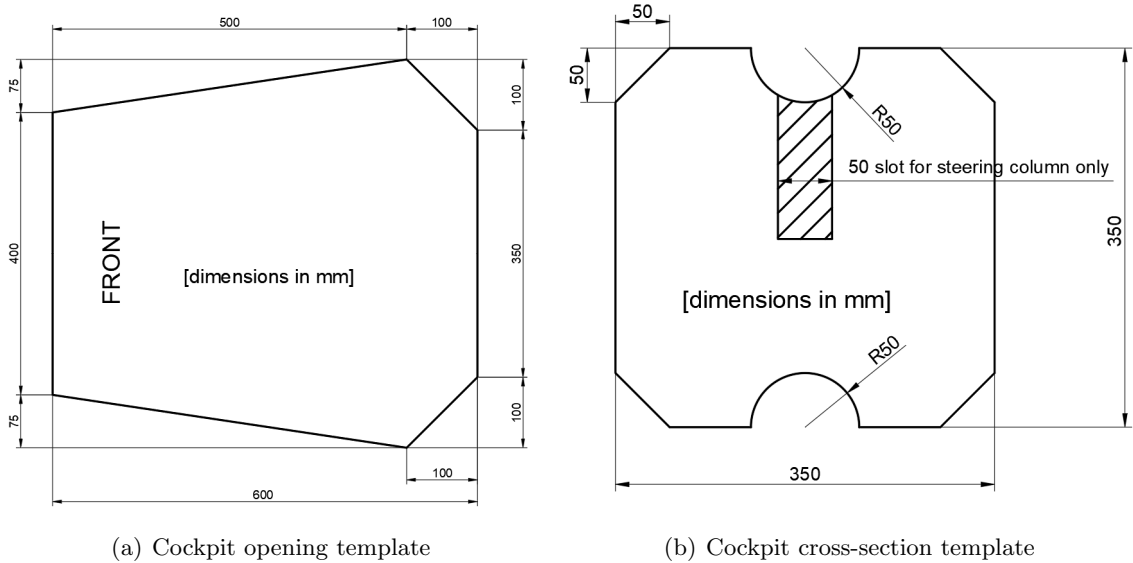


Figure 1.7: Cockpit templates (3)

Driver's positions in the cockpit must be such that adequate heat insulation is provided so driver is not able to be in contact with any material that can reach temperature above 60 degrees Celsius. The Firewall must separate the Cockpit from engine bay, fuel supply, engine oil or liquid cooling systems. Each Firewall must be made of stiff and fire resistant material, must seal completely against passage of fluids and any holes for seat belts cannot be there.

### 1.2.10 95th Percentile Male Template

95th percentile male template serve as measure for frame design. The template is comprised of three circles, two of 200 mm and one of 300 mm in diameter connected together. Whole template is shown in Fig. 1.8 with its dimensions according to Formula SAE<sup>®</sup> rules.

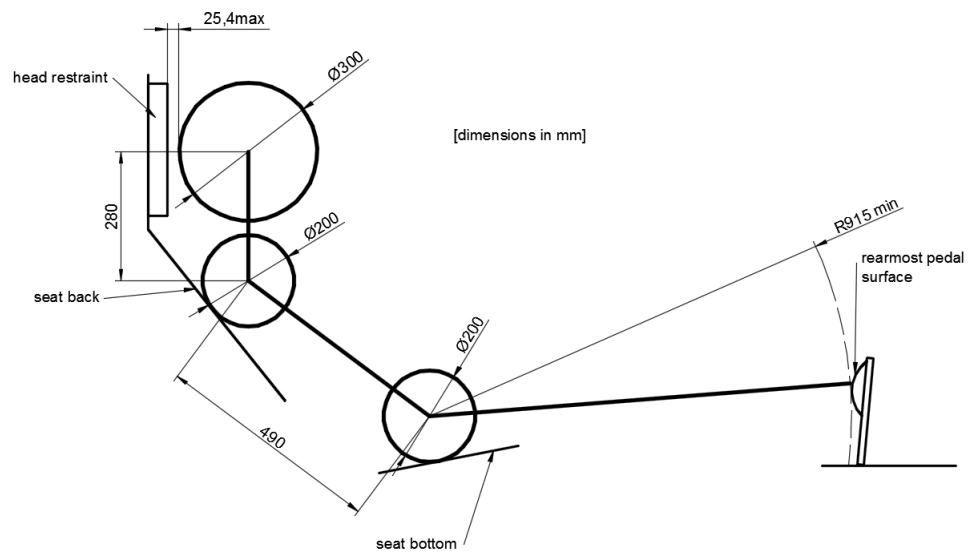


Figure 1.8: 95th percentile male template (3)

The 95th percentile male template's helmet and even all team's drivers must meet the requirements shown in Fig 1.9. This is safety condition for rollover cases thus the driver's head is not possible to touch the ground during such accident.

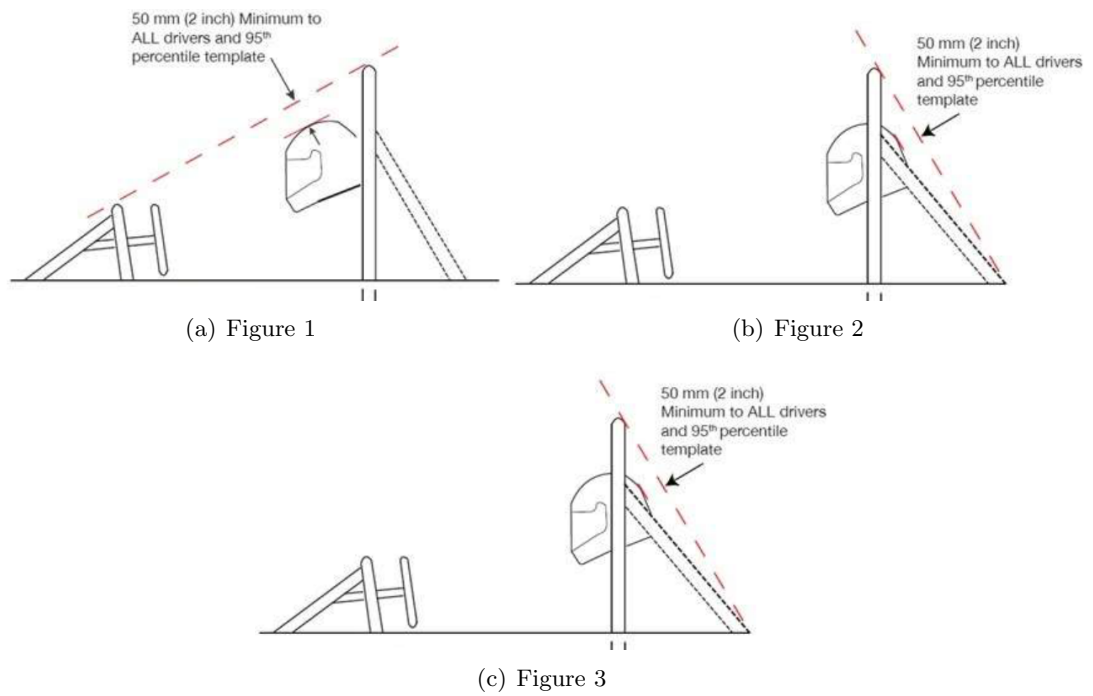


Figure 1.9: Helmet clearance (3)

### 1.2.11 Torsion Stiffness of Frame

The key property of each vehicle's frame, it is longitudinal torsional stiffness (see Fig. 1.10). It means the resistance against twist around longitudinal axis while cornering or while one wheel goes over a bump. If the frame is not adequately stiff the suspension does not work properly. Because of this, the torsional stiffness affects vehicle's performance and behavior significantly (6).

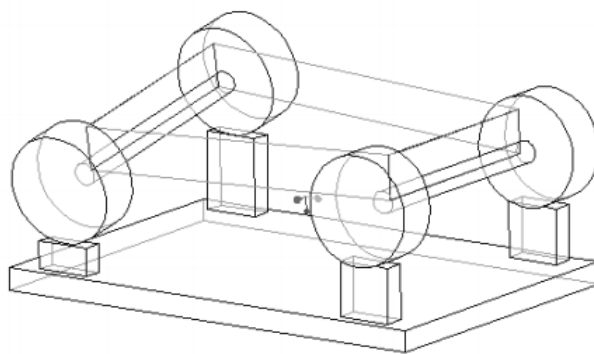


Figure 1.10: Longitudinal torsion mode (7)

Teams are evaluating the torsion stiffness of the frame to prove quality of the design and to find out whether the frame is enough stiff compared to roll stiffness of the suspension. The frames are usually tested with suspension only. However, one can say that there is not only frame racing around the track. There are also another parts (such as engine, body panels,

etc.) affecting the stiffness. Thus, it is good to test the torsion stiffness of whole vehicle or at least with parts with significant effect on the stiffness.

Torsion stiffness, it is a good property for comparison of frames with each other. There is also ratio between frame stiffness and its mass which could help during optimization of the frame. Drawback of this ratio, it is that the ratio can be little bit confusing. One can imagine very stiff (significantly exceeding roll stiffness of suspension) but very heavy frame, then the ratio is high but vehicle's performance suffers from the great mass of the frame. Due to this fact, the team must find adequate design to get as stiff and lightweight frame as possible. Of course, with higher torsion stiffness than roll stiffness of suspension.

Generally applies that torsion stiffness of frame should be higher than roll stiffness. There is no fixed value of torsion stiffness of the frame, with respect to roll stiffness of suspension, which should be exceeded. The more sources one have, the more recommendations can find (e.g. (6), (20)). According to the sources, the torsion stiffness should be 2 to 10 times higher than roll stiffness of suspension. For most Formula SAE<sup>®</sup> cars, it is sufficient to have the frame four times stiffer than suspension (6).

## Chapter 2

# Geometric and Finite Element Model of Frame

### 2.1 Model of Frame

#### 2.1.1 Geometric Model of Frame

The initial point for design of the frame was the last year's car Vector 03 frame (season 2016-2017). After discussion with other Formula TU Ostrava team members, I have proposed and then designed new version of the frame for the new vehicle Vector 04 for season 2017-2018. Main changes touched the front part of the frame where the Front Hoop was tilted in forward direction in 16 degrees and changed in shape. Front Bulkhead went upwards little bit thus there should be more air under the car. That allows us to better utilize the aerodynamic devices located in this area. Beside the rules, there was a restriction that mounting points of A-arms of suspension to the frame must be preserved.

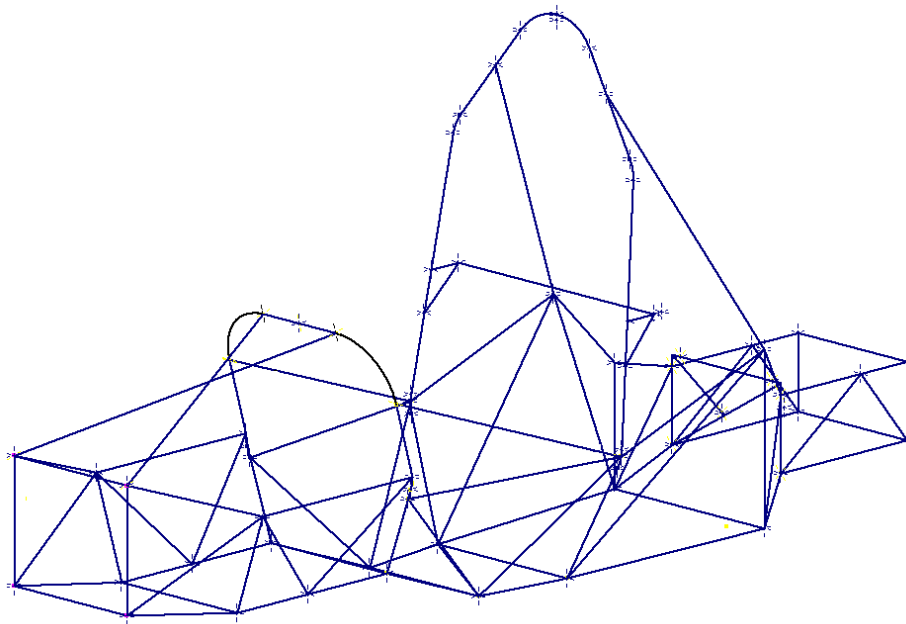


Figure 2.1: Wire-frame model of the new frame

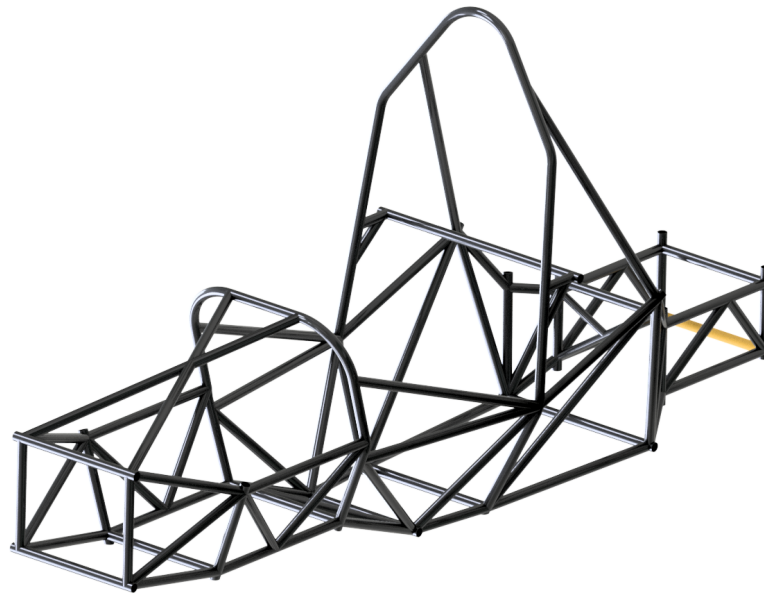


Figure 2.2: 3D model of the new frame

The geometric model of frame, I have designed in software Autodesk Inventor initially as a wire-frame structure (see Fig. 2.1) and at the end as 3D model (see Fig. 2.2). The 3D model served also as a source for generating of drawings for manufacture of the frame. The manufactured and sandblasted frame already with some components attached, one can see in the Fig. 2.3.



Figure 2.3: Sandblasted frame

### 2.1.2 Finite Element Model of Frame

For creation the finite element model, I have utilized the wire-frame structure model designed in Inventor. This model, I have imported into Ansys Design Modeler as line bodies. For each line body, I have assigned a cross-section acc. to Fig. 2.5. Wire-frame model with assigned cross-sections is in Fig. 2.4.

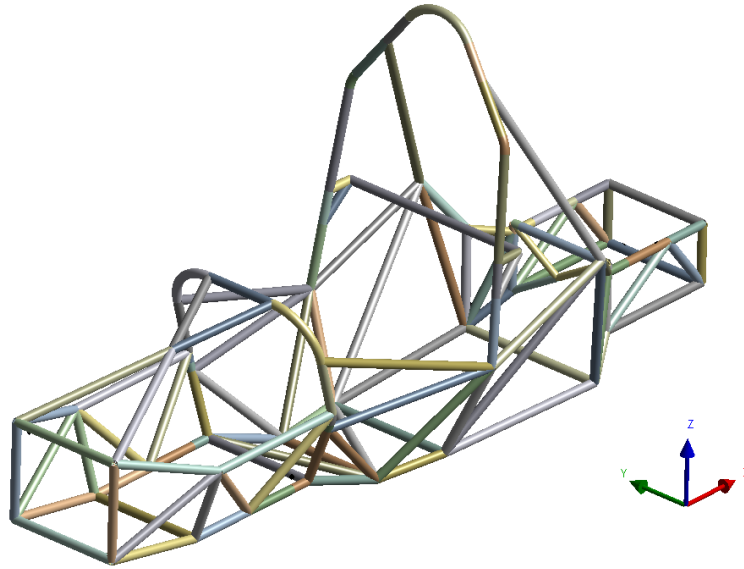


Figure 2.4: Imported wire-frame model with assigned cross-sections



Figure 2.5: Cross-section assignment



## 2.2 Finite Element Model

Though the frame is fundamental part of analysis, there are also another components necessary for establishing adequate analysis environment. Such parts as suspension A-arms or ARB system was included into finite element model to have as exact model compared to real testing as possible.

I have moved on to model other components such as A-arms, front and rear ARB system and testing beams according to real testing environment which one follow to the Chapter 4. For the finite element model, I have decided to model all parts as line bodies with assigned cross-section. Below, there is displayed line model with all parts needed in Ansys Design Modeler (Fig. 2.6).

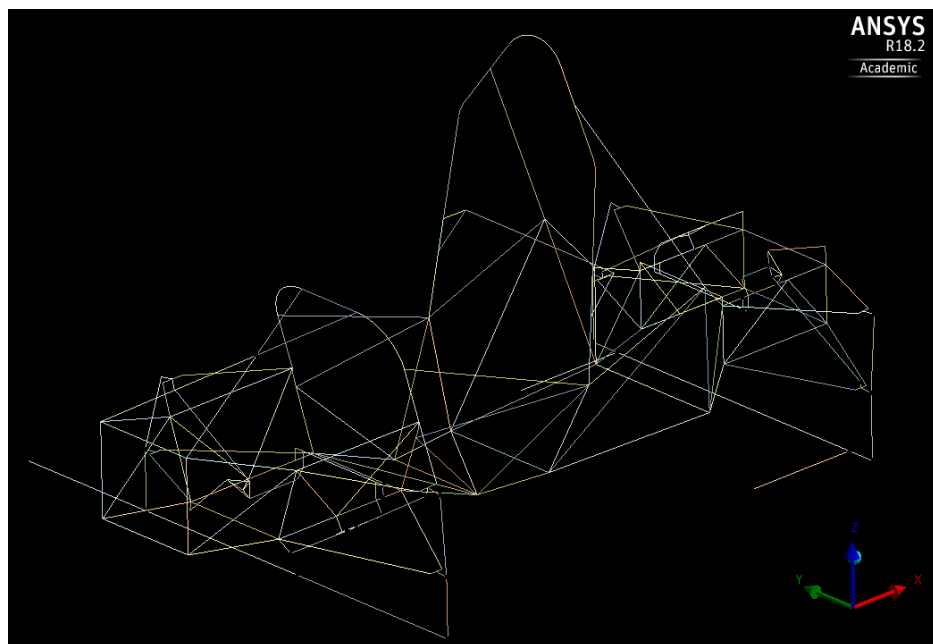


Figure 2.6: Line model

After assigning of cross-sections to all line bodies, I have got the final finite element model.

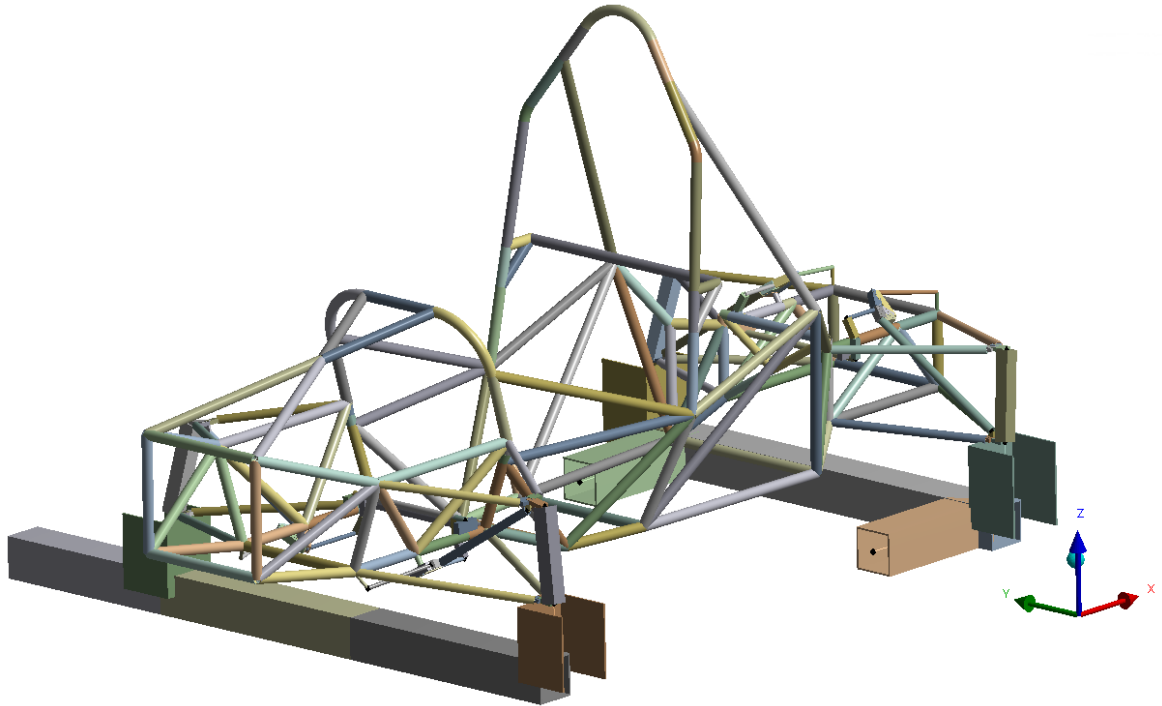


Figure 2.7: Final finite element model for analysis

Now follows description of individual parts in more detail.

- **A-arms with uprights**

Each A-arm is comprised of two carbon-fibre tubes with diameter of 20 mm and wall thickness of 2 mm glued to aluminum bracket on upright's side. The bracket is then connected with an upright by a spherical bearing. At the frame's side, to each carbon-fibre tube is glued an aluminum insert with spherical bearing connecting the whole assembly to the frame (see Fig. 2.8(a)).

Each bracket (made of aluminum AW7075) was simplified as 2 line bodies with rectangular cross-sections of 20x9.5 mm and of 26x9.5 mm respectively. This applies for all 8 A-arms of the vehicle. Front upper and rear lower A-arms, however, have even holder for ARB system. Thus for this A-arms, I have assigned also rectangular cross-section of 14x6 mm.

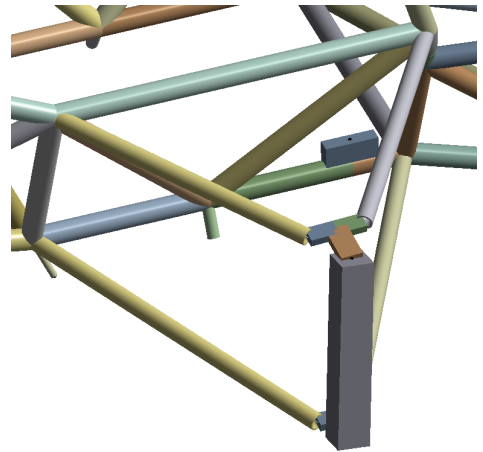
Uprights are made of aluminum AW7022. Because of its complexity in shape, I have decided to simplify them as a line bodies with assigned square cross-section of 38x38 mm for the front ones and of 33x33 mm for the rear ones<sup>1</sup>.

---

<sup>1</sup>I have estimated the dimension of cross-sections for the uprights but during the search for the causes of inaccuracies in the simulation, I have determined the new cross-section dimensions acc. to procedure in Appendix B



(a) Real front A-arms



(b) Simplified model of front A-arms

Figure 2.8: Modeling of front A-arms and uprights

In Fig. 2.9, one can see described simplified A-arms together with an upright.

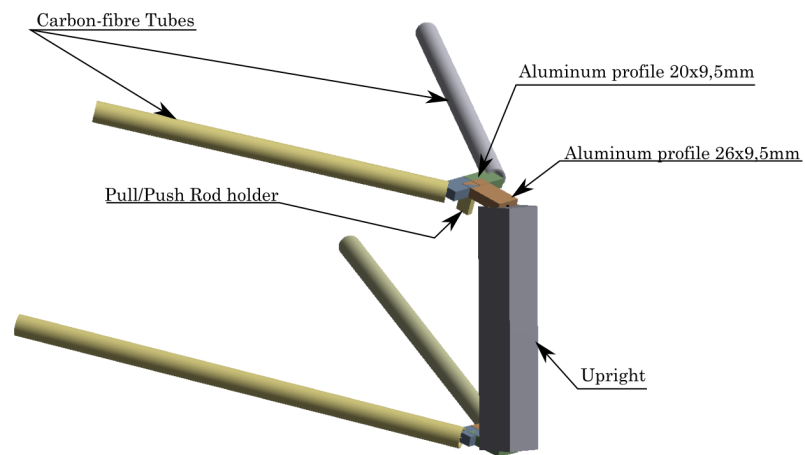


Figure 2.9: Description of individual parts of A-arms together with upright

- Front and rear ARB system

The ARB system, I have also modeled as line bodies with assigned cross-section. Such ARB system, does not matter if front or rear, consists of pull or push rod going from A-arm to the bell-crank. Then, from the bell-crank there goes damper-replacing rod to the frame and ARB link to the lever connecting bell-crank with ARB. Figure 2.10 below shows the situation with cross-sections assigned.

Pull or push rod (it matters if it is loaded in tension or compression) is tube of carbon-

fibre material. It has the same cross-section as A-arm tubes (of 20x2 mm). The bell-crank, I have simplified in way that it satisfy connection of all necessary parts. The bell-crank itself is attached to the frame and preserve its basic shape. Square cross-section of 20x20 mm, I have used for the bell-crank. Then, the Rod is steel tube of 10x2 mm, ARB link is aluminum (AW7075) tube of 10x2.5 mm, ARB lever is of steel with square cross-section of 16x16 mm, ARB is full rod with circular cross-section of 16 mm. ARB holder is of plastic Igumid G with rectangular cross-section of 62x16 mm, bell-crank holder is steel rod with diameter of 14 mm and Holder is steel rod with diameter of 8 mm. Names of individual parts are according to Fig. 2.10.

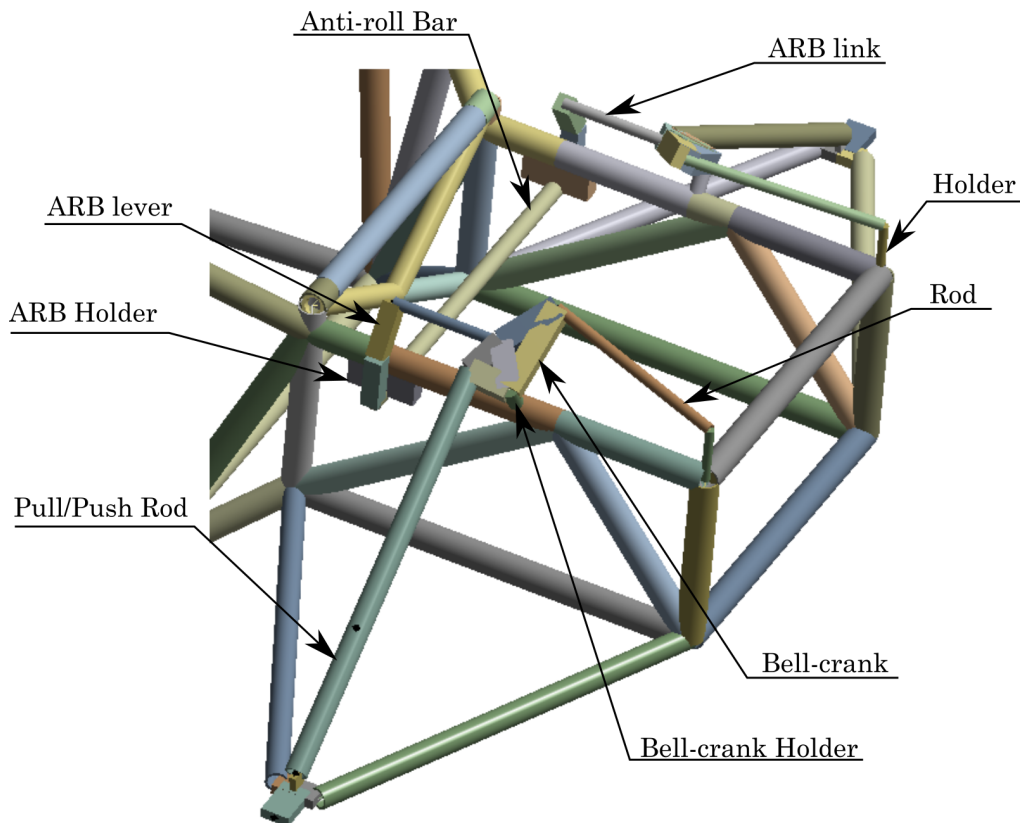


Figure 2.10: Description of individual parts of ARB system

- Beams

Whole frame with A-arms and ARB system is attached to two beams. Rear axle is mounted to the fixed one and front axle is mounted to another one which is allowed to rotate around  $x$  axis (longitudinal axis of the frame).

The beams are of steel and have standard square-tube profile of 100x100 mm with wall thickness of 4 mm. Connection between beams and suspension (or frame) is provided by a connection holder. The model of the connection holder, I have derived and simplified

from the real part (see Fig. 2.11) as a line body with U-profile of steel with cross-section of 136x147 mm with wall thickness of 5 mm (mid-section of the holder). Beams and all its parts, I have also modeled as line bodies with assigned cross-sections. Figure 2.12 below depicts finished model of beams with connection holders (U-profiles).



Figure 2.11: Connection holder

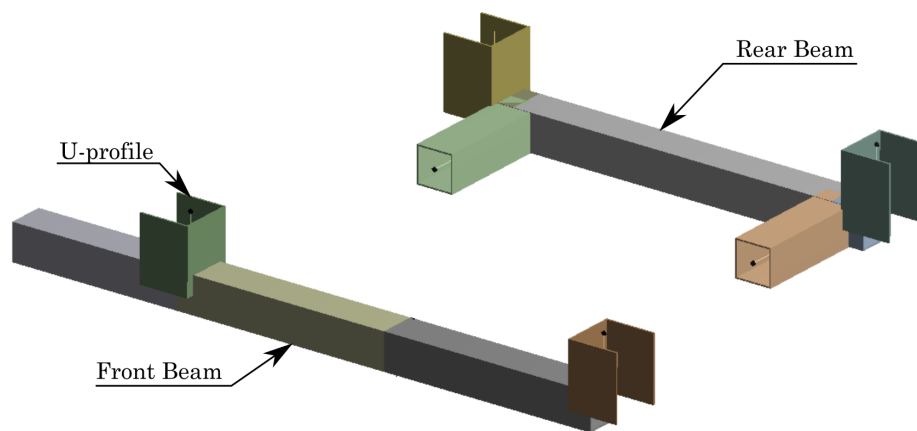


Figure 2.12: Description of beams design

- Connections

After creation of model, I have connected the parts together by either inserting them into *Part* (used for the firmly connected together - welded or bolted, for example the beams are one *Part* with connecting holders because they are welded together) or by using of joints.

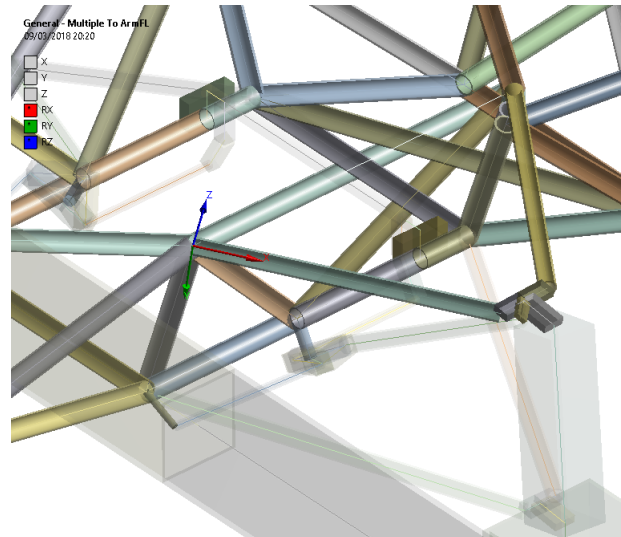
Type of joint, I have applied according to real connection between components. I have used two types of joints:

- General joint

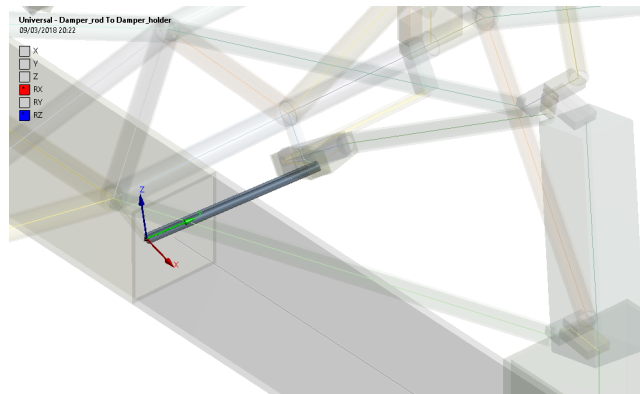
Using this one, I have set one or all rotations free according to my needs. For example, for connection between A-arms and frame structure, I have set all rotations free because it is connected with spherical bearing in reality (see Fig 2.13(a)). I have set rotation free only about one axis, for example, for connection of bell-crank with frame, because it is allowed to rotate only about one axis which is the axis of the peg the bell-crank is mounted on.

- Universal joint

This type of joint, I have applied because it allowed me to set free rotations about two axis. This, I have widely used for connections within ARB system (there are spherical bearings at both ends of the link thus I have needed to fix rotation about link's axis, see Fig. 2.13(b)).



(a) Example of general joint, A-arm to frame



(b) Example of universal joint, ARB link to frame

Figure 2.13: Examples of joints used (grey rectangle means the translation or rotation is fixed, the colourful one means free translation or rotation)

### 2.2.1 Properties of Materials Used

For all components of the simulation model described above, I have used the material properties as in Tab. 2.1.

Material	Young's modulus[MPa]	Poisson's ratio[-]	Density[kg/m <sup>3</sup> ]
Steel (8)	200 000	0.3	7850
Carbon-fibre tube <sup>2</sup>	12 280	0.3	1430
Aluminum AW7022 (10)	72 000	0.34 (8)	2760
Aluminum AW7075 (11)	71 000	0.34 (8)	2800
Plastic Igumid G (9)	8000	0.3	1370

Table 2.1: Mechanical properties for materials used in model



## Chapter 3

# Mesh, Boundary Conditions and Settings of Analysis

### 3.1 Element Type and Mesh Used

#### 3.1.1 Element Type

There are 3 basic element types: beams, shells and solids. From the 3 basic element types, I have chosen beams as the most convenient element type for this simulation model. I have not chosen shells because that would require significantly more time to model all parts and issues with connection of complex frame nodes would probably occur (13). Reasons, why I have not chosen solid elements are quite similar to shell elements. If I would use solid elements, the modeling time would be much higher but main reason is mesh. It is recommended that solid elements should be at least 3 elements per wall thickness. Tubes of the frame have wall thickness about 2 mm. Thus, very tiny elements would be used. Resulting in huge amount of elements which would probably need great computational time for both generating such dense mesh and calculation. The beam elements, in other hand, provided good modeling time and not very high elements amount. Thus, computation has lasted in order of seconds. The most importantly, very close results to reality has been achieved.

I have used the beam elements in Ansys so called BEAM188. Their mathematical background is based on Timoshenko beam theory including shear-deformation effects. The element is linear, quadratic or cubic two-node beam element in 3-D. The element has six or seven DOF at each node (translations in the x, y and z directions and rotations about the x, y and z directions, 7th DOF is warping magnitude which is optional) (12). The BEAM188's geometry is displayed in Fig. 3.1 below.

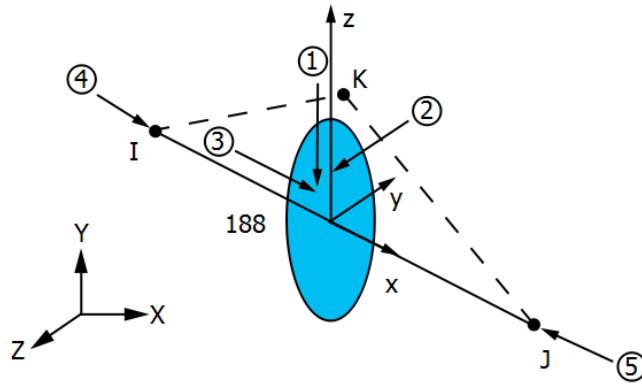
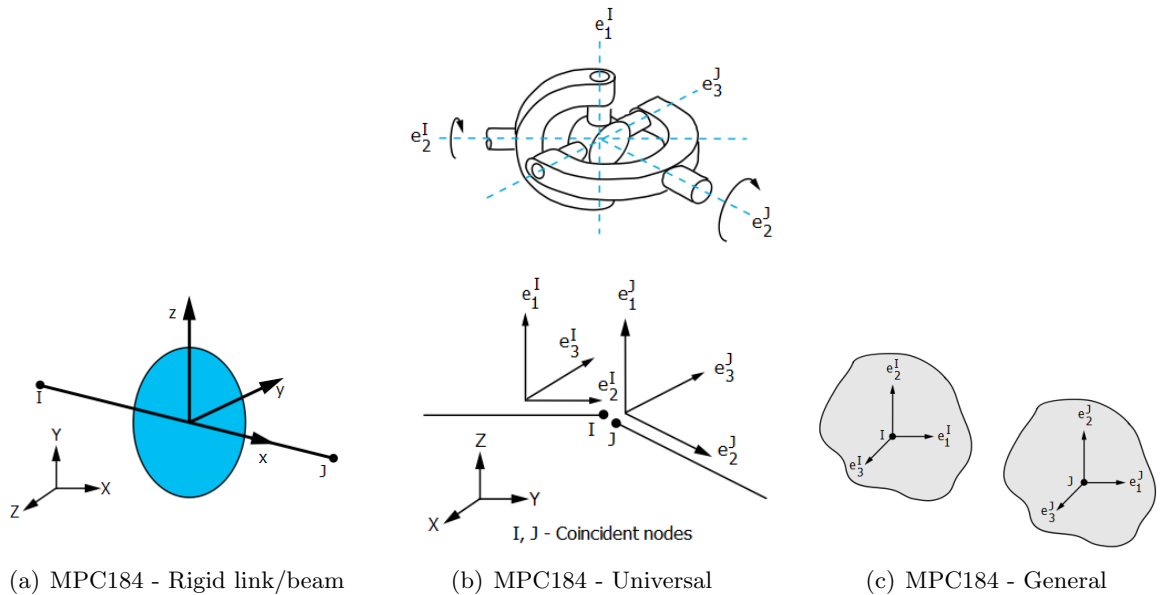


Figure 3.1: Geometry of so called BEAM188 element (12)

Another element type used in this simulation is multipoint constraint element in ANSYS so called MPC184. This element type is used because it provides kinematic constraint between nodes. I have used it for joints between components of simulated system. The MPC184 can be classified as constraint element (rigid link/beam) and joint element (universal, general, revolute, etc.) (14). In this analysis are used MPC184 - Universal and MPC184 - General and MPC184 - Rigid link/beam. In figure 3.2, one can see geometry of MPC184 joints according to ANSYS Help Viewer.



(a) MPC184 - Rigid link/beam

(b) MPC184 - Universal

(c) MPC184 - General

Figure 3.2: Geometry of discussed MPC184 elements (14)

### 3.1.2 Mesh

I have created mesh using automatic mesh generator in ANSYS Mechanical. At first, I have decided to use no sizing method for mesh but the resulting mesh was extremely coarse. Then, I have refined mesh by adding sizing method with the mesh sizing of 20 mm per element (see Fig. 3.3 below). Number of nodes and elements is in Tab. 3.1 below.

Number of nodes	Number of elements
5238	2638

Table 3.1: Number of nodes and elements when using mesh size of 20 mm

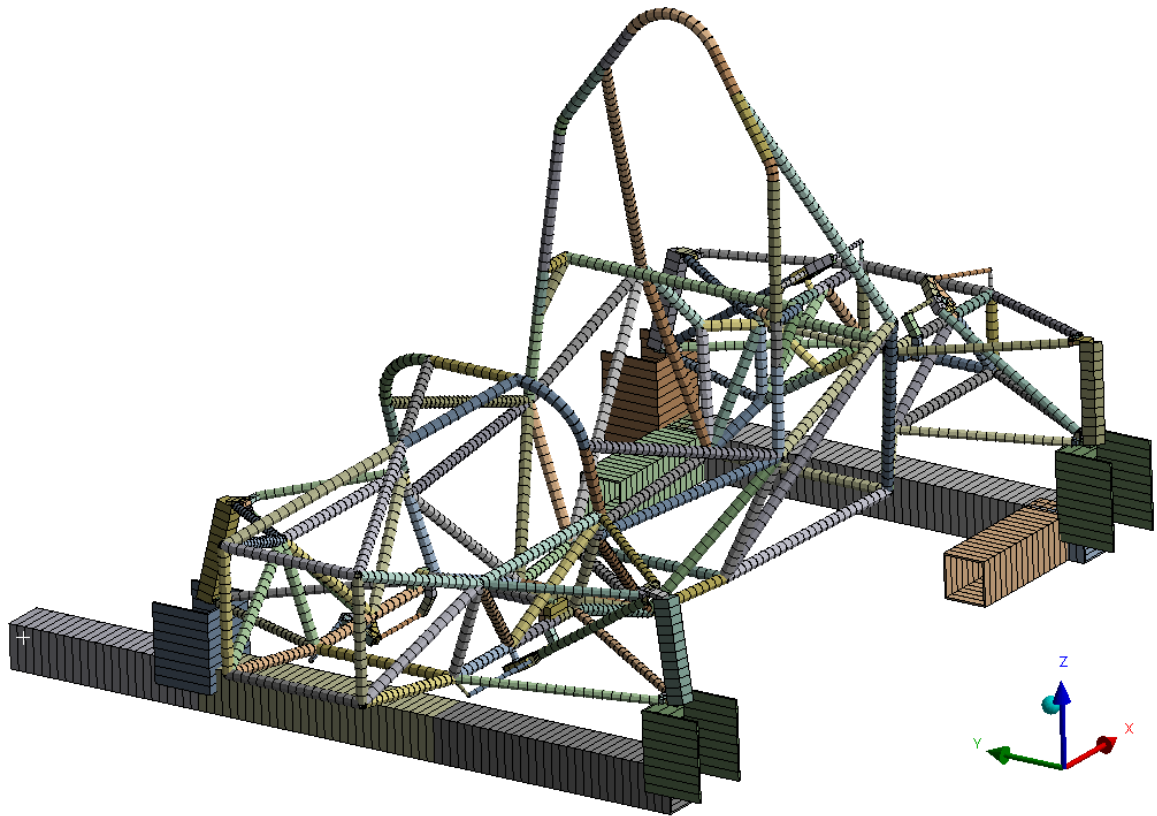


Figure 3.3: Mesh with sizing of 20 mm

Then, to prove mesh quality (or if such mesh sizing is sufficient), I have decided to reduce sizing from 20 mm per element to 10 mm per element. Resulting in higher number of nodes and elements (see Tab. 3.2). The new finer mesh is depicted in Fig. 3.4 below.

Number of nodes	Number of elements
10198	5118

Table 3.2: Number of nodes and elements when using mesh size of 10 mm

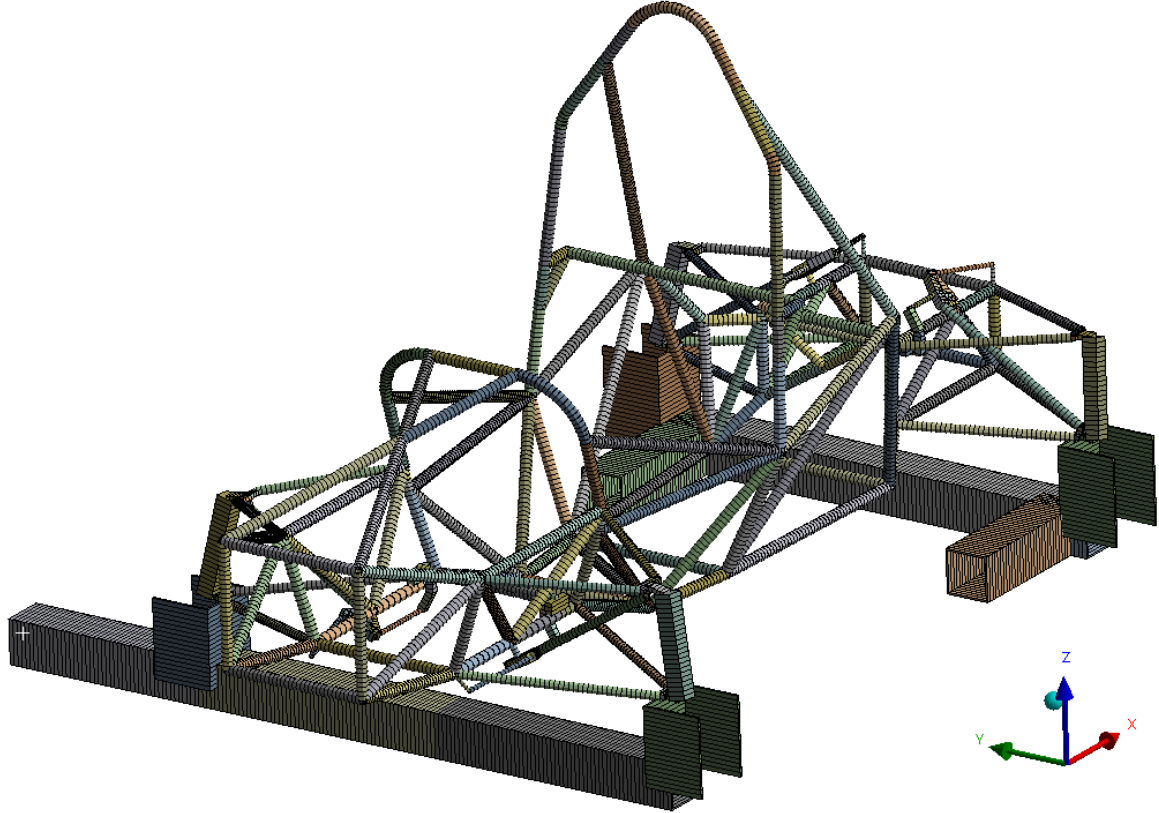


Figure 3.4: Mesh with sizing of 10 mm

Finally, comparison of results is in Tab. 3.3 below.

Mesh sizing [mm]	20	10	Difference [%]	0.25
Torsion stiffness [Nm/deg]	753	754.9		

Table 3.3: Table of comparison of results for different mesh sizing

From the comparison in the Tab. 3.3 above, one can see that the results are almost the same<sup>1</sup>. Difference is 0.25 percent. Thus, I have decided to use mesh with sizing of 20 mm for all simulations because it is sufficient.

<sup>1</sup>The results are evaluated according to procedure discussed in Chapter 4 and the evaluation table, one can follow to Appendix E.

## 3.2 Boundary Conditions

The boundary conditions discussed below are based on the real testing procedure and the setting of the testing fixture (see Chapter 4).

Figure 3.5 shows the boundary conditions of the whole model as set for the simulation.

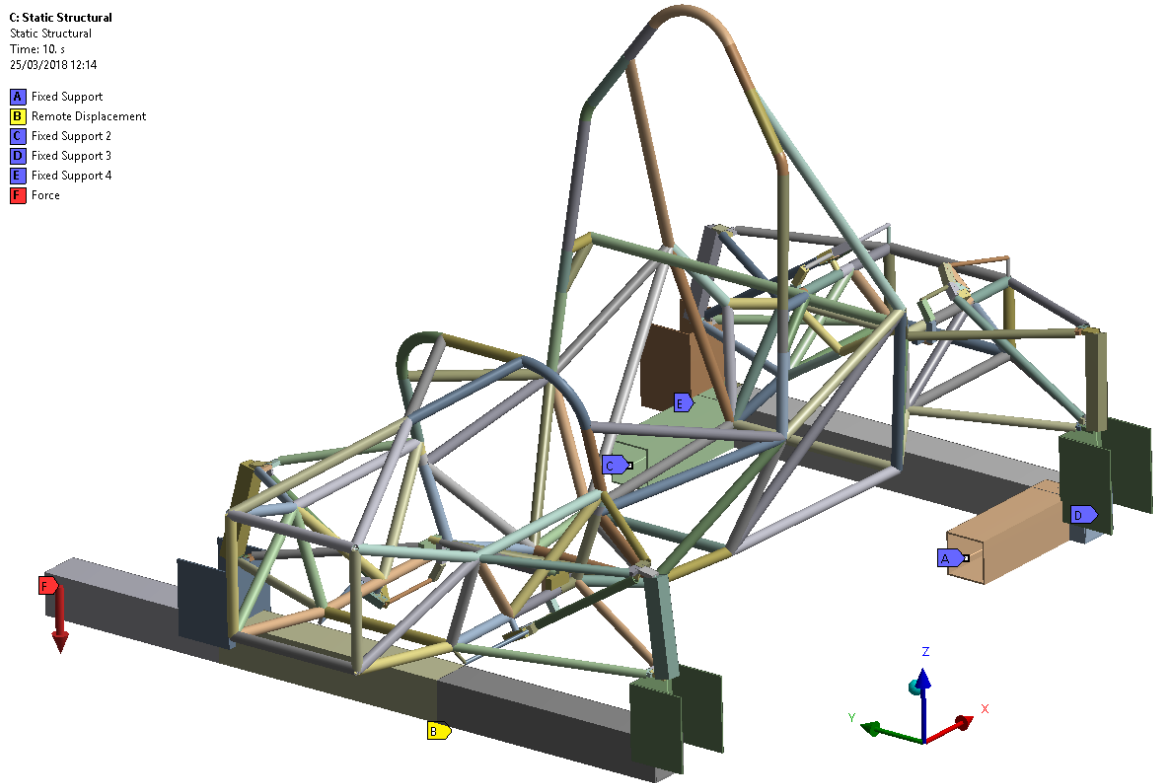


Figure 3.5: Overview of boundary conditions of the model

### 3.2.1 Force

The desired loading (torsion), I have achieved by application of force at the one end of the revolving beam. The force's magnitude, number of steps and even point of application were the same as during the real testing. In the Tab. 3.4 below, one can see magnitude of the applied force during all load steps. Progress of adding of force is depicted in the Fig. 3.6 (sign "minus" is only because of orientation of coordinate system in Ansys and has no influence on the simulation).

Step	1	2	3	4	5	6	7	8	9	10
Force [N]	49.1	144.2	195.2	246.2	295.3	343.4	392.4	441.5	496.4	551.3

Table 3.4: Table of loading steps

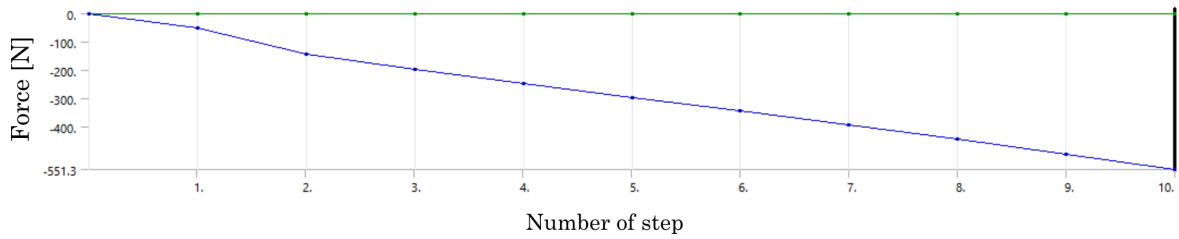


Figure 3.6: Progress of the force within all steps

### 3.2.2 Constraints

As discussed above, the rear beam is fixed thus I have applied so called Fixed constraint at all points (four) where attached (welded) to the table (see Fig. 3.5). The situation, in more detail, is depicted in Fig. 3.7 below.

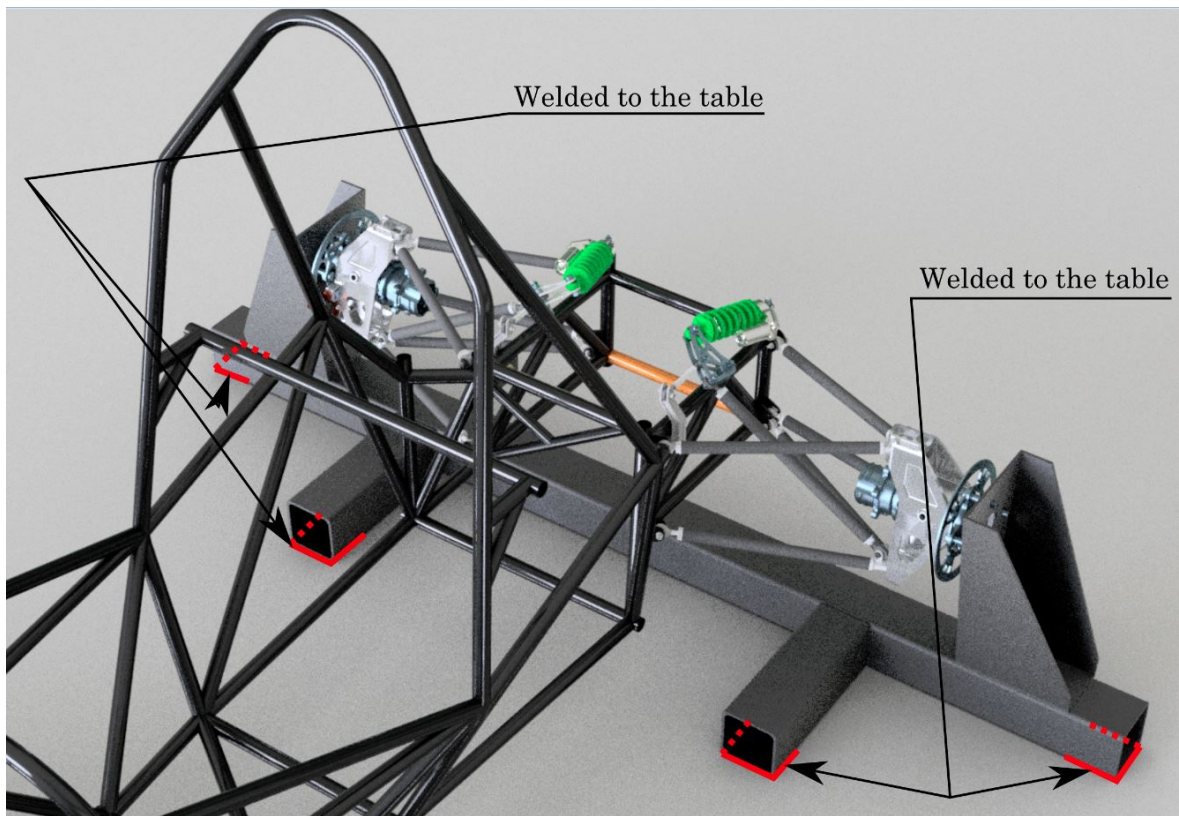


Figure 3.7: Detail of rear beam situation

Then, the front beam is able to rotate around longitudinal axis of the frame, the situation is depicted in Fig. 3.8 below.

In the simulation, I have set so called "Remote displacement" constraint (see Fig. 3.5). This constraint has connected the middle part of the front beam with point of rotation (the point where the front beam touches the table) by a rigid link. Then, I have set the Remote displacement as free to rotate about x axis (the frame's longitudinal one).

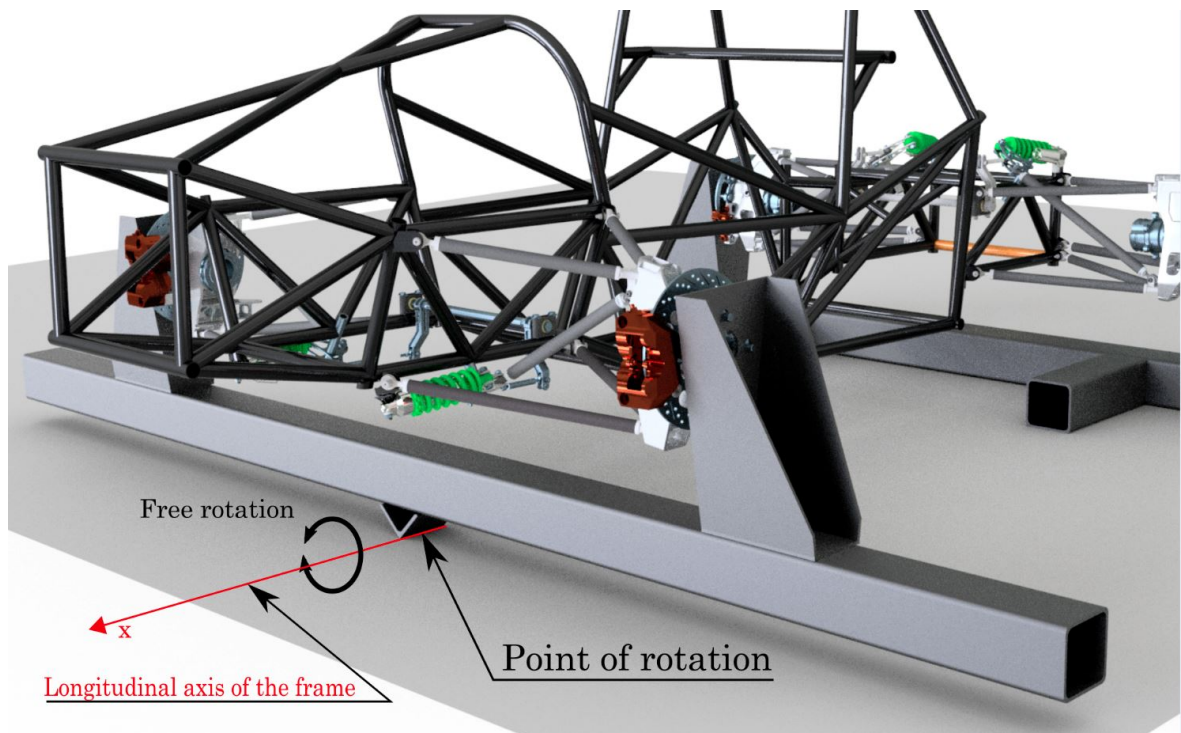


Figure 3.8: Detail of front beam situation

### 3.3 Settings of Simulation

I have carried out the simulation by several ways. I have simulated it as a linear model at first. After that, I have simulated it as a non-linear model with enabled so called "Large deflections" because translations from linear simulation were quite large (maximum about 15 mm).

To see the influence of ARB system on torsion stiffness of the frame, I have performed both linear and non-linear simulation even for the model without ARB system.

Results, comparisons and conclusions, one can follow in Chapter 4 and Chapter 6, respectively.

### 3.4 Modal Analysis of Finite Element Model

Since I have imported the wire-frame model of the frame and added other components and connected them together with joints, I have needed to prove that all parts are connected together properly. This, I have easily carried out by a modal analysis in Ansys Workbench 18.2. For setting up analysis, I have decided to apply no boundary conditions. It means no loading and even no constrains. The mesh sizing, I have set of 20 mm per element. Thus, if all bodies are connected together properly then only the first six natural frequencies of the system are zero. It means that the system is free to move in  $x$ ,  $y$  and  $z$  direction and rotate about those three axes (16).

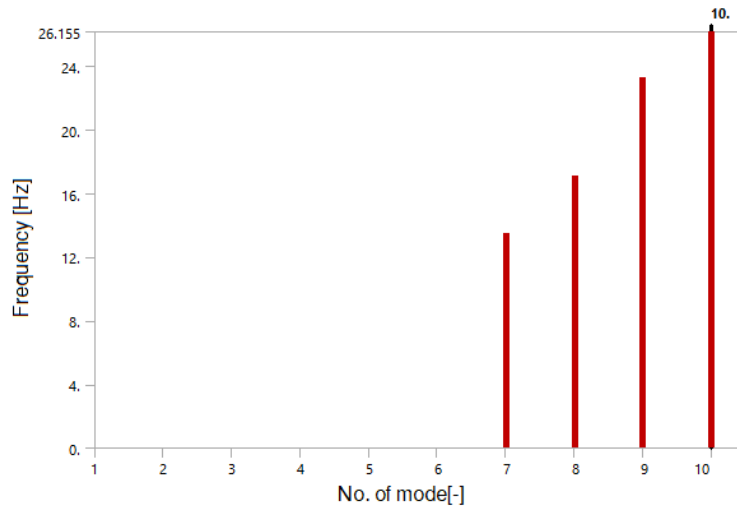


Figure 3.9: Result of natural frequencies in graphical layout

Results show that all line bodies are connected together because first six natural frequencies are zero and other frequencies are not zero (see Fig. 3.9). The exact values of first ten natural frequencies are in the Tab. 3.5 below. Figure 3.10 displays the 7th deformation shape within the 7th natural frequency.

Mode	Frequency [Hz]
1	0
2	0
3	0
4	0
5	0
6	0
7	13.517
8	17.112
9	23.269
10	25.155

Table 3.5: Table of frequencies in first ten modes



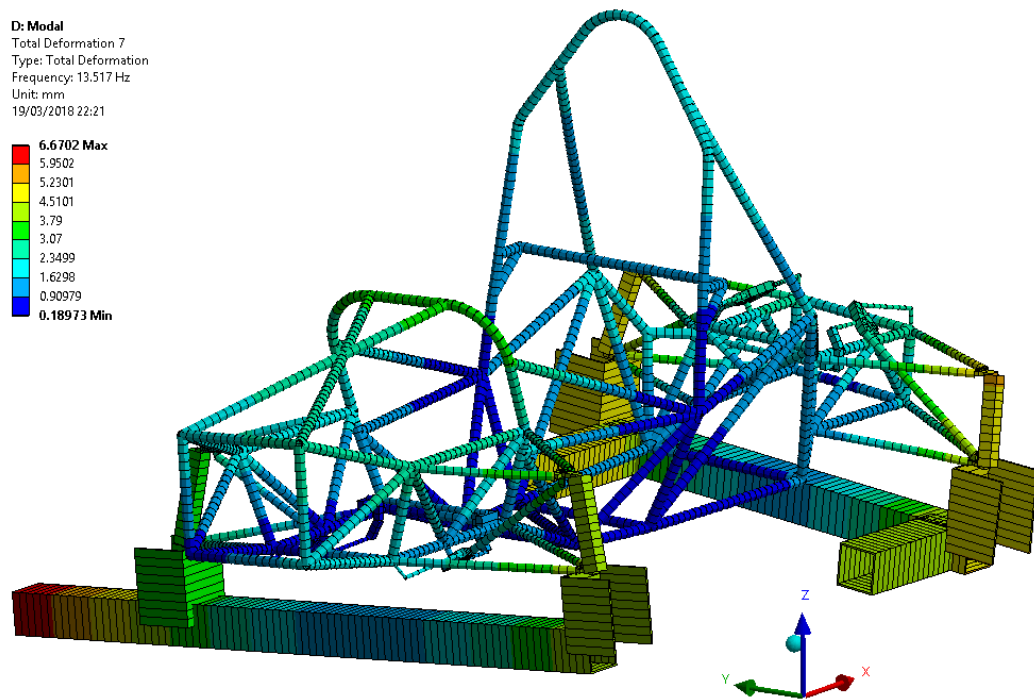


Figure 3.10: Deformation shape of 7th natural frequency of the system.

## Chapter 4

# Evaluation of the Frame Stiffness

### 4.1 Description of Testing and Simulation Procedure

There are several options how to measure or evaluate torsion stiffness of the frame of vehicle. For example, one can fix one axle into a rigid beam and then apply torque on the other axle while measuring displacement (see Fig. 4.1(b)). Another procedure is to fix three wheels in certain manner and translate upwards the fourth wheel resulting in torsional loading (similar to this Fig. 4.1(a)). Some procedures are described more in detail here (7).

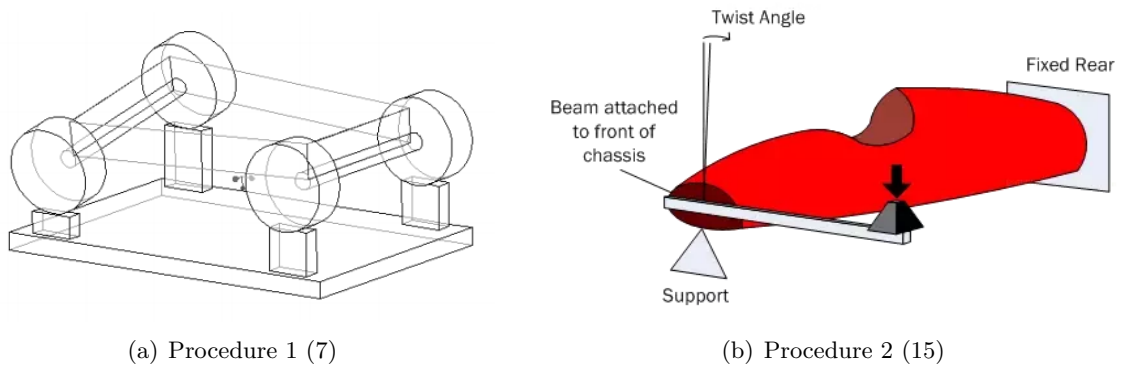


Figure 4.1: Possible testing procedures

Each procedure has its benefits and drawbacks of course. I have decided to use procedure with two beams generally displayed in Fig. 4.1(b). The idea is that one axle is fixed to a rigid beam and second axle is attached to another beam which is allowed to rotate about longitudinal axis of the frame. On one side of revolving beam, there is applied loading resulting into torque. Thus, the frame twists and displacement of the frame is measured. From the displacement, the torsional stiffness is determined as ratio between applied torque and deformation angle. The model of the testing situation can look like in the Fig. 4.2. Advantage of this procedure is its easy feasibility, drawback could be that the frame is loaded in quite artificial manner (the frame would not be loaded as once the vehicle racing around the track) (7). This type of procedure is the favorite one of many Formula SAE<sup>®</sup> (and Formula Student) teams.

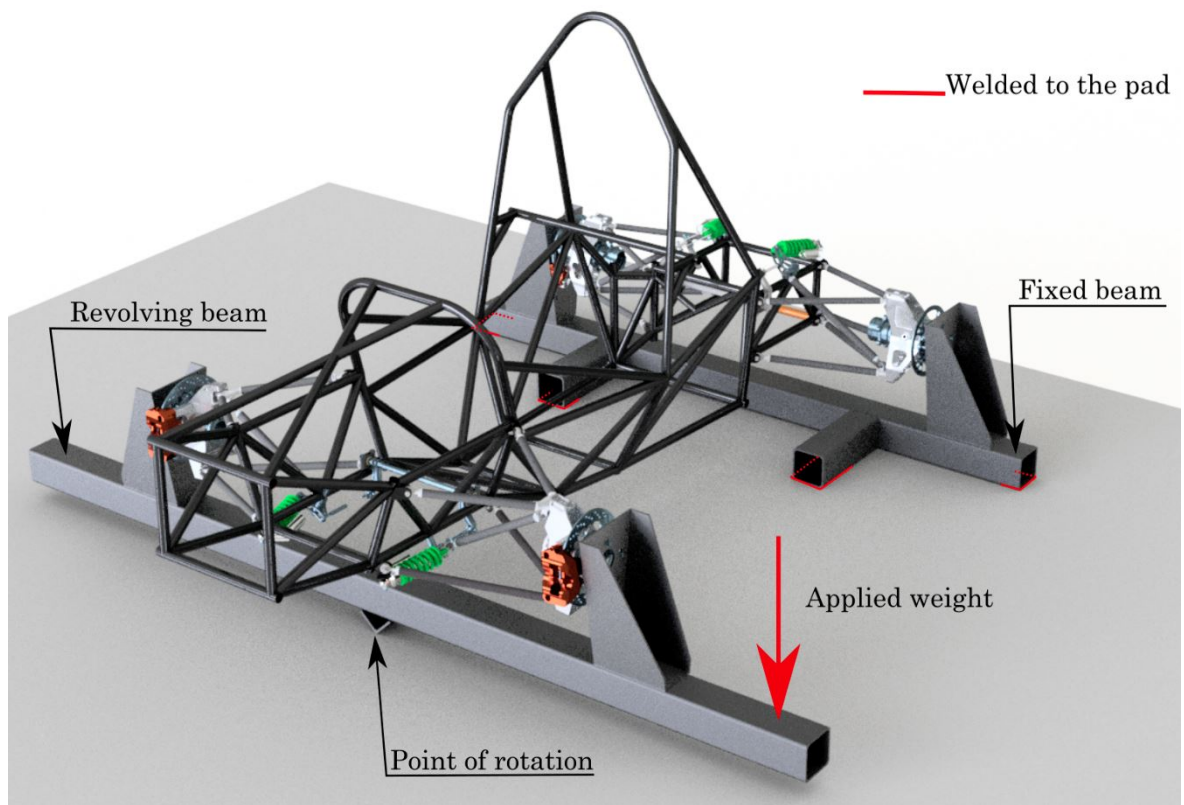


Figure 4.2: Testing model with frame and complete suspension

The torsion stiffness determination is then derived from Fig. 4.3.

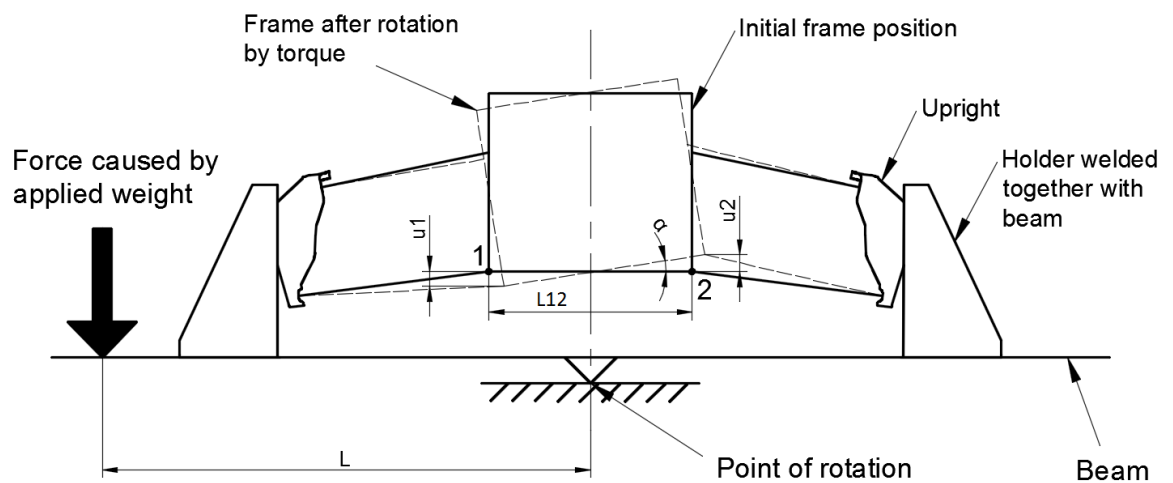


Figure 4.3: Simplified situation at revolving beam in front view

During applying of weight the revolving beam move in some angle so the vertical displacement  $u_1$  and  $u_2$  is measured (horizontal displacement is neglected in this case because of its very small influence on the change of dimension  $L_{12}$  which would be affected by rotation).

From deformation triangle in Fig. 4.4, the angle  $\alpha$  is determined as follows:

$$\alpha = \arctan \left( \frac{u_1 + u_2}{L_{12}} \right) [deg] \quad (4.1)$$

where  $L_{12}$  is pitch of points 1 and 2.

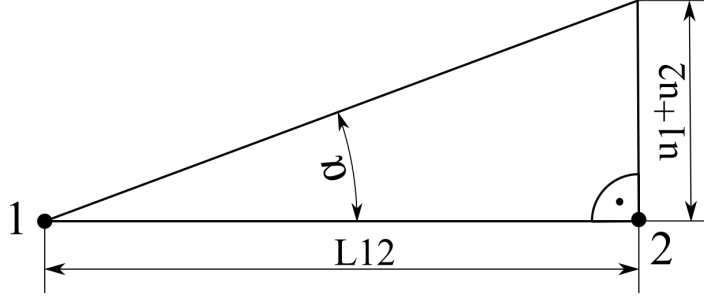


Figure 4.4: Deformation triangle

The torsion stiffness  $C_T$  (Eq. 4.2) is determined as ratio between applied torque  $T$  (Eq. 4.3) and angle of deformation  $\alpha$  (Eq. 4.1).

$$C_T = \frac{T}{\alpha} [Nm/deg] \quad (4.2)$$

$$T = F \cdot L [Nm] \quad (4.3)$$

where  $F$  is force caused by applied mass (4.4) and  $L$  is length from point of the force to the point of rotation (see Fig. 4.3).

$$F = m \cdot g [N] \quad (4.4)$$

where  $m$  is weight of applied mass and  $g$  is gravity acceleration which equals to  $9.81m/s^2$ .

Evaluating of torsion stiffness for both simulation and experimental part is according to above mentioned formulas and procedure. For the evaluation, I have utilized the software Microsoft Excel.

## 4.2 Experimental Part

Simulation is substitution of reality with simulation (or mathematical) model with several simplifications. The simplifications can be more or less significant in order to have as similar results to reality as possible. Sometimes, it is not easy to determine the influence of individual simplifications on simulation results. That is why each simulation is, at least initially once it is not tuned up yet, recommended to be supported by analytic calculation or experiment.

### 4.2.1 Testing Environment

As I mentioned above, I have chosen the testing procedure with two beams, one fixed and second one allowed to rotate. Both beams are composed of square steel profiles of cross-sectional dimensions of 100x100x4 mm. I have set the length to be sufficient for attachment of the frame and application of mass.

Real testing I have carried out, is according to testing model in the Fig. 4.2. The only change is that dampers with springs were replaced with steel rods (see Fig. 4.5) to ensure locked and rigid suspension (in other case, the torsion stiffness of the frame would be affected by stiffness of the springs and the results would be distorted).



Figure 4.5: Rod replacing dampers

The final testing environment is displayed in Fig. 4.6 where the Vector 04 vehicle frame is attached to two beams. For the experiment, I have used the frame with suspension with ARB system. The displacement at six points is measured (see Fig. 4.7) with dial indicators while mass is applied on the front beam resulting into torque loading of the frame.

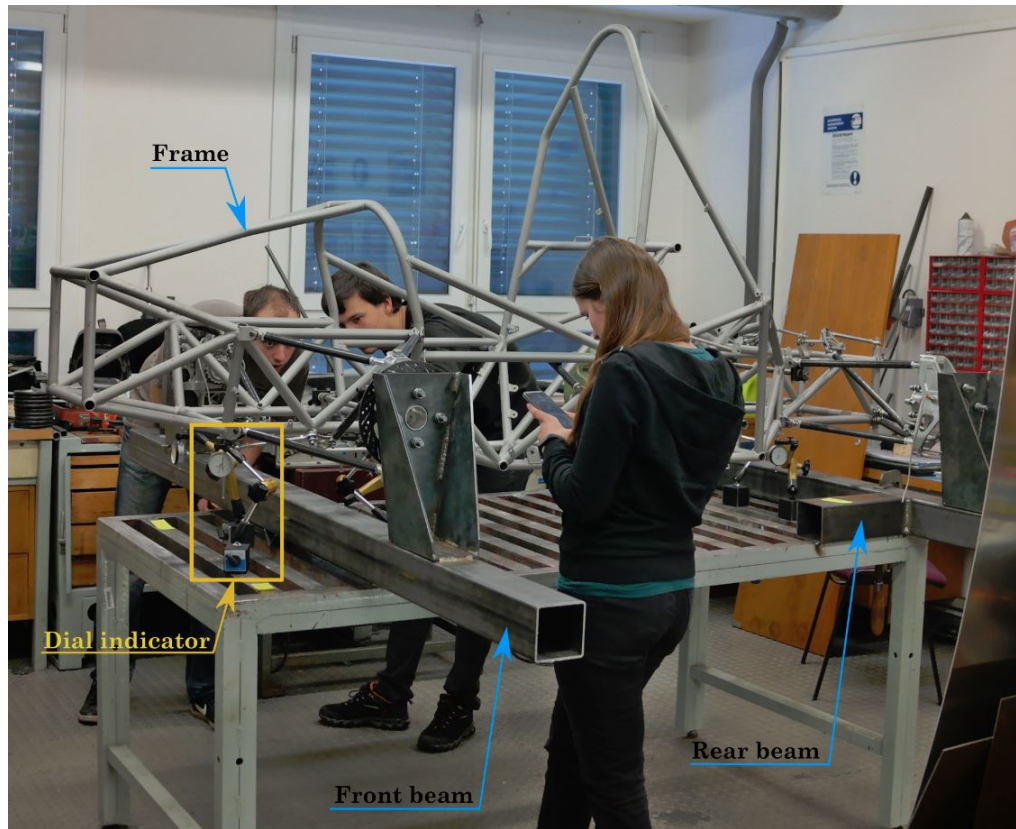


Figure 4.6: Experimental setup

#### 4.2.2 Measuring Procedure

The measurement, I have carried out three times. I have measured displacement at the six points of the frame (see Fig. 4.7) during step adding of mass and even during step releasing of mass. Within each step (there was 10 steps), I have added (or released) certain mass. Maximal applied mass was of 56.2 kg.

Step	1	2	3	4	5	6	7	8	9	10
Mass [kg]	5	9.7	5.2	5.2	5	4.9	5	5	5.6	5.6

Table 4.1: Table of individual added or released masses within all steps

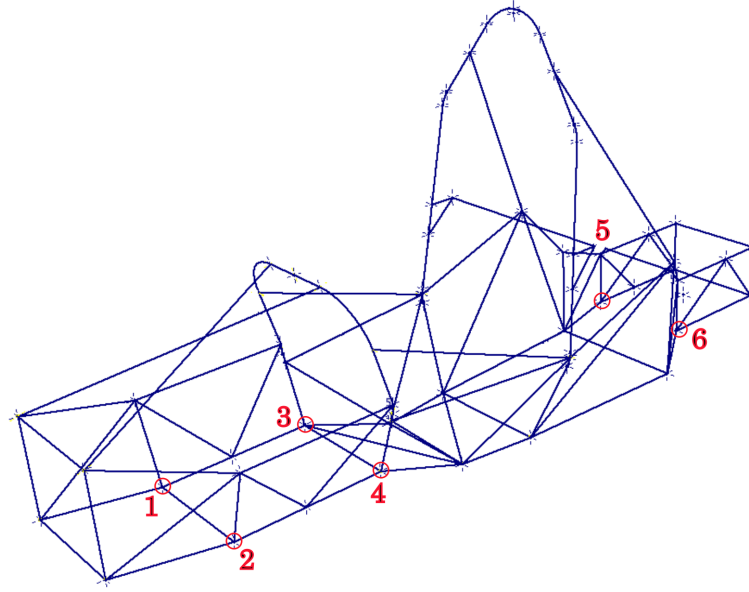


Figure 4.7: Six measured points of the frame

### 4.2.3 Evaluation of the Torsion Stiffness from Experiment

#### Overall Torsion Stiffness of the Frame

Overall (axle-to-axle) torsion stiffness, I have determined from displacement at points 1 and 2 (see Fig. 4.7). Averaged values of displacements from all three measurements with respect to applied mass at point 1 and 2 are displayed in Fig. 4.8<sup>1</sup>. There is visible that during releasing of mass the displacement is the same besides couple steps where are minor fluctuations. The graphs have also proven that response of the frame on loading is rather linear and all deformations are elastic. No residual deformations have remained after the mass is completely released.

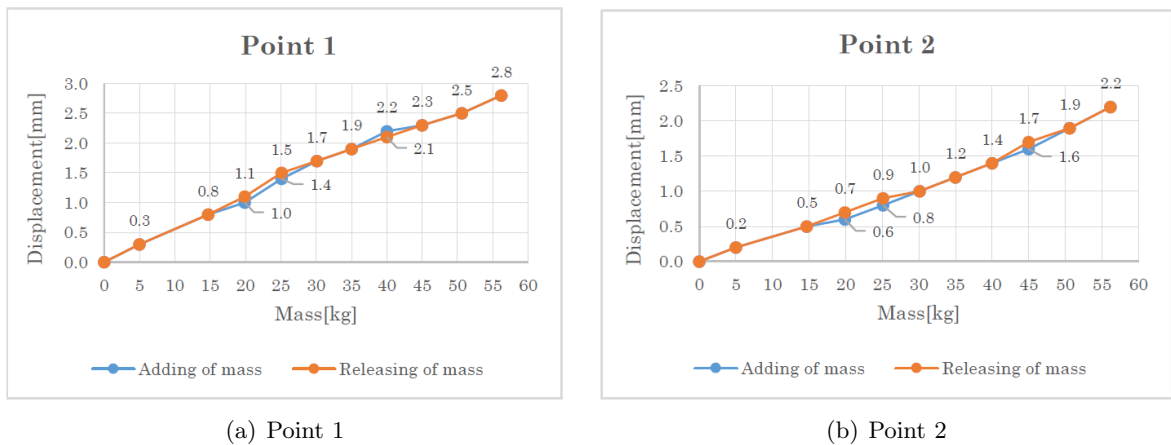


Figure 4.8: Averaged values of displacement at point 1 and point 2 with respect to loading

<sup>1</sup>The graphs for other points (i.e. 3, 4, 5, 6) one can find in the Appendix D.

In the Fig. 4.9, one can see example of results from the first measurement while adding of mass<sup>2</sup>. Gathered data are the green cells where is displacement of individual point in millimeters within each load step.

			First measurement - ADDING MASS					
			POINT					
STEP	MASS[KG]	FORCE[N]	1	2	3	4	5	6
0	0.0	0.0	0.0	0.0	0.0	0.0	0.0	0.0
1	5.0	49.1	0.3	0.2	0.2	0.2	0.1	0.1
2	14.7	144.2	0.8	0.5	0.7	0.4	0.3	0.2
3	19.9	195.2	1.0	0.7	0.9	0.6	0.4	0.3
4	25.1	246.2	1.4	0.9	1.1	0.8	0.4	0.5
5	30.1	295.3	1.7	1.0	1.4	1.0	0.4	0.7
6	35.0	343.4	1.9	1.2	1.6	1.2	0.5	0.8
7	40.0	392.4	2.2	1.4	1.8	1.4	0.5	0.9
8	45.0	441.5	2.4	1.6	2.0	1.5	0.6	1.0
9	50.6	496.4	2.5	2.0	2.1	1.9	0.6	1.1
10	56.2	551.3	2.8	2.2	2.3	2.1	0.7	1.2

Figure 4.9: Displacements of individual points from first measurement - adding mass

Now follows description of evaluation of torsional stiffness of the frame from the experiment.

First measurement - adding mass							
Point							
STEP	MASS[KG]	FORCE[N]	Torque[Nm]	u1[mm]	u2[mm]	Alpha12[deg]	C[Nm/deg]
0	0.0	0.0	0	0.0	0.0	0	N/A
1	5.0	49.1	51.50	0.3	0.2	0.08425844	611.24
2	14.7	144.2	151.42	0.8	0.5	0.21907103	691.18
3	19.9	195.2	204.98	1.0	0.7	0.28647651	715.52
4	25.1	246.2	258.54	1.4	0.9	0.38758318	667.06
5	30.1	295.3	310.05	1.7	1.0	0.45498633	681.44
6	35.0	343.4	360.52	1.9	1.2	0.52238822	690.13
7	40.0	392.4	412.02	2.2	1.4	0.60663853	679.19
8	45.0	441.5	463.52	2.4	1.6	0.67403690	687.68
9	50.6	496.4	521.21	2.5	2.0	0.75828222	687.35
10	56.2	551.3	578.89	2.8	2.2	0.84252426	687.09

L[mm]	L12[mm]
1050	340

Figure 4.10: Example of evaluation table

In the Fig. 4.10, one can see table for evaluation of the overall torsion stiffness (in this case, for the first measurement - adding mass). Each measurement include twenty loading steps (ten for adding of mass and ten for releasing of mass). During each step, certain mass is applied or released (in yellow box, there is total mass of individual load step) resulting into twenty pairs of displacement in vertical direction per measurement (red box). The displacement is, then, used for calculation of torsion stiffness for each load step (blue box).

<sup>2</sup>Gathered data from all measurements, one can reach in Appendix D.



Now follows an example of calculation of the third line of the table.

- Firstly, the applied mass  $m$  is recalculated to force  $F$ :

$$F = m \cdot g = 19.9 \cdot 9.81 = 195.2N \quad (4.5)$$

where  $g$  is gravity acceleration ( $9.81 \text{ m/s}^2$ ).

- Then, torque is evaluated from the force:

$$T = F \cdot L = 195.2 \cdot 1.05 = 204.98Nm \quad (4.6)$$

where  $T$  is torque and  $L$  is length from point of the force to point of rotation.

- Deformation angle  $\alpha_{12}$  is determined as:

$$\alpha_{12} = \arctan\left(\frac{u_1 + u_2}{L_{12}}\right) = \arctan\left(\frac{1 + 0.7}{340}\right) = 0.286deg \quad (4.7)$$

where  $u_1$  and  $u_2$  are displacements of points 1 and 2, respectively and  $L_{12}$  is length between the points.

- Finally, the torsion stiffness for the third load step  $C_{T3}$  is calculated as:

$$C_{T3} = \frac{T}{\alpha_{12}} = \frac{204.98}{0.286} = 715.52Nm/deg. \quad (4.8)$$

According to procedure above, all further lines of the table and all further measurements, I have evaluated.

Since I have obtained 60 values of torsion stiffness from all measurements eventually, I have calculated an arithmetic mean from them using the formula (4.9):

$$\bar{x} = \frac{1}{n} \cdot \sum_{i=1}^n x_i \quad (4.9)$$

where  $x_i$  is the individual value of stiffness from individual load step<sup>3</sup> and  $n$  means total number of values  $x_i$ , in this case  $n = 60$ .

I have thus obtained result of overall torsion stiffness from experiment:

$$\mathbf{C_{Texp}=679,4 \text{ Nm/deg}}$$

---

<sup>3</sup>All values, one can find in Appendix D.

## Sectional Stiffness of the Frame

In previous section, I have determined overall torsion stiffness of the frame from experiment. Each frame is as stiff as its the weakest part. One can imagine 3 springs connected in series (see Fig. 4.11(a)) where two of them are very stiff and the middle one is significantly more compliant. Then during loading, the overall stiffness of this system is highly influenced by the middle weak spring and the other two other springs can be as stiff as possible. The similar situation is for torsion stiffness of the frame. One can imagine torsion bars connected in series (see Fig. 4.11(b)) instead of springs. Behavior of such system is the same as mentioned above.

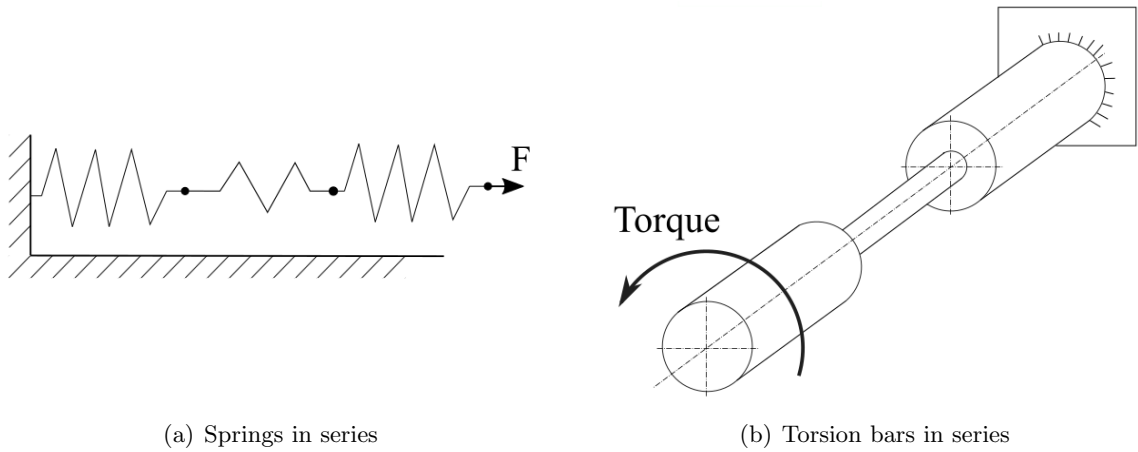


Figure 4.11: Imagination of set of springs and torsion bars in series

Thus, not only overall torsion stiffness but even sectional torsion stiffness is significant in order to evaluate the frame quality or in order to design the frame properly. In this case the sectional (or relative) stiffness, I have determined from averaged displacements (average from all measurements for individual load steps) at all 6 measured points according to procedure described below:

- Firstly, I have divided the frame into 4 sections (see Fig. 4.14), with respect to measured points at which I have determined relative torsion stiffness to evaluate the influence of each section on overall stiffness.
- Secondly, I have determined angle of deformation  $\alpha$  according to formulas (4.10), (4.11) and (4.12) for all three pairs of points (i.e. 1,2; 3,4; 5,6) for all 10 steps respectively:

$$\alpha_{12} = \arctg \left( \frac{u_1 + u_2}{L_{12}} \right) [deg] \quad (4.10)$$

$$\alpha_{34} = \arctg \left( \frac{u_3 + u_4}{L_{34}} \right) [deg] \quad (4.11)$$

$$\alpha_{56} = \arctg \left( \frac{u_5 + u_6}{L_{56}} \right) [deg] \quad (4.12)$$

where  $u_1$  to  $u_6$  are averaged displacement at each point within all 10 loading steps and  $L_{12} = 340mm$ ,  $L_{34} = 340mm$ ,  $L_{56} = 320mm$  are distances between each pair of points.

Below in the Fig. 4.12, one can see all averaged displacement together with results of deformation angle  $\alpha$  for all three spots within the frame. The table follows an example of calculation of deformation angle for the seventh line of the table.

Averaged translations [mm]							Deformation angle Alpha [deg]		
Step	u1	u2	u3	u4	u5	u6	Alpha12	Alpha34	Alpha56
0	0.0	0.0	0.0	0.0	0.0	0.0	0	0	0
1	0.3	0.2	0.3	0.1	0.1	0.0	0.0843	0.0688	0.0281
2	0.8	0.5	0.7	0.4	0.3	0.2	0.2191	0.1918	0.0886
3	1.1	0.7	0.9	0.6	0.4	0.3	0.2921	0.2570	0.1173
4	1.5	0.9	1.2	0.8	0.3	0.6	0.3904	0.3404	0.1623
5	1.7	1.0	1.4	1.0	0.4	0.7	0.4578	0.4101	0.1946
6	1.9	1.2	1.6	1.2	0.4	0.8	0.5252	0.4693	0.2220
7	2.2	1.4	1.8	1.4	0.5	0.9	0.5982	0.5364	0.2507
8	2.3	1.7	1.9	1.6	0.5	1.0	0.6740	0.5979	0.2757
9	2.5	1.9	2.1	1.8	0.6	1.1	0.7470	0.6634	0.3047
10	2.8	2.2	2.3	2.1	0.7	1.2	0.8425	0.7336	0.3330

L12[mm]	L34[mm]	L56[mm]
340	340	320

Figure 4.12: Results of deformation angle  $\alpha$  for all three sites within the frame

Deformation angle for spot between points 1 and 2:

$$\alpha_{12} = \arctg\left(\frac{u_1 + u_2}{L_{12}}\right) = \arctg\left(\frac{2.2 + 1.4}{340}\right) = 0.5982deg. \quad (4.13)$$

Deformation angle for spot between points 3 and 4:

$$\alpha_{34} = \arctg\left(\frac{u_3 + u_4}{L_{34}}\right) = \arctg\left(\frac{1.8 + 1.4}{340}\right) = 0.5364deg. \quad (4.14)$$

Deformation angle for spot between points 5 and 6:

$$\alpha_{56} = \arctg\left(\frac{u_5 + u_6}{L_{56}}\right) = \arctg\left(\frac{0.5 + 0.9}{320}\right) = 0.2507deg. \quad (4.15)$$

- Then, I have calculated the sectional deformation angle<sup>4</sup>  $\alpha_B$  and  $\alpha_C$  (index B means that the angle is for section B and index C means that the angle is for section C):

$$\alpha_B = \alpha_{12} - \alpha_{34}[deg] \quad (4.16)$$

$$\alpha_C = \alpha_{34} - \alpha_{56}[deg] \quad (4.17)$$

Example of calculation of  $\alpha_B$  and  $\alpha_C$  for seventh line of table in Fig. 4.13.

$$\alpha_{B7} = \alpha_{12} - \alpha_{34} = 0.5982 - 0.5364 = 0.0618deg \quad (4.18)$$

$$\alpha_{C7} = \alpha_{34} - \alpha_{56} = 0.5364 - 0.2507 = 0.2858deg \quad (4.19)$$

- The torsion stiffness for section B and C is determined:

$$C_B = \frac{T}{\alpha_B}[Nm/deg] \quad (4.20)$$

and

$$C_C = \frac{T}{\alpha_C}[Nm/deg]. \quad (4.21)$$

where torque is calculated according to (4.4) and (4.3) respectively.

The example of calculation of  $C_B$  and  $C_C$  for the seventh line of table in Fig. 4.13.

Firstly, the torque for the seventh load step  $T_7$ :

$$T_7 = m_7 \cdot g \cdot L = 40 \cdot 9.81 \cdot 1.05 = 412.02Nm \quad (4.22)$$

where  $m_7$  is applied mass within seventh load step,  $g$  is gravity acceleration considered as  $9.81 \text{ m/s}^2$  and  $L$  is length from point of force to point of rotation.

Torsion stiffness of section B  $C_{B7}$  from seventh line of the table:

$$C_{B7} = \frac{T_7}{\alpha_{B7}} = \frac{412.02}{0.0618} = 6668.77Nm/deg. \quad (4.23)$$

And torsion stiffness of section C  $C_{C7}$  from seventh line of the table:

$$C_{C7} = \frac{T_7}{\alpha_{C7}} = \frac{412.02}{0.2858} = 1441.83Nm/deg. \quad (4.24)$$

- Final torsion stiffness of section B and section C is determined as an average value of individual line's values (green and blue box in the table in Fig. 4.13) according to general formula (4.9).

Step	Section B		Section C	
	Aplha B [deg]	C <sub>B</sub> [Nm/deg]	Aplha C [deg]	C <sub>C</sub> [Nm/deg]
0	0	0	0	0
1	0.0154	3334.06	0.0408	1263.55
2	0.0272	5557.98	0.1032	1467.24
3	0.0351	5838.74	0.1397	1467.19
4	0.0500	5171.75	0.1781	1451.97
5	0.0477	6493.94	0.2155	1438.83
6	0.0559	6450.80	0.2473	1457.88
7	0.0618	6668.77	0.2858	1441.83
8	0.0761	6090.64	0.3222	1438.62
9	0.0837	6228.25	0.3587	1453.10
10	0.1090	5313.16	0.4005	1445.26
	Average C <sub>B</sub> [Nm/deg]	5714.81	Average C <sub>C</sub> [Nm/deg]	1432.55

Figure 4.13: Results deformation angles  $\alpha$  and sectional torsion stiffness of section B and C

From the procedure above, I have obtained averaged value of torsion stiffness for section B as:

$$C_B = 5714.81 Nm/deg$$

and for section C as:

$$C_C = 1432,55 Nm/deg.$$

Because each section has different length, it is necessary to calculate its torsion stiffness on unit of length for comparison. Thus, torsion stiffness on unit of length is calculated as sectional torsion stiffness times length of the section:

$$C_l = C \cdot l [Nm^2/deg] \quad (4.25)$$

where  $C_l$  is torsion stiffness on unit of length,  $C$  is overall torsion stiffness of individual section and  $l$  is length of the section.

Thus for section B:

$$C_{lB} = C_B \cdot l_B = 5714.81 \cdot 0,44 = 2514.5 Nm^2/deg \quad (4.26)$$

and for section C

$$C_{lC} = C_C \cdot l_C = 1432,55 \cdot 1,169 = 1674,6 Nm^2/deg. \quad (4.27)$$

<sup>4</sup>The angle that the section would twist while the frame is loaded.

Below (in the Fig. 4.14), follows depicted curve of deformation angle along the frame. For creation of the graph, I have used dependency of deformation angle (on the vertical axis) and length of the frame (on the horizontal axis). Since I have measured six points of the frame, I have ended up with three values of deformation angle within the frame. That is the reason, why the curve is composed of straight lines. For better imagination of the reader, I have also displayed the silhouette of the frame in the graph. Now one can easily see how the deformation angle goes down from the front (free axle) to the rear (fixed axle) and can estimate the possible weak and strong sections of the frame<sup>5</sup>.

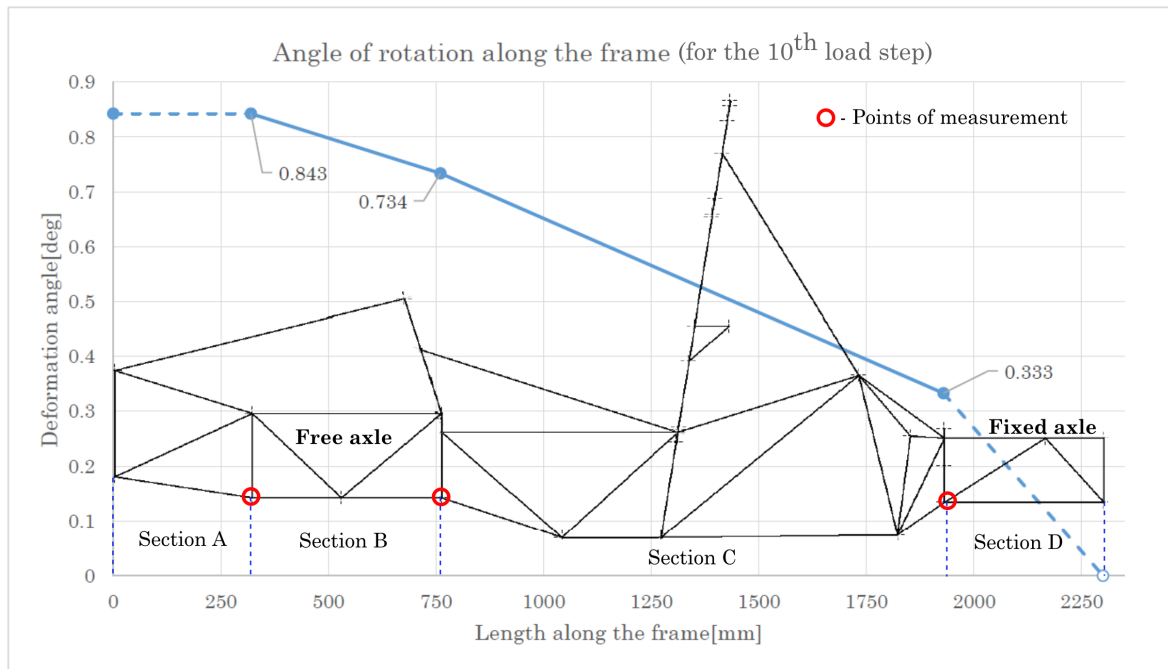


Figure 4.14: Change of deformation angle  $\alpha$  along the frame

<sup>5</sup>Sections A and D, I have not evaluated for sectional torsion stiffness because of there were no measured points at the very front and at the very rear point of the frame. That is also the meaning of the dashed-lines in the graph.

### 4.3 Simulation Part

After the frame was tested experimentally, I have evaluated the simulation which I have build in accordance with procedures used for the experimental testing.

#### 4.3.1 Points of Interest Within the Frame

The points of interest (where the displacements were evaluated) are depicted in Fig. 4.15 below. I have determined the overall torsion stiffness of the frame from points 1 and 2 and the length between them. I have also used so called Path function in ANSYS Mechanical for evaluating deformation (deformation angle) along the whole frame.

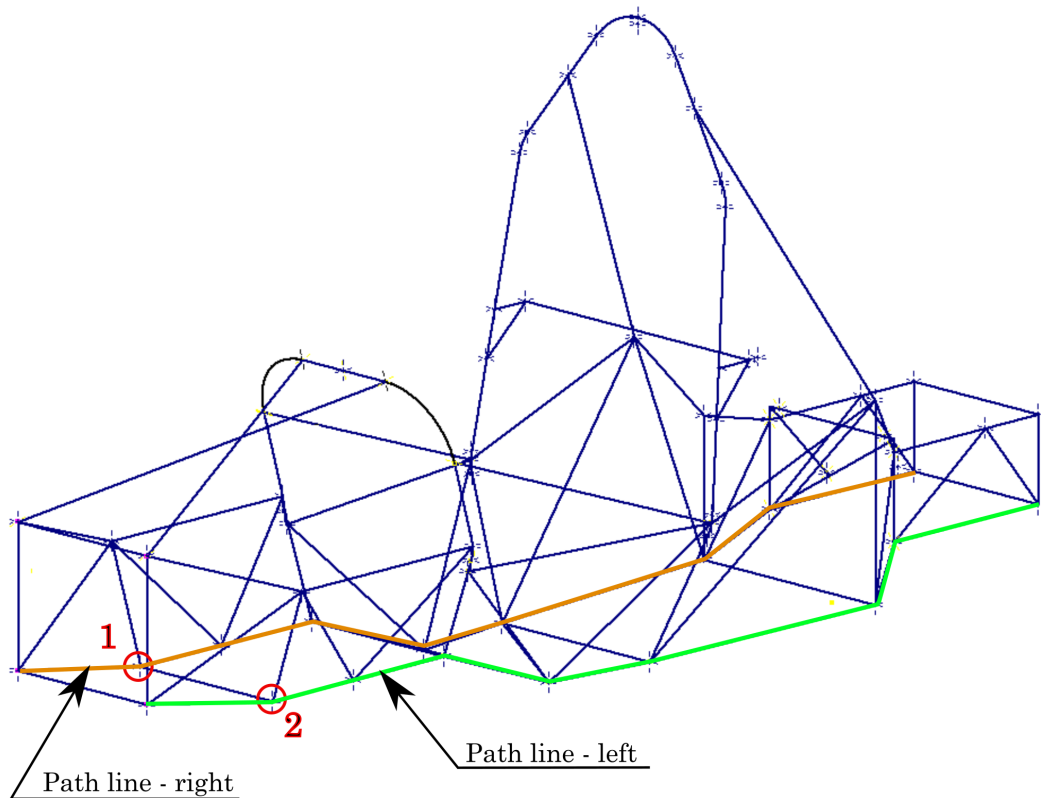


Figure 4.15: Places of interest within the frame

Figure 4.16 displays deformation from the simulation with linear setting with ARB system and with points of interest in which the displacement in z-axis was examined.

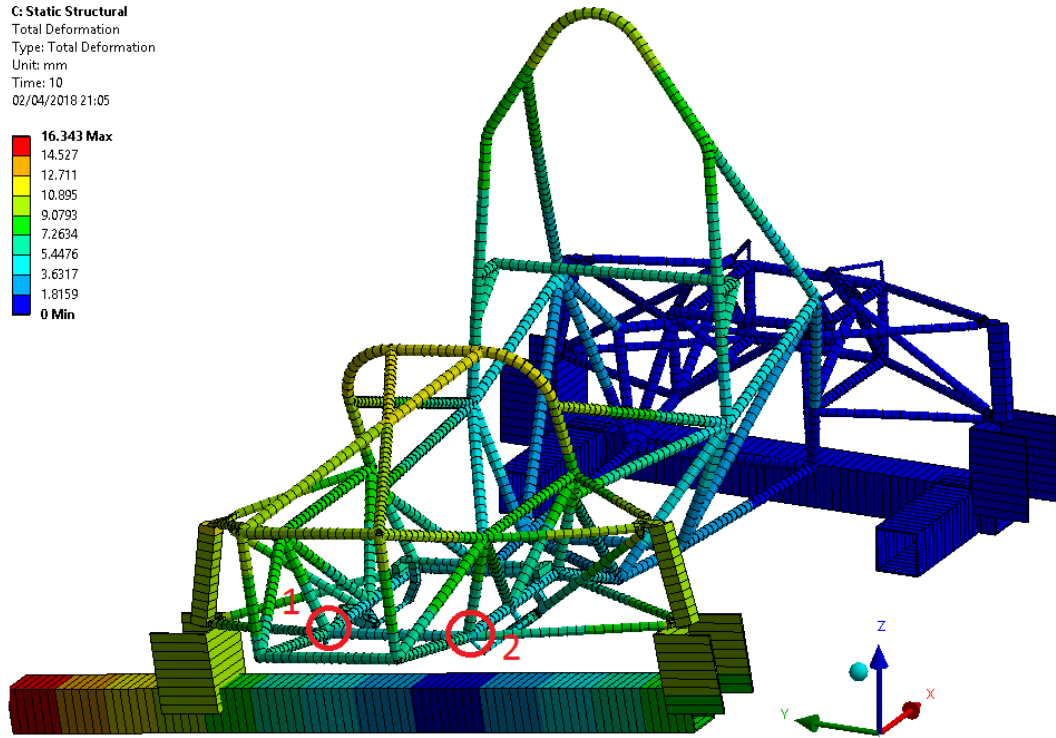


Figure 4.16: Deformation plot from the simulation with linear setting with ARB system

### 4.3.2 Evaluation of the Torsion Stiffness from Simulation

Because of four different settings of the simulation (for more detail one can see Chapter 3, section 3.3), I have evaluated four results of overall torsion stiffness and even four results of deformation angle along the whole frame.

Description and example of the evaluation procedure for the first simulation setting (linear simulation model with ARB system) follows below.



STEP	MASS[KG]	FORCE[N]	Torque[Nm]	Point		LINEAR SIMULATION - with ARB	
				u1	u2	Alpha12[deg]	C_T[Nm/deg]
0	0.0	0.0	0	0.0	0.0	0	N/A
1	5.0	49.1	51.50	0.2	0.2	0.06740677	764.06
2	14.7	144.2	151.42	0.7	0.5	0.20221956	748.78
3	19.9	195.2	204.98	0.9	0.7	0.26962521	760.24
4	25.1	246.2	258.54	1.1	0.9	0.33703011	767.12
5	30.1	295.3	310.05	1.3	1.1	0.40443408	766.61
6	35.0	343.4	360.52	1.6	1.3	0.48868745	737.73
7	40.0	392.4	412.02	1.8	1.5	0.55608863	740.93
8	45.0	441.5	463.52	2.0	1.7	0.62348828	743.43
9	50.6	496.4	521.21	2.2	1.9	0.69088621	754.40
10	56.2	551.3	578.89	2.5	2.1	0.77513090	746.83

L[mm]	L12[mm]
1050	340

Overall torsional stiffness -C_T[Nm/deg]	753.01
--	--------

Figure 4.17: Evaluation of overall torsion stiffness for linear simulation of model with ARB system

In the Fig. 4.17, one can see whole table for evaluation of the overall torsion stiffness of simulation. The simulation include ten load steps. During each load step, certain mass is applied (in yellow box, there is total mass within individual load step) resulting into ten pairs of displacement in vertical direction in millimetres (red box). The displacements are output from simulation and it is used for calculation of torsion stiffness for each load step (green box). In the blue box, there is result of overall torsion stiffness determined as the arithmetic mean of stiffness from individual load steps.

Now, follows an example of calculation of the ninth line of the table:

- Firstly, force  $F$  is calculated as:

$$F = m \cdot g = 50.6 \cdot 9.81 = 496.4N. \quad (4.28)$$

- Then, the torque is evaluated from the force:

$$T = F \cdot L = 496.4 \cdot 1.05 = 521.21Nm \quad (4.29)$$

- Deformation angle  $\alpha_{12}$  is determined as:

$$\alpha_{12} = \arctan\left(\frac{u_1 + u_2}{L_{12}}\right) = \arctan\left(\frac{2.2 + 1.9}{340}\right) = 0.691deg \quad (4.30)$$

where  $u_1$  and  $u_2$  is displacement of points 1 and 2, respectively and  $L_{12}$  is length between the points.

- Then, torsion stiffness for ninth load step  $C_{T9}$  is calculated as:

$$C_{T9} = \frac{T}{\alpha_{12}} = \frac{521.21}{0.691} = 754.4 Nm/deg. \quad (4.31)$$

According to such procedure, all lines of tables in Figures 4.18, 4.19 and 4.20 are evaluated. Below, one can see results of remaining simulations.

STEP	MASS[KG]	FORCE[N]	Torque[Nm]	Point		NON-LINEAR SIM. - with ARB	
				u1	u2	Alpha12[deg]	C[Nm/deg]
0	0.0	0.0	0	0.0	0.0	0	N/A
1	5.0	49.1	51.50	0.2	0.2	0.06740677	764.06
2	14.7	144.2	151.42	0.7	0.5	0.20221956	748.78
3	19.9	195.2	204.98	0.9	0.7	0.26962521	760.24
4	25.1	246.2	258.54	1.1	0.9	0.33703011	767.12
5	30.1	295.3	310.05	1.4	1.1	0.42128490	735.95
6	35.0	343.4	360.52	1.6	1.3	0.48868745	737.73
7	40.0	392.4	412.02	1.8	1.5	0.55608863	740.93
8	45.0	441.5	463.52	2.0	1.6	0.60663853	764.08
9	50.6	496.4	521.21	2.3	1.8	0.69088621	754.40
10	56.2	551.3	578.89	2.6	2.0	0.77513090	746.83

L[mm]	L12[mm]	Overall torsional stiffness -C[Nm/deg]	752.0105679
1050	340		

Figure 4.18: Evaluation of overall torsion stiffness for non-linear simulation of model with ARB system

STEP	MASS[KG]	FORCE[N]	Torque[Nm]	Point		LINEAR SIMULATION - no ARB	
				u1	u2	Alpha12[deg]	C_T[Nm/deg]
0	0.0	0.0	0	0.0	0.0	0	N/A
1	5.0	49.1	51.50	0.3	0.2	0.08425844	611.24
2	14.7	144.2	151.42	0.9	0.5	0.23592246	641.81
3	19.9	195.2	204.98	1.2	0.7	0.32017896	640.20
4	25.1	246.2	258.54	1.5	0.9	0.40443408	639.27
5	30.1	295.3	310.05	1.7	1.1	0.47183693	657.10
6	35.0	343.4	360.52	2.0	1.3	0.55608863	648.31
7	40.0	392.4	412.02	2.3	1.5	0.64033793	643.44
8	45.0	441.5	463.52	2.6	1.6	0.70773540	654.94
9	50.6	496.4	521.21	2.9	1.8	0.79197945	658.10
10	56.2	551.3	578.89	3.2	2.0	0.87622008	660.67

L[mm]	L12[mm]	Overall torsional stiffness -C_T[Nm/deg]	645.51
1050	340		

Figure 4.19: Evaluation of overall torsion stiffness for linear simulation of model without ARB system

STEP	MASS[KG]	FORCE[N]	Torque[Nm]	Point		NON-LINEAR SIM. - no ARB	
				u1	u2	Alpha12[deg]	C_T[Nm/deg]
0	0.0	0.0	0	0.0	0.0	0	N/A
1	5.0	49.1	51.50	0.3	0.2	0.08425844	611.24
2	14.7	144.2	151.42	0.9	0.5	0.23592246	641.81
3	19.9	195.2	204.98	1.2	0.7	0.32017896	640.20
4	25.1	246.2	258.54	1.5	0.9	0.40443408	639.27
5	30.1	295.3	310.05	1.8	1.1	0.48868745	634.44
6	35.0	343.4	360.52	2.1	1.2	0.55608863	648.31
7	40.0	392.4	412.02	2.4	1.4	0.64033793	643.44
8	45.0	441.5	463.52	2.7	1.5	0.70773540	654.94
9	50.6	496.4	521.21	3.1	1.7	0.80882786	644.40
10	56.2	551.3	578.89	3.4	1.9	0.89306776	648.20

L[mm]	L12[mm]	Overall torsional stiffness -C_T[Nm/deg]	640.63
1050	340		

Figure 4.20: Evaluation of overall torsion stiffness for non-linear simulation of model without ARB system

Table 4.2 sums up all results of torsion stiffness of the frame from all simulations<sup>6</sup>.

	Overall torsion stiffness [Nm/deg]
Linear - no ARB	645.51
Linear - with ARB	753.01
Non-linear - no ARB	640.63
Non-linear - with ARB	752.01

Table 4.2: Overall results from the simulations

Now follow the results of the deformation (angle of rotation) along the frame. The deformation is, also, determined for all four simulation settings.

Firstly, I have set the so called Path at both sides of the frame (see Fig. 4.15), ensured that both Paths have the same number of nodes (in case of mesh sizing of 20 mm per element, the number of nodes per one Path is 123) and evaluated displacement in vertical (z-axis) direction for each node within both left and right Path. Values of displacement at all nodes from all simulations, one can follow to Appendix A. Then, I have determined the deformation angle at each site along the frame (by site, I mean section of the frame defined by individual pair of nodes along the Path, i.e. 123 sites) according to procedure below.

The Fig. 4.21 shows data for first 16 lines of the Path evaluation table. The example of evaluation of the deformation angle of the highlighted line in the table follows below. Other lines of the table are evaluated in the same manner.

<sup>6</sup>The results are from final tuned up finite element simulation model, i.e. cross-section of simplified uprights is optimized as well as the material properties of carbon-fibre tubes. Influence of upright simplification and influence of change of carbon-fibre material properties on results are described in Appendix B and Appendix C.

PATH RESULTS						
Number of node	Length [mm]	Right path		Left path		Angle[deg]
		u_r [mm]	u_l [mm]	Width between nodes [mm]		
1	0	-2.675	2.164	332	0.8351	
2	19.10	-2.667	2.161	332.471	0.8318	
3	38.20	-2.658	2.157	332.941	0.8285	
4	57.30	-2.648	2.153	333.412	0.8251	
5	76.40	-2.638	2.149	333.882	0.8215	
6	95.51	-2.628	2.145	334.353	0.8179	
7	114.61	-2.618	2.141	334.824	0.8143	
8	133.71	-2.607	2.136	335.294	0.8105	
9	152.81	-2.597	2.131	335.765	0.8067	
10	171.91	-2.586	2.126	336.235	0.8028	
11	191.01	-2.574	2.121	336.706	0.7989	
12	210.11	-2.563	2.115	337.176	0.7949	
13	229.21	-2.551	2.109	337.647	0.7908	
14	248.31	-2.540	2.103	338.118	0.7866	
15	267.41	-2.528	2.096	338.588	0.7824	
16	286.51	-2.516	2.089	339.059	0.7781	

Figure 4.21: Part of the Path evaluation table for linear model with ARB

Firstly, description of the Path evaluation table. Column "Length" denotes distance of the certain node to the very front point of the frame (for graph purposes). Columns " $u_r$ " and " $u_l$ " are values of displacement of certain node on left or right Path (always the opposite of nodes) in vertical (z-axis) direction<sup>7</sup>. Column "Width between nodes" includes values of length between each pair of opposite nodes. Column "Angle" contains values of deformation angle along the frame.

Now follows the example of evaluating procedure for highlighted line (pair of nodes with number 6) in Fig. 4.21.

- Once the data for Length,  $u_r$ ,  $u_l$  and Width between nodes columns are gathered, one can go on right to calculation of deformation angle.
- Thus, deformation angle  $\alpha_D$ :

$$\alpha_D = \arctan\left(\frac{|u_r| + u_l}{l_n}\right) = \arctan\left(\frac{|-2.628| + 2.145}{334.353}\right) = 0.8179deg \quad (4.32)$$

where  $l_n$  is length between the nodes.

The utilization of the deformation angle along the frame is to see deformation of the frame at certain sections. The output, one can see in Fig. 4.22. The curve is smooth because it is composed of 123 values along the frame.

<sup>7</sup>Negative values within the  $u_r$  column are caused by the nodes within the right path are translated in opposite direction than the z-axis is defined in the simulation.

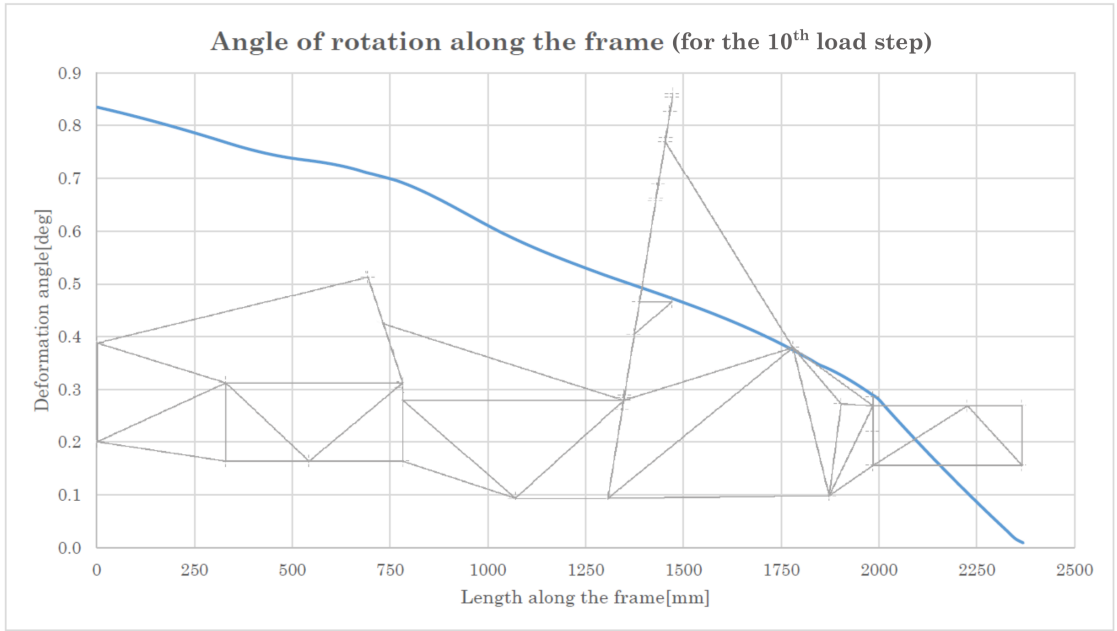


Figure 4.22: Deformation angle along the frame for linear model with ARB

## 4.4 Comparison of the Results from the Experiment and from Simulations

### 4.4.1 Overall Comparison of the Results

In this section, one can see comparison of results from all simulations with results from experiment and comparison of results from simulations respectively.

Table 4.3 shows overall comparison of results from the experiment with results from all simulations (sign minus means that the certain result is lower than the result from experiment, in other words - the certain simulation is less stiff).

	Overall torsion stiffness [Nm/deg]	Difference [%]
Experiment	679.4	—
Linear - no ARB	645.51	-5.3
Linear - with ARB	753.01	9.7
Non-linear - no ARB	640.63	-6.1
Non-linear - with ARB	752.01	9.6

Table 4.3: Overall comparison of results

In the Table 4.4, one can see influence of usage of ARB system within simulation model. The difference fluctuates from 14 to 15 percent.

	Overall torsion stiffness [Nm/deg]	Difference [%]
Linear - no ARB	645.51	—
Linear - with ARB	753.01	14.3
Non-linear - no ARB	640.63	—
Non-linear - with ARB	752.01	14.8

Table 4.4: Influence of usage ARB system within the simulation model

In the Table 4.5, one can see influence of usage of linear or non-linear simulation model. The difference is up to 1 percent.

	Overall torsion stiffness [Nm/deg]	Difference [%]
Linear - no ARB	645.51	—
Non-linear - no ARB	640.63	-0.8
Linear - with ARB	753.01	—
Non-linear - with ARB	752.01	-0.1

Table 4.5: Influence of usage linear or non-linear simulation model

Fig. 4.23 depicts comparison of the deformation angle  $\alpha$  along the frame from all simulation models with deformation angle from experimental measurement. The smooth curves display the results from simulation and the straight-line curve displays the results from experiment<sup>8</sup>.

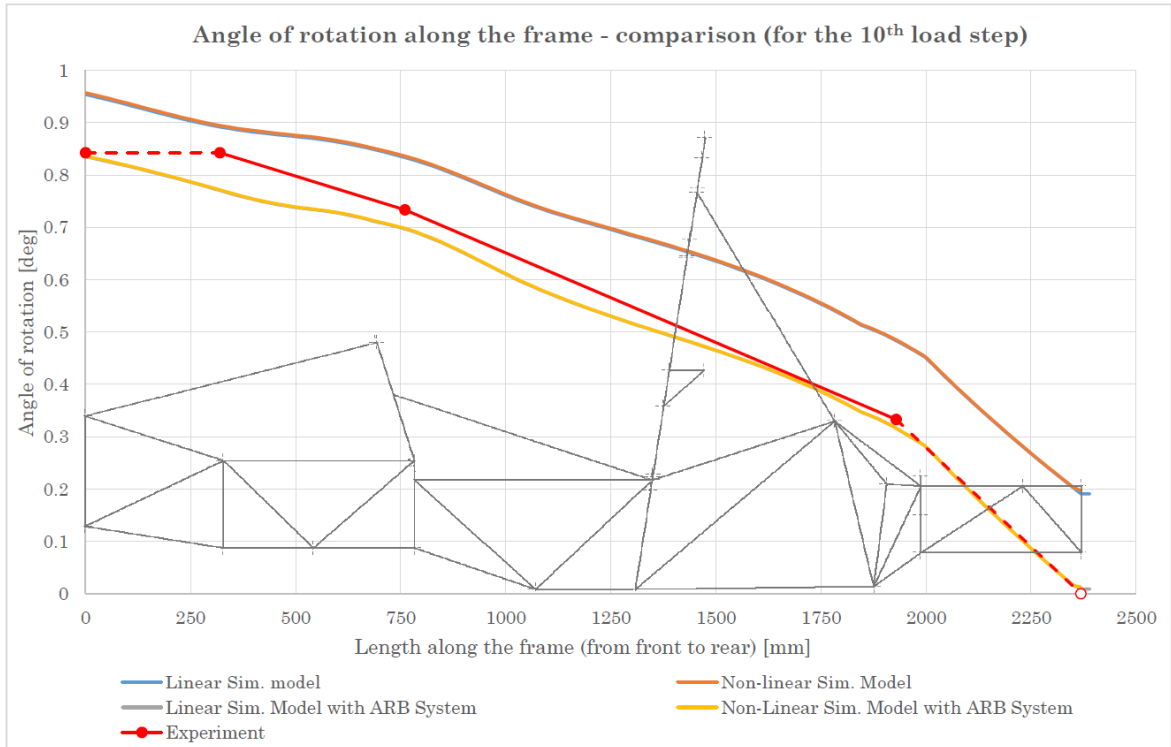


Figure 4.23: Comparison of the deformation angle alpha along the frame

#### 4.4.2 Comparison with Roll Stiffness of the Suspension

The value of torsion stiffness is useless if there is nothing to compare with. The torsion stiffness is usually compared with roll stiffness of the suspension.

Because the vehicle has two axles and each can have different roll stiffness (roll stiffness is calculated for just 1 axle), I have determined total roll stiffness of suspension as follows.

Firstly, Ing. Tomáš Pasterňák kindly provided me the roll stiffness of individual axles (see Tab. 4.6 below).

Then, one can imagine the system front axle - frame - rear axle as system of springs connected in series. The situation is depicted in Fig. 4.24 below.

<sup>8</sup>Blue and grey curves are barely visible because they are under orange and yellow curve respectively. This shows proximity of the results.

	Roll stiffness [Nm/deg]
Front axle	599
Rear axle	456

Table 4.6: Table of roll stiffnesses of individual axles

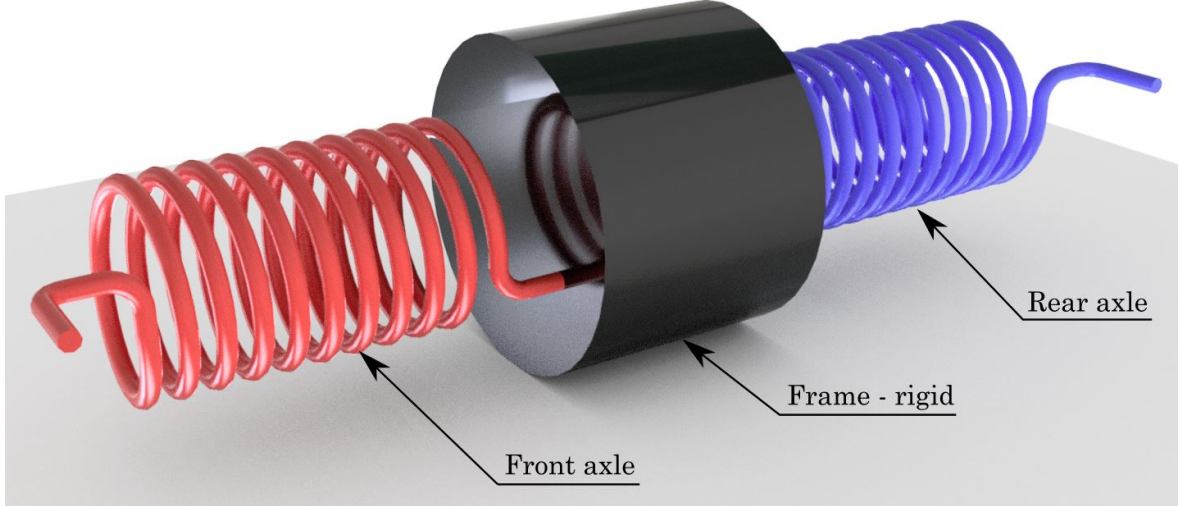


Figure 4.24: Imagination of frame/suspension connection as springs

Front and rear axle has its roll stiffness but the frame is considered as rigid. Then, I can calculate total roll stiffness according to formulas for total stiffness of system of springs in series.

Thus, total roll stiffness  $C_R$ :

$$C_R = \frac{1}{\frac{1}{C_{Rf}} + \frac{1}{C_{Rr}}} = \frac{1}{\frac{1}{599} + \frac{1}{456}} = 258.9 Nm/deg \quad (4.33)$$

where  $C_{Rf}$  is roll stiffness of the front axle and  $C_{Rr}$  is roll stiffness of the rear axle.

Finally, the torsion stiffness/roll stiffness ratio  $c_{TR}$ :

$$c_{TR} = \frac{C_T}{C_R} [-] \quad (4.34)$$

where  $C_T$  is torsion stiffness of the frame.



Tab. 4.7 denotes results of torsion stiffness/roll stiffness ratio for experimental and for simulation results.

	Torsion stiffness [Nm/deg]	$c_{TR}$ [-]
Experiment	679.4	2.6
Linear - no ARB	645.51	2.5
Linear - with ARB	753.01	2.9
Non-linear - no ARB	640.63	2.5
Non-linear - with ARB	752.01	2.9

Table 4.7: Results of torsion stiffness/roll stiffness ratio  $c_{TR}$

Example of the calculation of the torsion stiffness/roll stiffness ratio  $c_{TR}$  for result from the experiment:

$$c_{TRexp} = \frac{C_{Texp}}{C_R} = \frac{679.4}{258.9} = 2.6[-]. \quad (4.35)$$

## Chapter 5

# Possibilities of Optimization of the Frame

By optimization of the frame, I mean, to make it stiffer and, in ideal case, reduce its mass. This can be achieved by many approaches. Change of cross-section, dimensions of cross-sections, material or placement of the tubes are some of them.

Firstly, I need to set aim of the optimization. Then, I need to establish the restrictions or boundary conditions the optimization should meet. Finally, I need to find out the sections (or parts) of the frame which are the most compliant or exceedingly (or unnecessary) stiff. Thus, I know where the region of application of optimization should be.

The aim is to increase torsion stiffness and try to keep or even reduce mass of the frame.

The restrictions (or boundary conditions) are more complex. Because the frame is already designed from tubes with minimal possible cross-section dimensions, the further reducing of them would be permitted only within Alternative frame rules (see Chapter 1). The same applies for other material than steel (except Main Hoop and Main Hoop Bracing which must be of steel under any circumstances). Thus, the one possible change could be change of the cross-section of tubing from round to square. But this is possible only for some parts of the frame (SIS, Front Bulkhead, Hoops Bracing and Driver's Restraint Harness Attachment) and this step could negatively affect the manufacturability. Also placement of vehicle's components (such as engine or drive-train) within the frame must be taken into consideration. Because of such restrictions, the easiest way to satisfy the optimization aim is to change the placement of the tubing and adding (or removing) the additional tubes.

## 5.1 Examination of the Sectional Stiffness of the Frame

The examination of the sectional torsion stiffness from the experiment, I have already mentioned in Chapter 4, section 4.2.3. It follows that the most compliant section of the frame is the section C and D. This confirmed also the graph of deformation angle  $\alpha$  along the frame eventually<sup>1</sup> (see Fig. 4.14).

The examination of the sectional torsion stiffness from the simulation follows now. For the examination, I have chosen the linear simulation model with ARB system (the ARB system was used during the experiment. Linear model because there is almost no difference between linear and non-linear simulation model, see Tab. 4.5). In the Fig. 5.1, one can see the frame divided into sections together with progress of deformation angle along the frame from the simulation.

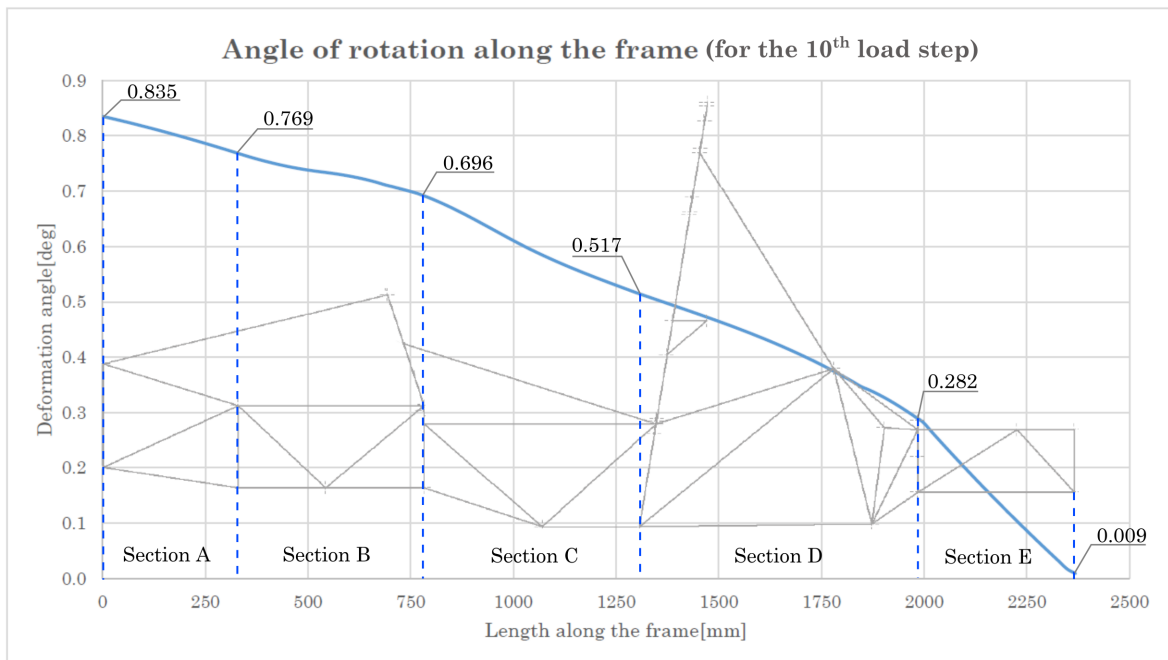


Figure 5.1: Frame divided into sections

<sup>1</sup>From the experiment, I have got 4 sections A, B, C and D (it depends on number of measured points) and exact values of deformation angle only at the measured points. Then, I have used linear interpolation and assumptions, for the section A that the deformation remains approximately the same and for section D that the deformation goes to zero because of fixed axle, to create the whole curve.

In the Fig. 5.2, one can see the results of sectional torsion stiffness together with sectional torsion stiffness on unit of length<sup>2</sup>.

Section length		Angle between sections		Angle difference	
Section	Length [mm]	Site	Angle [deg]	Section	Angle [deg]
A	320	Alpha AA	0.835	Alpha A	0.066
B	440	Alpha AB	0.769	Alpha B	0.073
C	510	Alpha BC	0.696	Alpha C	0.179
D	659	Alpha CD	0.517	Alpha D	0.235
E	371	Alpha DE	0.282	Alpha E	0.273
		Alpha EE	0.009		

Sectional torsion stiffness		Torsion stiffness on unit of length	
Section	Stiffness [Nm/deg]	Section	Stiffness [Nm <sup>2</sup> /deg]
A	8771.03	A	2806.73
B	7929.97	B	3489.19
C	3234.01	C	1649.35
D	2463.35	D	1623.35
E	2120.47	E	786.69

Figure 5.2: Results of calculation of the sectional torsion stiffness from simulation

Now follows the example of calculation for highlighted line in Fig. 5.2:

- Firstly the length of each section, I have determined from the model of the frame.
- Then, from displacement of points on boundaries of each section (dashed-lines in the Fig. 5.1), I have calculated the angle of rotation on boundaries of each section (the values one can also see in the Fig. 5.1) according to the formula (4.1).
- After that, I have calculated the angle difference (the angle in which the section is twisted) as follows:

$$\alpha_C = \alpha_{BC} - \alpha_{CD} = 0.696 - 0.517 = 0.179deg. \quad (5.1)$$

- Then, I have could determine the sectional stiffness for the section C as:

$$C_C = \frac{T_{10}}{\alpha_C} = \frac{578.89}{0.179} = 3234.01Nm/deg \quad (5.2)$$

where  $T_{10}$  is the torque during the 10th load step.

- Finally, the sectional torsion stiffness of the section C on unit of length:

$$C_{lC} = C_C \cdot l_c = 3234.01 \cdot 0.51 = 1649.35Nm^2/deg \quad (5.3)$$

where  $l_C$  is the length of the section C.

<sup>2</sup>I have calculated the results from displacement at 10th load step. I have decided to do not use the average value from all 10 steps as for the experiment because as one can see in Fig. 4.13 the fluctuation of the values is very small.

From the results (Fig. 5.2), one can see that the most compliant section is section E and then section C and D, when compared with the other sections. It follows that, the sections C, D and E should be taken into consideration for the optimization process (the stiffness should be increased).

## 5.2 Example of Optimization

By the procedure above, I have determined the most compliant sections of the frame: C, D and E. Based on it below, I have introduced an example how the optimization could look like.

I have added bracing within section E, D and even section B. The section C is cockpit area thus it is one of the most open part of the frame and there is a minimal possibility to change placement of tubes. Thus, I have decided to add a tube on each side of the frame within the section B to provide a triangulation for the brace going rearward from the Front Hoop. Placement of added tubes, one can see in Fig. 5.3.

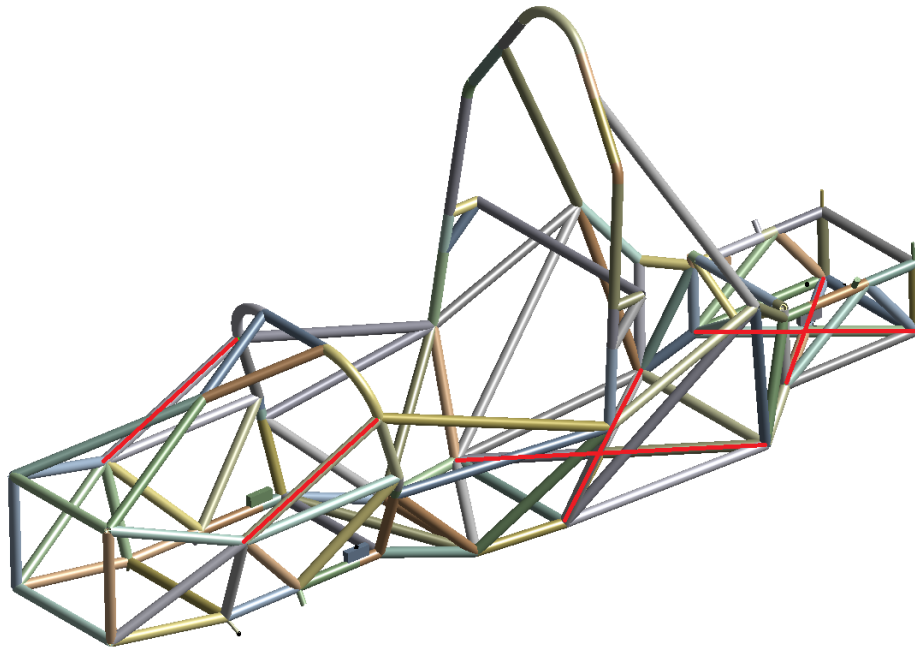


Figure 5.3: The frame structure with added tubes highlighted in red

According to procedures I have discussed in previous chapters, I have simulated the frame with the new tubes (linear simulation model with ARB system) and evaluated its overall torsion stiffness<sup>3</sup>.

Summary of results of the optimized frame follows below:

- 8 additional tubes of steel of round cross-section. Diameter 25 mm, wall thickness 1.5 mm.
- Total length of added tubes - 3204 mm, resulting in mass of 2.8 kg.

---

<sup>3</sup>The evaluation table, one can follow to Appendix E.

- The new overall torsion stiffness is 1014 Nm/deg (approx. 26% increase<sup>4</sup>).
- The new mass of the frame - 38.8 kg (increase of 2.8 kg or 7.2% compared with the default design).
- Torsion stiffness/roll stiffness ratio - 3.9 (increase of approx. 25%<sup>4</sup>)

### 5.3 Assessment of the Optimization

In the previous section, I have determined that the new frame design is about 26% stiffer and about 2.8 kg heavier. But how one knows whether the optimization was successful (increase of stiffness prevailed the mass increase for example). There is a ratio between torsion stiffness and frame mass which can help to assess the optimization (or the frame) quality with respect to torsion stiffness and mass. For the ratio applies, the higher value, the better. But one must be aware even if the ratio is high, the frame does not have to be properly optimized (or designed). One can imagine a very stiff frame but even very heavy, then the ratio could be the same as for a less stiff frame but also more lightweight. This is why I have mentioned that the ratio could only *help* to assess the frame. The assessment of the frame according to this ratio only, it would not be proper. The maximum desired mass or comparison with the roll stiffness of the suspension should be taken into consideration while assessing the frame with respect to torsion stiffness and mass.

Thus, the torsion stiffness/mass ratio (I have established it in this thesis as  $C_T/m$ ):

$$C_T/m = \frac{C_T}{m} [-]^5 \quad (5.4)$$

where  $C_T$  is overall torsion stiffness of the frame and  $m$  is the mass of the frame.

Then for the base frame, I have calculated the ratio  $C_T/m_b$  as follows.

$$C_T/m_b = \frac{C_T}{m} = \frac{753.01}{36} = 20.9 [-] \quad (5.5)$$

Now, the ratio for the new optimized frame  $C_T/m_o$ .

$$C_T/m_o = \frac{C_T}{m} = \frac{1014.01}{28.8} = 26.1 [-] \quad (5.6)$$

---

<sup>4</sup>Compared with the result of the linear simulation with ARB system.

<sup>5</sup>Although the unit would be  $\frac{m^2}{s^2 \cdot deg}$ , I have decided to write it as a dimensionless formula because there is no physical meaning of the formula (or unit). The ratio serves only as a helpful tool for assessment of the frame quality with respect to torsion stiffness and mass.

## Chapter 6

# Discussion of Results and Conclusion

In the Introduction, I have discussed the brief history, description, objectives and competition event of the Formula SAE<sup>®</sup>. I have also discussed main types of frames for Formula SAE<sup>®</sup> vehicles. Formulation of the topic and targets of this thesis, I have introduced at the end of the chapter.

In the Chapter 1, I have discussed technical requirements for the Formula SAE<sup>®</sup> vehicles in general. Requirements are prescribed by Formula SAE<sup>®</sup> rules document which serves as the official competition and evaluating document. I have introduced also requirements for frames of Formula SAE<sup>®</sup> vehicles, including description of the frame parts, material requirements and design requirements. The discussion about torsion stiffness of the frame and the importance of the torsion stiffness and its influence on the vehicle performance concludes the Chapter 1.

In the next part of this thesis, I have dealt with geometric and finite element model of the frame. Firstly, I have prepared wire-frame model of the frame using software Autodesk Inventor. Subsequently, I have imported the geometry of the wire-frame model into ANSYS Design Modeler. Since the simulation was supposed to be compared with the real testing, the creation of the other parts of the simulation system (such as beams, suspension, ARB system), has been my next step. Because of complexity of the simulation system, I have prepared the finite element model for the so called beam elements. Thus, by assignment of the cross-sections and joints to the geometry, I have concluded the creation of the model. I have written down material properties of each material used in the Tab. 2.1.

Chapter 3 of the thesis begins with a discussion of all element types used. The mesh, I have generated using mesh generator within the ANSYS Mechanical, I have introduced together with comparison of 2 mesh sizes, concluding that the mesh sizing of 20 mm per element is sufficient. The final mesh is depicted in the Fig. 3.3 and number of nodes and elements is written down in the Tab. 3.1. Then, the chapter goes on with an introduction of the boundary conditions used, including description of the force and constraints settings which are based on the real testing environment. How I have set the simulation and why I have performed even modal analysis is answered at the very end of this chapter.

With the model prepared, I have gone on to carry out the simulation and the experiment.

The experimental environment, measuring procedure and evaluation, I have explained step by step. I have ended up with value of torsion stiffness of the frame  $C_T = 679.4Nm/deg$  from the experiment eventually. Then, I have discussed and determined sectional torsion stiffness concluding that the most compliant is section C<sup>1</sup>.

Then, I have carried out and evaluated simulations according to the same procedure as the experiment. Thus, I have could afford to compare the experiment and simulations eventually. I have compared the results in Tabs. 4.3, 4.4 and 4.5. From the results, the difference of simulations with respect to experiment is up to 10%. I consider this difference as acceptable. The biggest difference (9.7%) is for the linear simulation model with ARB system (torsion stiffness  $C_T = 753Nm/deg$ ) which I have considered as the reference for comparison with the experiment and for tuning the simulation to get as close result to experiment as possible.<sup>2</sup> Main sources of differences and inaccuracies between the experiment and analysis could be the simplifications of the model (simplified cross-sections, joints without friction and gaps), approximate values of mechanical properties of carbon-fibre material (the influence of the change of Young's modulus of the carbon-fibre on results, one can find in Appendix C) and rounding of simulated displacements on one decimal eventually. There could be also inaccuracies within the experiment such as the rounding on one decimal and inaccuracy of dial indicators.

Then, to assess the influence of the ARB system on the results, I have utilized the Fig. 4.23. There is clearly visible that despite the difference of overall torsion stiffness of simulation with ARB system is bigger (compared to the experiment), the overall progress of the deformation angle curve is much closer to the experimental curve, than the curve for simulation without ARB system. Thus, the ARB system should be included into simulations. In the Tab. 4.5, one can see the influence of non-linear setting on the simulation compared with the linear setting. The difference fluctuates up to 1% thus I consider it as negligible and simulations are possible to be performed linear simulation model.

After evaluating the torsion stiffness, I have moved on to comparison of the torsion stiffness of the frame with the roll stiffness of the suspension. In the Tab.4.7, one can see results for experiment and all simulations. The ratio for the experiment ( $c_{TR} = 2.6$ ) and for the linear simulation model with ARB system ( $c_{TR} = 2.9$ ) is higher than 1 thus from that, I can conclude that the frame is stiffer than the suspension. Moreover, the frame is simulated (and measured) without any component (besides suspension)<sup>3</sup> thus with engine and another components, I presume, the vehicle would be even stiffer.

The last part of this thesis is dedicated to discussion and proposal of optimization of the frame to increase of torsion stiffness (and in ideal case to reduce of mass). Within this part, I have discussed possibilities of the optimization and what the *optimization* actually means. Firstly, I have carried out the examination of the most compliant sections of the frame (for linear simulation model with ARB system). Then, I have proposed changes of the frame design (see Fig. 5.3), based on the examination (Fig. 5.2). I have ended up with the new design of the frame which is about 2.8 kg heavier but about 25% (1014 Nm/deg) stiffer compared with the linear simulation model with ARB system eventually. Even the torsion stiffness/roll stiffness ratio increased by approx. 25% to 3.9. Whether the optimization was worth it, I have as-

---

<sup>1</sup>Nevertheless, from the Fig. 4.14, the section D should be also considered as the weak part of the frame because of very sharp fall of the deformation angle within the section.

<sup>2</sup>The influence of main regions where could be the significant inaccuracies (simplification of uprights and A-arms material), one can follow to Appendix B, C and F.

<sup>3</sup>Performing the simulations and experiment with the whole car was not in my forces because of its complexity and new parts of the vehicle were not available at the time of performing.



essed according to the ratio between the torsion stiffness and mass of the frame, followed with a notification about usage of the ratio within assessing the overall quality of the frame design.

# Acknowledgement

I would like to sincerely thank my supervisor **Ing. Zdeněk Poruba, Ph.D.** for his advice and professional guidance. I also would like to thank my closest family for their support during study. I would like to address my thanks to **doc. Ing. Aleš Slíva, Ph.D.** for his support of Formula TU Ostrava team which I am member of, to **Ing. Šárka Tichá, Ph.D.** and **Ing. Lenka Čepová, Ph.D.** who kindly provided measuring tools for experiment. And last but not least I thank to members of **Formula TU Ostrava team** for their help with the performance of the experiment.

# List of Figures

1	1982 University of Houston Formula SAE <sup>®</sup> car(2)	11
2	Skid-pad layout according to Formula SAE rules (3)	14
3	Steel tube frame (4)	15
4	Carbon fibre monocoque (5)	16
1.1	Unobstructed zones (3)	17
1.2	Description of frame structure of Vector 04 vehicle	21
1.3	Impact Attenuator with Anti-Intrusion Plate mounted on the Front Bulkhead	22
1.4	Example of triangulation (3)	23
1.5	Prescribed dimensions and positions (3)	25
1.6	Side impact structure requirements (3)	26
1.7	Cockpit templates (3)	26
1.8	95th percentile male template (3)	27
1.9	Helmet clearance (3)	28
1.10	Longitudinal torsion mode (7)	28
2.1	Wire-frame model of the new frame	30
2.2	3D model of the new frame	31
2.3	Sandblasted frame	31
2.4	Imported wire-frame model with assigned cross-sections	32
2.5	Cross-section assignment	32
2.6	Line model	33
2.7	Final finite element model for analysis	34
2.8	Modeling of front A-arms and uprights	35
2.9	Description of individual parts of A-arms together with upright	35
2.10	Description of individual parts of ARB system	36
2.11	Connection holder	37
2.12	Description of beams design	37
2.13	Examples of joints used (grey rectangle means the translation or rotation is fixed, the colourful one means free translation or rotation)	39
3.1	Geometry of so called BEAM188 element (12)	42
3.2	Geometry of discussed MPC184 elements (14)	42
3.3	Mesh with sizing of 20 mm	43
3.4	Mesh with sizing of 10 mm	44
3.5	Overview of boundary conditions of the model	45
3.6	Progress of the force within all steps	46
3.7	Detail of rear beam situation	46
3.8	Detail of front beam situation	47

3.9	Result of natural frequencies in graphical layout . . . . .	48
3.10	Deformation shape of 7th natural frequency of the system. . . . .	49
4.1	Possible testing procedures . . . . .	50
4.2	Testing model with frame and complete suspension . . . . .	51
4.3	Simplified situation at revolving beam in front view . . . . .	51
4.4	Deformation triangle . . . . .	52
4.5	Rod replacing dampers . . . . .	53
4.6	Experimental setup . . . . .	54
4.7	Six measured points of the frame . . . . .	55
4.8	Averaged values of displacement at point 1 and point 2 with respect to loading . . . . .	55
4.9	Displacements of individual points from first measurement - adding mass . . . . .	56
4.10	Example of evaluation table . . . . .	56
4.11	Imagination of set of springs and torsion bars in series . . . . .	58
4.12	Results of deformation angle $\alpha$ for all three sites within the frame . . . . .	59
4.13	Results deformation angles $\alpha$ and sectional torsion stiffness of section B and C . . . . .	61
4.14	Change of deformation angle $\alpha$ along the frame . . . . .	62
4.15	Places of interest within the frame . . . . .	63
4.16	Deformation plot from the simulation with linear setting with ARB system . . . . .	64
4.17	Evaluation of overall torsion stiffness for linear simulation of model with ARB system . . . . .	65
4.18	Evaluation of overall torsion stiffness for non-linear simulation of model with ARB system . . . . .	66
4.19	Evaluation of overall torsion stiffness for linear simulation of model without ARB system . . . . .	66
4.20	Evaluation of overall torsion stiffness for non-linear simulation of model without ARB system . . . . .	67
4.21	Part of the Path evaluation table for linear model with ARB . . . . .	68
4.22	Deformation angle along the frame for linear model with ARB . . . . .	69
4.23	Comparison of the deformation angle $\alpha$ along the frame . . . . .	71
4.24	Imagination of frame/suspension connection as springs . . . . .	72
5.1	Frame divided into sections . . . . .	75
5.2	Results of calculation of the sectional torsion stiffness from simulation . . . . .	76
5.3	The frame structure with added tubes highlighted in red . . . . .	77
6.1	Table's lines from 1 to 46 . . . . .	91
6.2	Table's lines from 47 to 97 . . . . .	92
6.3	Table's lines from 98 to 123 . . . . .	93
6.4	Table's lines from 1 to 45 . . . . .	94
6.5	Table's lines from 46 to 95 . . . . .	95
6.6	Table's lines from 96 to 123 . . . . .	96
6.7	Table's lines from 1 to 44 . . . . .	97
6.8	Table's lines from 45 to 93 . . . . .	98
6.9	Table's lines from 94 to 123 . . . . .	99
6.10	Table's lines from 1 to 48 . . . . .	100
6.11	Table's lines from 49 to 101 . . . . .	101
6.12	Table's lines from 102 to 123 . . . . .	102
6.13	Imported models of uprights in Ansys Design Modeler . . . . .	103

6.14	Imported models of uprights in Ansys Design Modeler . . . . .	104
6.15	Design of the simplified uprights . . . . .	105
6.16	Evaluation table for 10% reduction . . . . .	106
6.17	Evaluation table for 20% reduction . . . . .	107
6.18	Evaluation table for 30% reduction . . . . .	107
6.19	Evaluation table for 40% reduction . . . . .	107
6.20	Evaluation table for 50% reduction . . . . .	108
6.21	Progress of influence of reduction of Young's modulus . . . . .	108
6.22	Gathered data from measurement (values of displacement at 6 points of the frame [mm]) . . . . .	109
6.23	Evaluation tables for all measurements . . . . .	110
6.24	Averaged values of displacement at point 3 and point 4 with respect to applied mass . . . . .	111
6.25	Averaged values of displacement at point 5 and point 6 with respect to applied mass . . . . .	111
6.26	Evaluation tables of mesh sizing comparison . . . . .	112
6.27	Evaluation table of optimization . . . . .	113
6.28	Testing specimen . . . . .	114
6.29	Specimen after testing procedure . . . . .	114
6.30	Resulting graph of force in relation to deflection . . . . .	115

# List of Tables

1	Maximal available points for disciplines (3)	14
1.1	Minimal profile and C-S requirements	23
1.2	Minimal material properties	24
2.1	Mechanical properties for materials used in model	40
3.1	Number of nodes and elements when using mesh size of 20 mm	43
3.2	Number of nodes and elements when using mesh size of 10 mm	44
3.3	Table of comparison of results for different mesh sizing	44
3.4	Table of loading steps	45
3.5	Table of frequencies in first ten modes	48
4.1	Table of individual added or released masses within all steps	54
4.2	Overall results from the simulations	67
4.3	Overall comparison of results	69
4.4	Influence of usage ARB system within the simulation model	70
4.5	Influence of usage linear or non-linear simulation model	70
4.6	Table of roll stiffnesses of individual axles	72
4.7	Results of torsion stiffness/roll stiffness ratio $c_{TR}$	73
6.1	Guide for evaluation tables	90
6.2	Stiffness of uprights	104
6.3	Evaluated influence of reduction	106

# Bibliography

- (1) FORMULA SAE®. *History of Formula SAE* [online]. SAE International [cit. 6.2.2018]  
Available from: <https://www.fsaeonline.com/page.aspx?pageid=c4c5195a-60c0-46aa-acbf-2958ef545b72>
- (2) HOUSTON FORMULA SAE®. *History of Houston Formula SAE*. [online] [cit. 7.2.2018].  
Available from: <http://uh.edu/fsae/history.htm>
- (3) 2017 - 18 Formula SAE® Rules. *Formula SAE* [online]. SAE International [cit. 8.2.2018].  
Available from: <https://www.fsaeonline.com/content/2017-18%20FSAE%20Rules%209.2.16a.pdf>
- (4) VICTOR BARO. *untitled.85.jpg* [online]. [cit. 10.2.2018]. Available from:  
<http://victorbaro.com/wp-content/uploads/2013/04/untitled.85.jpg>
- (5) ABLOAD. *mc\_vollstaendig.16ciq9.jpg* [online]. [cit. 10.2.2018].  
Available from: [http://www.abload.de/img/mc\\_vollstaendig.16ciq9.jpg](http://www.abload.de/img/mc_vollstaendig.16ciq9.jpg)
- (6) van KERKHOVEN, Janis D.G. *Design of a Formula Student race car chassis: Master Thesis* [online]. Eindhoven: Eindhoven University of Technology, Department Mechanical Engineering, 2008. Thesis head: Prof. dr. ir. Steinbuch, M. [cit. 12.2.2018].  
Available from: <http://www.mate.tue.nl/mate/pdfs/10019.pdf>
- (7) RILEY, William B., GEORGE, Albert R. *Design, Analysis and Testing of a Formula SAE Car Chassis* [online]. SAE International, 2002. [cit. 12.2.2018] ISSN 0148-7191.  
Available from DOI: 10.4271/2002-01-3300.
- (8) LEINVEBER, J., VÁVRA, P. *Strojnické tabulky: pomocná učebnice pro školy technického zaměření*. 4. dopl. vyd. Úvaly: Albra, 2008. ISBN 978-80-7361-051-7.
- (9) IGUS. *Material Data igumid & igus® e-chain® Colors* [online]. Igus® 2018. [cit. 9.3.2018].  
Available from: [https://www.igus.eu/wpck/2921/designing\\_materialdata](https://www.igus.eu/wpck/2921/designing_materialdata).
- (10) GLEICH. *CERTAL®: technický list* [online]. Gleich Aluminum, 2018. [cit. 9.3.2018].  
Available from: [https://gleich.de/cz/wp-content/uploads/sites/8/2017/04/cz\\_certal.pdf](https://gleich.de/cz/wp-content/uploads/sites/8/2017/04/cz_certal.pdf)

- (11) GLEICH. *EN AW 7075: technický list* [online]. Gleich Aluminum, 2018. [cit. 9.3.2018]. Available from: [https://gleich.de/cz/wp-content/uploads/sites/8/2017/04/cz\\_en\\_aw\\_7075.pdf](https://gleich.de/cz/wp-content/uploads/sites/8/2017/04/cz_en_aw_7075.pdf)
- (12) ANSYS®. *Academic Teaching Advanced, Release 18.2: help system* [online]. ANSYS, Inc. [cit. 26.3.2018]. Available from: [help/ans\\_elem/Hlp\\_E\\_BEAM188.html](help/ans_elem/Hlp_E_BEAM188.html)
- (13) BLOKEŠ, J. *Stress-strain Analysis of the Student Formula Frame: Bachelor Thesis* [online]. Ostrava: VSB - Technical University of Ostrava, Faculty of Mechanical Engineering, Department of Mechanics, 64p. Thesis head: Poruba, Z. [cit. 20.3.2018]. Available from : <http://hdl.handle.net/10084/104955>.
- (14) ANSYS®. *Academic Teaching Advanced, Release 18.2: help system* [online]. ANSYS, Inc. [cit. 26.3.2018]. Available from: [help/ans\\_elem/Hlp\\_E\\_MPC184.html](help/ans_elem/Hlp_E_MPC184.html)
- (15) BUILD YOUR OWN RACE CAR. *Diagram TR2. Method to measure torsional rigidity* [online]. [cit. 18.2.2018]. Available from: <http://www.buildyourownracecar.com/race-car-chassis-basics-and-design/>.
- (16) ONDROUCH, J., PODEŠVA, J. *Teorie a příklady k předmětu Technické kmitání* [online]. Ostrava, 2012. ISBN 978-80-248-2762-9. [cit. 26.2.2018]. Available from: <http://projekty.fs.vsb.cz/147/ucebniopory/978-80-248-2762-9.pdf>
- (17) CHALUPA, P. *Analýza torzní tuhosti upravené varianty rámu vozidla Formule Student: diplomová práce* [online]. Brno: Vysoké učení technické v Brně, Fakulta strojního inženýrství, 2010. Vedoucí diplomové práce Ing. Pavel Ramík. [cit. 26.2.2018]. Available from: <http://hdl.handle.net/11012/15688>.
- (18) TICHÁ, Š., ADAMEC, J. *Návody do cvičení z předmětu strojírenská metrologie* [online]. Ostrava, 2008. [cit. 24.2.2018]. Available from: <https://www.fs.vsb.cz/export/sites/fs/346/cs/studium/studijni-literatura/NAVODY-DO-CVICENI-Z-PREDMETU-strojirenska-metrologie.pdf>.
- (19) TULIS, V. *Vliv směru vláken dlouhovláknového kompozitu v okolí díry na napětí: bakalářská práce* [online]. Brno: Vysoké učení technické v Brně, Fakulta strojního inženýrství, 2016. 55 s. Vedoucí bakalářské práce: Polzer, S. [cit. 15.3.2018]. Available from: [https://www.vutbr.cz/www\\_base/zav\\_prace\\_soubor\\_verejne.php?file\\_id=126475](https://www.vutbr.cz/www_base/zav_prace_soubor_verejne.php?file_id=126475).
- (20) HLADÍK, O. *Návrh prostorového trubkového rámu vozu kategorie Formula Student: bakalářská práce* [online]. Praha: České vysoké učení technické v Praze, Fakulta strojní, 2015. 54 s. Vedoucí bakalářské práce: Astraverkhau, N. [cit. 12.2.2018]. Available from: <https://dspace.cvut.cz/bitstream/handle/10467/63703/F2-BP-2015-Hladik-Ondrej-BAKALARKA.pdf?sequence=1&isAllowed=y>.



# Table of Contents for Appendix

<b>Appendix</b>	<b>Number of pages</b>
A Evaluation Tables of Path Results	13
B Evaluation of Cross-Section Area of Simplified Uprights	3
C Influence of Young's Modulus of Carbon-Fibre Material on Torsional Stiffness	3
D Data from Measurement	3
E Evaluation Tables	2
F Carbon-Fibre Tube Material Testing	3

## A Evaluation Tables of Path Results

Simulation	Number of figure with relevant evaluation table
Linear, no ARB system	Figs. 6.1, 6.2, 6.3
Non-linear, no ARB system	Figs. 6.4, 6.5, 6.6
Linear with ARB system	Figs. 6.7, 6.8, 6.9
Non-linear with ARB system	Figs. 6.10, 6.11, 6.12

Table 6.1: Guide for evaluation tables

PATH RESULTS - linear simulation model without ARB system					
Node No.	Length from zero[mm]	Right path	Left path	Width between nodes[mm]	Angle[deg]
		Displacement [mm]	Displacement [mm]		
1	0.00	-3.439	2.090	332.000	0.954076
2	19.10	-3.429	2.088	332.471	0.950538
3	38.20	-3.418	2.085	332.941	0.946855
4	57.30	-3.406	2.082	333.412	0.943045
5	76.40	-3.394	2.079	333.882	0.939126
6	95.51	-3.382	2.075	334.353	0.935149
7	114.61	-3.370	2.072	334.824	0.931114
8	133.71	-3.358	2.068	335.294	0.927057
9	152.81	-3.346	2.064	335.765	0.923012
10	171.91	-3.333	2.060	336.235	0.918977
11	191.01	-3.321	2.057	336.706	0.915039
12	210.11	-3.309	2.054	337.176	0.911163
13	229.21	-3.297	2.051	337.647	0.907399
14	248.31	-3.286	2.048	338.118	0.903782
15	267.41	-3.275	2.046	338.588	0.900327
16	286.51	-3.265	2.044	339.059	0.897050
17	305.62	-3.255	2.043	339.529	0.894002
18	324.72	-3.246	2.043	340.000	0.891198
19	343.53	-3.234	2.039	340.000	0.888620
20	362.35	-3.223	2.037	340.000	0.886278
21	381.17	-3.213	2.034	340.000	0.884105
22	399.99	-3.202	2.033	340.000	0.882134
23	418.81	-3.193	2.032	340.000	0.880297
24	437.63	-3.183	2.031	340.000	0.878579
25	456.44	-3.174	2.030	340.000	0.876928
26	475.26	-3.165	2.030	340.000	0.875361
27	494.08	-3.156	2.030	340.000	0.873811
28	512.90	-3.147	2.030	340.000	0.872278
29	531.72	-3.138	2.029	340.000	0.870728
30	551.13	-3.128	2.029	340.000	0.868908
31	570.55	-3.117	2.027	340.000	0.866785
32	589.97	-3.105	2.025	340.000	0.864359
33	609.38	-3.092	2.022	340.000	0.861664
34	628.80	-3.078	2.018	340.000	0.858715
35	648.22	-3.064	2.013	340.000	0.855548
36	667.63	-3.050	2.008	340.000	0.852144
37	687.05	-3.034	2.001	340.000	0.848539
38	706.47	-3.019	1.994	340.000	0.844765
39	725.88	-3.003	1.987	340.000	0.840806
40	745.30	-2.987	1.979	340.000	0.836712
41	764.72	-2.971	1.970	340.000	0.832500
42	784.66	-2.944	1.950	338.667	0.827912
43	804.61	-2.916	1.929	337.333	0.822880
44	824.56	-2.887	1.907	336.000	0.817415
45	844.51	-2.856	1.885	334.667	0.811617
46	864.45	-2.825	1.862	333.333	0.805514

Figure 6.1: Table's lines from 1 to 46

47	884.40	-2.793	1.838	332.000	0.799173
48	904.35	-2.761	1.814	330.667	0.792641
49	924.29	-2.728	1.790	329.333	0.786005
50	944.24	-2.695	1.766	328.000	0.779279
51	964.19	-2.662	1.743	326.667	0.772552
52	984.14	-2.630	1.720	325.333	0.765910
53	1004.10	-2.597	1.697	324.000	0.759337
54	1024.00	-2.566	1.675	322.667	0.752976
55	1044.00	-2.535	1.654	321.333	0.746847
56	1063.90	-2.505	1.634	320.000	0.741044
57	1083.30	-2.516	1.657	325.000	0.735567
58	1102.60	-2.528	1.679	330.000	0.730412
59	1121.90	-2.540	1.702	335.000	0.725497
60	1141.20	-2.553	1.724	340.000	0.720793
61	1160.60	-2.566	1.747	345.000	0.716243
62	1179.90	-2.579	1.769	350.000	0.711806
63	1199.20	-2.592	1.791	355.000	0.707414
64	1218.60	-2.605	1.813	360.000	0.703064
65	1237.90	-2.618	1.834	365.000	0.698691
66	1257.20	-2.630	1.854	370.000	0.694267
67	1276.50	-2.642	1.873	375.000	0.689747
68	1295.90	-2.653	1.891	380.000	0.685104
69	1315.50	-2.648	1.892	382.143	0.680663
70	1335.20	-2.642	1.894	384.286	0.676182
71	1354.90	-2.635	1.895	386.429	0.671633
72	1374.60	-2.628	1.896	388.571	0.667015
73	1394.20	-2.620	1.897	390.714	0.662316
74	1413.90	-2.611	1.898	392.857	0.657537
75	1433.60	-2.602	1.898	395.000	0.652665
76	1453.30	-2.592	1.898	397.143	0.647687
77	1472.90	-2.581	1.898	399.286	0.642590
78	1492.60	-2.569	1.897	401.429	0.637347
79	1512.30	-2.557	1.895	403.571	0.632005
80	1532.00	-2.544	1.893	405.714	0.626506
81	1551.60	-2.530	1.890	407.857	0.620841
82	1571.30	-2.516	1.886	410.000	0.615040
83	1591.00	-2.500	1.881	412.143	0.609062
84	1610.70	-2.484	1.875	414.286	0.602897
85	1630.30	-2.467	1.869	416.429	0.596562
86	1650.00	-2.450	1.861	418.571	0.590032
87	1669.70	-2.431	1.852	420.714	0.583309
88	1689.30	-2.412	1.842	422.857	0.576384
89	1709.00	-2.392	1.831	425.000	0.569245
90	1728.70	-2.371	1.818	427.143	0.561870
91	1748.40	-2.349	1.804	429.286	0.554274
92	1768.00	-2.326	1.789	431.429	0.546462
93	1787.70	-2.302	1.772	433.571	0.538396
94	1807.40	-2.278	1.754	435.714	0.530082
95	1827.10	-2.252	1.734	437.857	0.521534
96	1846.70	-2.226	1.712	440.000	0.512705
97	1865.60	-2.137	1.625	425.000	0.507075

Figure 6.2: Table's lines from 47 to 97

98	1884.50	-2.047	1.536	410.000	0.500766
99	1903.40	-1.957	1.448	395.000	0.493819
100	1922.30	-1.867	1.359	380.000	0.486324
101	1941.20	-1.777	1.270	365.000	0.478307
102	1960.10	-1.688	1.182	350.000	0.469848
103	1979.00	-1.601	1.095	335.000	0.461059
104	1997.90	-1.514	1.011	320.000	0.452036
105	2017.40	-1.472	0.966	320.000	0.436439
106	2036.90	-1.430	0.922	320.000	0.421091
107	2056.40	-1.389	0.878	320.000	0.405982
108	2076.00	-1.349	0.836	320.000	0.391107
109	2095.50	-1.309	0.794	320.000	0.376462
110	2115.00	-1.269	0.753	320.000	0.362024
111	2134.50	-1.230	0.712	320.000	0.347788
112	2154.10	-1.192	0.672	320.000	0.333769
113	2173.60	-1.154	0.633	320.000	0.319943
114	2193.10	-1.117	0.594	320.000	0.306306
115	2212.60	-1.080	0.555	320.000	0.292834
116	2232.20	-1.044	0.518	320.000	0.279562
117	2251.70	-1.008	0.480	320.000	0.266429
118	2271.20	-0.972	0.443	320.000	0.253477
119	2290.70	-0.937	0.407	320.000	0.240671
120	2310.30	-0.903	0.371	320.000	0.228013
121	2329.80	-0.868	0.335	320.000	0.215494
122	2349.30	-0.835	0.300	320.000	0.203109
123	2368.90	-0.801	0.265	320.000	0.190848

Figure 6.3: Table's lines from 98 to 123

PATH RESULTS - non-linear simulation without ARB system					
Node No.	Length from zero [mm]	Right path	Left path	Width between nodes [mm]	Angle[deg]
		Displacement [mm]	Displacement [mm]		
1	0.00	-3.581	1.965	332.000	0.957130
2	19.10	-3.572	1.962	332.471	0.953605
3	38.20	-3.562	1.958	332.941	0.949900
4	57.30	-3.552	1.954	333.412	0.946086
5	76.40	-3.541	1.950	333.882	0.942145
6	95.51	-3.530	1.945	334.353	0.938147
7	114.61	-3.520	1.940	334.824	0.934091
8	133.71	-3.509	1.934	335.294	0.930013
9	152.81	-3.498	1.929	335.765	0.925963
10	171.91	-3.487	1.924	336.235	0.921924
11	191.01	-3.476	1.919	336.706	0.917948
12	210.11	-3.465	1.914	337.176	0.914068
13	229.21	-3.455	1.910	337.647	0.910283
14	248.31	-3.445	1.906	338.118	0.906662
15	267.41	-3.436	1.902	338.588	0.903186
16	286.51	-3.427	1.899	339.059	0.899905
17	305.62	-3.419	1.896	339.529	0.896836
18	324.72	-3.411	1.894	340.000	0.893994
19	343.53	-3.401	1.889	340.000	0.891417
20	362.35	-3.392	1.884	340.000	0.889058
21	381.17	-3.384	1.880	340.000	0.886902
22	399.99	-3.376	1.876	340.000	0.884914
23	418.81	-3.368	1.872	340.000	0.883060
24	437.63	-3.361	1.869	340.000	0.881308
25	456.44	-3.354	1.866	340.000	0.879674
26	475.26	-3.348	1.864	340.000	0.878090
27	494.08	-3.341	1.861	340.000	0.876523
28	512.90	-3.334	1.859	340.000	0.874990
29	531.72	-3.327	1.856	340.000	0.873423
30	551.13	-3.320	1.853	340.000	0.871587
31	570.55	-3.311	1.849	340.000	0.869430
32	589.97	-3.301	1.844	340.000	0.867004
33	609.38	-3.291	1.839	340.000	0.864292
34	628.80	-3.280	1.832	340.000	0.861343
35	648.22	-3.268	1.825	340.000	0.858142
36	667.63	-3.255	1.817	340.000	0.854739
37	687.05	-3.242	1.809	340.000	0.851117
38	706.47	-3.228	1.800	340.000	0.847309
39	725.88	-3.214	1.791	340.000	0.843350
40	745.30	-3.200	1.781	340.000	0.839239
41	764.72	-3.185	1.770	340.000	0.834993
42	784.66	-3.159	1.749	338.667	0.830398
43	804.61	-3.132	1.728	337.333	0.825342
44	824.56	-3.103	1.705	336.000	0.819871
45	844.51	-3.073	1.682	334.667	0.814047

Figure 6.4: Table's lines from 1 to 45

46	864.45	-3.043	1.658	333.333	0.807920
47	884.40	-3.011	1.634	332.000	0.801571
48	904.35	-2.979	1.609	330.667	0.795032
49	924.29	-2.947	1.585	329.333	0.788370
50	944.24	-2.915	1.560	328.000	0.781620
51	964.19	-2.882	1.536	326.667	0.774884
52	984.14	-2.850	1.512	325.333	0.768199
53	1004.10	-2.818	1.489	324.000	0.761635
54	1024.00	-2.787	1.467	322.667	0.755231
55	1044.00	-2.756	1.445	321.333	0.749112
56	1063.90	-2.727	1.425	320.000	0.743264
57	1083.30	-2.739	1.446	325.000	0.737770
58	1102.60	-2.752	1.468	330.000	0.732582
59	1121.90	-2.766	1.489	335.000	0.727651
60	1141.20	-2.779	1.511	340.000	0.722950
61	1160.60	-2.793	1.533	345.000	0.718385
62	1179.90	-2.808	1.554	350.000	0.713934
63	1199.20	-2.822	1.575	355.000	0.709528
64	1218.60	-2.836	1.596	360.000	0.705180
65	1237.90	-2.849	1.615	365.000	0.700794
66	1257.20	-2.863	1.634	370.000	0.696357
67	1276.50	-2.876	1.653	375.000	0.691840
68	1295.90	-2.888	1.670	380.000	0.687200
69	1315.50	-2.884	1.670	382.143	0.682732
70	1335.20	-2.878	1.671	384.286	0.678240
71	1354.90	-2.873	1.671	386.429	0.673693
72	1374.60	-2.866	1.672	388.571	0.669064
73	1394.20	-2.859	1.672	390.714	0.664383
74	1413.90	-2.851	1.672	392.857	0.659593
75	1433.60	-2.842	1.672	395.000	0.654710
76	1453.30	-2.833	1.671	397.143	0.649721
77	1472.90	-2.823	1.670	399.286	0.644627
78	1492.60	-2.812	1.668	401.429	0.639388
79	1512.30	-2.800	1.666	403.571	0.634035
80	1532.00	-2.788	1.663	405.714	0.628512
81	1551.60	-2.775	1.660	407.857	0.622864
82	1571.30	-2.761	1.655	410.000	0.617038
83	1591.00	-2.746	1.650	412.143	0.611050
84	1610.70	-2.730	1.644	414.286	0.604889
85	1630.30	-2.714	1.636	416.429	0.598529
86	1650.00	-2.697	1.628	418.571	0.591989
87	1669.70	-2.679	1.619	420.714	0.585257
88	1689.30	-2.660	1.608	422.857	0.578308
89	1709.00	-2.641	1.596	425.000	0.571146
90	1728.70	-2.620	1.583	427.143	0.563761
91	1748.40	-2.599	1.568	429.286	0.556142
92	1768.00	-2.577	1.552	431.429	0.548308
93	1787.70	-2.554	1.534	433.571	0.540220
94	1807.40	-2.530	1.515	435.714	0.531883
95	1827.10	-2.505	1.494	437.857	0.523274

Figure 6.5: Table's lines from 46 to 95

96	1846.70	-2.480	1.471	440.000	0.514437
97	1865.60	-2.391	1.383	425.000	0.508760
98	1884.50	-2.302	1.293	410.000	0.502429
99	1903.40	-2.213	1.203	395.000	0.495458
100	1922.30	-2.124	1.112	380.000	0.487907
101	1941.20	-2.035	1.022	365.000	0.479876
102	1960.10	-1.947	0.933	350.000	0.471390
103	1979.00	-1.860	0.845	335.000	0.462557
104	1997.90	-1.774	0.759	320.000	0.453488
105	2017.40	-1.733	0.712	320.000	0.437844
106	2036.90	-1.693	0.667	320.000	0.422456
107	2056.40	-1.653	0.622	320.000	0.407302
108	2076.00	-1.613	0.578	320.000	0.392377
109	2095.50	-1.575	0.535	320.000	0.377679
110	2115.00	-1.537	0.492	320.000	0.363206
111	2134.50	-1.499	0.450	320.000	0.348931
112	2154.10	-1.462	0.408	320.000	0.334870
113	2173.60	-1.425	0.367	320.000	0.321005
114	2193.10	-1.389	0.327	320.000	0.307328
115	2212.60	-1.354	0.287	320.000	0.293835
116	2232.20	-1.319	0.248	320.000	0.280525
117	2251.70	-1.284	0.209	320.000	0.267374
118	2271.20	-1.250	0.171	320.000	0.254379
119	2290.70	-1.216	0.133	320.000	0.241534
120	2310.30	-1.183	0.095	320.000	0.228857
121	2329.80	-1.150	0.058	320.000	0.216304
122	2349.30	-1.117	0.021	320.000	0.203874
123	2368.90	-1.085	-0.015	320.000	0.196956

Figure 6.6: Table's lines from 96 to 123



PATH RESULTS - linear simulation with ARB system					
Node No.	Length from zero [mm]	Right path	Left path	Width between nodes [mm]	Angle[deg]
		Displacement [mm]	Displacement [mm]		
1	0.00	-2.675	2.164	332.000	0.835130
2	19.10	-2.667	2.161	332.471	0.831846
3	38.20	-2.658	2.157	332.941	0.828486
4	57.30	-2.648	2.153	333.412	0.825066
5	76.40	-2.638	2.149	333.882	0.821535
6	95.51	-2.628	2.145	334.353	0.817947
7	114.61	-2.618	2.141	334.824	0.814282
8	133.71	-2.607	2.136	335.294	0.810542
9	152.81	-2.597	2.131	335.765	0.806728
10	171.91	-2.586	2.126	336.235	0.802839
11	191.01	-2.574	2.121	336.706	0.798893
12	210.11	-2.563	2.115	337.176	0.794873
13	229.21	-2.551	2.109	337.647	0.790779
14	248.31	-2.540	2.103	338.118	0.786646
15	267.41	-2.528	2.096	338.588	0.782423
16	286.51	-2.516	2.089	339.059	0.778144
17	305.62	-2.504	2.081	339.529	0.773809
18	324.72	-2.493	2.074	340.000	0.769419
19	343.53	-2.478	2.063	340.000	0.765055
20	362.35	-2.463	2.052	340.000	0.760894
21	381.17	-2.450	2.042	340.000	0.756968
22	399.99	-2.437	2.034	340.000	0.753295
23	418.81	-2.425	2.026	340.000	0.749858
24	437.63	-2.413	2.018	340.000	0.746673
25	456.44	-2.402	2.012	340.000	0.743775
26	475.26	-2.391	2.007	340.000	0.741113
27	494.08	-2.382	2.003	340.000	0.738754
28	512.90	-2.372	2.000	340.000	0.736682
29	531.72	-2.364	1.998	340.000	0.734879
30	551.13	-2.354	1.996	340.000	0.733009
31	570.55	-2.344	1.994	340.000	0.730937
32	589.97	-2.333	1.991	340.000	0.728628
33	609.38	-2.321	1.988	340.000	0.726000
34	628.80	-2.308	1.983	340.000	0.723018
35	648.22	-2.294	1.977	340.000	0.719631
36	667.63	-2.279	1.969	340.000	0.715806
37	687.05	-2.262	1.960	340.000	0.711442
38	706.47	-2.249	1.952	340.000	0.707853
39	725.88	-2.236	1.943	340.000	0.704130
40	745.30	-2.222	1.933	340.000	0.700271
41	764.72	-2.209	1.923	340.000	0.696244
42	784.66	-2.183	1.902	338.667	0.690967
43	804.61	-2.156	1.878	337.333	0.685071
44	824.56	-2.127	1.854	336.000	0.678667

Figure 6.7: Table's lines from 1 to 44

45	844.51	-2.096	1.828	334.667	0.671802
46	864.45	-2.065	1.801	333.333	0.664573
47	884.40	-2.033	1.774	332.000	0.657009
48	904.35	-2.000	1.747	330.667	0.649211
49	924.29	-1.967	1.719	329.333	0.641228
50	944.24	-1.934	1.691	328.000	0.633180
51	964.19	-1.900	1.664	326.667	0.625066
52	984.14	-1.867	1.637	325.333	0.617009
53	1004.10	-1.834	1.611	324.000	0.609081
54	1024.00	-1.801	1.586	322.667	0.601388
55	1044.00	-1.770	1.561	321.333	0.593935
56	1063.90	-1.739	1.539	320.000	0.586867
57	1083.30	-1.742	1.549	325.000	0.580184
58	1102.60	-1.745	1.560	330.000	0.573737
59	1121.90	-1.748	1.570	335.000	0.567518
60	1141.20	-1.752	1.580	340.000	0.561464
61	1160.60	-1.755	1.590	345.000	0.555602
62	1179.90	-1.759	1.600	350.000	0.549875
63	1199.20	-1.763	1.609	355.000	0.544277
64	1218.60	-1.767	1.618	360.000	0.538771
65	1237.90	-1.771	1.627	365.000	0.533369
66	1257.20	-1.775	1.635	370.000	0.528020
67	1276.50	-1.779	1.643	375.000	0.522706
68	1295.90	-1.782	1.650	380.000	0.517442
69	1315.50	-1.773	1.644	382.143	0.512337
70	1335.20	-1.763	1.639	384.286	0.507289
71	1354.90	-1.754	1.634	386.429	0.502267
72	1374.60	-1.743	1.629	388.571	0.497256
73	1394.20	-1.733	1.624	390.714	0.492241
74	1413.90	-1.722	1.619	392.857	0.487223
75	1433.60	-1.710	1.614	395.000	0.482172
76	1453.30	-1.698	1.609	397.143	0.477075
77	1472.90	-1.686	1.603	399.286	0.471918
78	1492.60	-1.673	1.597	401.429	0.466702
79	1512.30	-1.659	1.591	403.571	0.461399
80	1532.00	-1.645	1.584	405.714	0.456010
81	1551.60	-1.631	1.576	407.857	0.450496
82	1571.30	-1.616	1.568	410.000	0.444872
83	1591.00	-1.600	1.559	412.143	0.439111
84	1610.70	-1.583	1.549	414.286	0.433189
85	1630.30	-1.566	1.539	416.429	0.427136
86	1650.00	-1.548	1.527	418.571	0.420897
87	1669.70	-1.529	1.514	420.714	0.414478
88	1689.30	-1.510	1.501	422.857	0.407879
89	1709.00	-1.489	1.486	425.000	0.401064
90	1728.70	-1.468	1.470	427.143	0.394049
91	1748.40	-1.446	1.452	429.286	0.386810
92	1768.00	-1.423	1.433	431.429	0.379351
93	1787.70	-1.400	1.413	433.571	0.371623

Figure 6.8: Table's lines from 45 to 93

94	1807.40	-1.375	1.391	435.714	0.363654
95	1827.10	-1.349	1.367	437.857	0.355424
96	1846.70	-1.323	1.342	440.000	0.346935
97	1865.60	-1.255	1.274	425.000	0.340993
98	1884.50	-1.187	1.205	410.000	0.334324
99	1903.40	-1.118	1.136	395.000	0.326945
100	1922.30	-1.049	1.066	380.000	0.318938
101	1941.20	-0.981	0.996	365.000	0.310369
102	1960.10	-0.913	0.928	350.000	0.301317
103	1979.00	-0.846	0.860	335.000	0.291893
104	1997.90	-0.781	0.795	320.000	0.282210
105	2017.40	-0.738	0.748	320.000	0.266044
106	2036.90	-0.696	0.701	320.000	0.250055
107	2056.40	-0.653	0.655	320.000	0.234245
108	2076.00	-0.612	0.609	320.000	0.218606
109	2095.50	-0.570	0.564	320.000	0.203138
110	2115.00	-0.529	0.520	320.000	0.187842
111	2134.50	-0.489	0.476	320.000	0.172710
112	2154.10	-0.449	0.432	320.000	0.157746
113	2173.60	-0.409	0.389	320.000	0.142944
114	2193.10	-0.370	0.347	320.000	0.128303
115	2212.60	-0.331	0.305	320.000	0.113821
116	2232.20	-0.292	0.263	320.000	0.099498
117	2251.70	-0.254	0.222	320.000	0.085329
118	2271.20	-0.217	0.182	320.000	0.071314
119	2290.70	-0.179	0.141	320.000	0.057450
120	2310.30	-0.143	0.102	320.000	0.043735
121	2329.80	-0.106	0.062	320.000	0.030167
122	2349.30	-0.070	0.023	320.000	0.016742
123	2368.90	-0.035	-0.016	320.000	0.009056

Figure 6.9: Table's lines from 94 to 123

PATH RESULTS - non-linear simulation with ARB system					
Node No.	Length from zero [mm]	Right path	Left path	Width between nodes [mm]	Angle[deg]
		Displacement [mm]	Displacement [mm]		
1	0.00	-2.731	2.115	332.000	0.836304
2	19.10	-2.722	2.112	332.471	0.833018
3	38.20	-2.712	2.109	332.941	0.829656
4	57.30	-2.703	2.106	333.412	0.826217
5	76.40	-2.693	2.102	333.882	0.822685
6	95.51	-2.683	2.098	334.353	0.819094
7	114.61	-2.672	2.094	334.824	0.815428
8	133.71	-2.661	2.089	335.294	0.811670
9	152.81	-2.650	2.084	335.765	0.807854
10	171.91	-2.639	2.079	336.235	0.803964
11	191.01	-2.628	2.074	336.706	0.800016
12	210.11	-2.617	2.068	337.176	0.795994
13	229.21	-2.605	2.062	337.647	0.791899
14	248.31	-2.593	2.056	338.118	0.787747
15	267.41	-2.582	2.049	338.588	0.783540
16	286.51	-2.570	2.042	339.059	0.779259
17	305.62	-2.558	2.035	339.529	0.774923
18	324.72	-2.546	2.027	340.000	0.770531
19	343.53	-2.531	2.016	340.000	0.766167
20	362.35	-2.517	2.005	340.000	0.762006
21	381.17	-2.504	1.995	340.000	0.758097
22	399.99	-2.492	1.986	340.000	0.754407
23	418.81	-2.480	1.977	340.000	0.750987
24	437.63	-2.468	1.970	340.000	0.747819
25	456.44	-2.458	1.963	340.000	0.744904
26	475.26	-2.448	1.957	340.000	0.742276
27	494.08	-2.439	1.952	340.000	0.739917
28	512.90	-2.430	1.949	340.000	0.737828
29	531.72	-2.422	1.946	340.000	0.736025
30	551.13	-2.413	1.944	340.000	0.734138
31	570.55	-2.403	1.941	340.000	0.732065
32	589.97	-2.393	1.938	340.000	0.729740
33	609.38	-2.382	1.933	340.000	0.727095
34	628.80	-2.369	1.928	340.000	0.724113
35	648.22	-2.356	1.921	340.000	0.720709
36	667.63	-2.341	1.913	340.000	0.716868
37	687.05	-2.325	1.903	340.000	0.712487
38	706.47	-2.312	1.895	340.000	0.708881
39	725.88	-2.299	1.886	340.000	0.705141
40	745.30	-2.285	1.877	340.000	0.701265
41	764.72	-2.271	1.867	340.000	0.697255
42	784.66	-2.245	1.845	338.667	0.691948
43	804.61	-2.217	1.823	337.333	0.686039
44	824.56	-2.187	1.799	336.000	0.679639
45	844.51	-2.156	1.774	334.667	0.672761
46	864.45	-2.124	1.748	333.333	0.665501
47	884.40	-2.091	1.722	332.000	0.657941
48	904.35	-2.058	1.695	330.667	0.650129

Figure 6.10: Table's lines from 1 to 48

49	924.29	-2.023	1.668	329.333	0.642150
50	944.24	-1.989	1.641	328.000	0.634053
51	964.19	-1.955	1.614	326.667	0.625926
52	984.14	-1.920	1.588	325.333	0.617872
53	1004.10	-1.887	1.563	324.000	0.609929
54	1024.00	-1.853	1.538	322.667	0.602205
55	1044.00	-1.821	1.515	321.333	0.594755
56	1063.90	-1.789	1.493	320.000	0.587655
57	1083.30	-1.791	1.504	325.000	0.580959
58	1102.60	-1.794	1.515	330.000	0.574501
59	1121.90	-1.796	1.526	335.000	0.568253
60	1141.20	-1.799	1.537	340.000	0.562205
61	1160.60	-1.802	1.548	345.000	0.556333
62	1179.90	-1.806	1.558	350.000	0.550595
63	1199.20	-1.809	1.568	355.000	0.544987
64	1218.60	-1.812	1.578	360.000	0.539487
65	1237.90	-1.816	1.587	365.000	0.534060
66	1257.20	-1.819	1.596	370.000	0.528686
67	1276.50	-1.822	1.604	375.000	0.523394
68	1295.90	-1.825	1.612	380.000	0.518121
69	1315.50	-1.815	1.607	382.143	0.513012
70	1335.20	-1.805	1.602	384.286	0.507945
71	1354.90	-1.794	1.598	386.429	0.502934
72	1374.60	-1.783	1.594	388.571	0.497905
73	1394.20	-1.772	1.590	390.714	0.492901
74	1413.90	-1.760	1.586	392.857	0.487865
75	1433.60	-1.748	1.581	395.000	0.482811
76	1453.30	-1.735	1.577	397.143	0.477724
77	1472.90	-1.722	1.572	399.286	0.472549
78	1492.60	-1.708	1.567	401.429	0.467329
79	1512.30	-1.694	1.561	403.571	0.462023
80	1532.00	-1.679	1.555	405.714	0.456632
81	1551.60	-1.663	1.548	407.857	0.451100
82	1571.30	-1.647	1.541	410.000	0.445459
83	1591.00	-1.630	1.533	412.143	0.439695
84	1610.70	-1.613	1.524	414.286	0.433770
85	1630.30	-1.595	1.514	416.429	0.427713
86	1650.00	-1.576	1.503	418.571	0.421459
87	1669.70	-1.557	1.491	420.714	0.415036
88	1689.30	-1.536	1.478	422.857	0.408421
89	1709.00	-1.515	1.464	425.000	0.401603
90	1728.70	-1.493	1.448	427.143	0.394559
91	1748.40	-1.470	1.432	429.286	0.387304
92	1768.00	-1.447	1.413	431.429	0.379829
93	1787.70	-1.422	1.394	433.571	0.372085
94	1807.40	-1.397	1.372	435.714	0.364101
95	1827.10	-1.370	1.349	437.857	0.355855
96	1846.70	-1.343	1.324	440.000	0.347325
97	1865.60	-1.275	1.257	425.000	0.341384
98	1884.50	-1.207	1.188	410.000	0.334701
99	1903.40	-1.138	1.119	395.000	0.327308
100	1922.30	-1.069	1.049	380.000	0.319270
101	1941.20	-1.000	0.980	365.000	0.310680

Figure 6.11: Table's lines from 49 to 101

102	1960.10	-0.931	0.911	350.000	0.301610
103	1979.00	-0.865	0.844	335.000	0.292163
104	1997.90	-0.799	0.778	320.000	0.282459
105	2017.40	-0.756	0.731	320.000	0.266266
106	2036.90	-0.713	0.685	320.000	0.250254
107	2056.40	-0.670	0.639	320.000	0.234417
108	2076.00	-0.628	0.594	320.000	0.218756
109	2095.50	-0.586	0.549	320.000	0.203267
110	2115.00	-0.545	0.505	320.000	0.187951
111	2134.50	-0.504	0.462	320.000	0.172800
112	2154.10	-0.463	0.418	320.000	0.157815
113	2173.60	-0.423	0.376	320.000	0.142997
114	2193.10	-0.383	0.334	320.000	0.128339
115	2212.60	-0.344	0.292	320.000	0.113841
116	2232.20	-0.305	0.251	320.000	0.099499
117	2251.70	-0.266	0.210	320.000	0.085317
118	2271.20	-0.228	0.170	320.000	0.071285
119	2290.70	-0.191	0.130	320.000	0.057405
120	2310.30	-0.153	0.090	320.000	0.043672
121	2329.80	-0.117	0.051	320.000	0.030088
122	2349.30	-0.080	0.013	320.000	0.016648
123	2368.90	-0.044	-0.026	320.000	0.012553

Figure 6.12: Table's lines from 102 to 123

## B Evaluation of Cross-Section Area of Simplified Uprights

Since the uprights have very complex shape (see Fig. 6.13) and the finite element model for simulations is based on usage of beam-type elements, I have decided to simplify them as aluminum boxes with square cross-section. The aim was to determine the length of the edge of the square cross-section, thus I could end up with aluminum box with the same (or approximate) stiffness as the original upright.

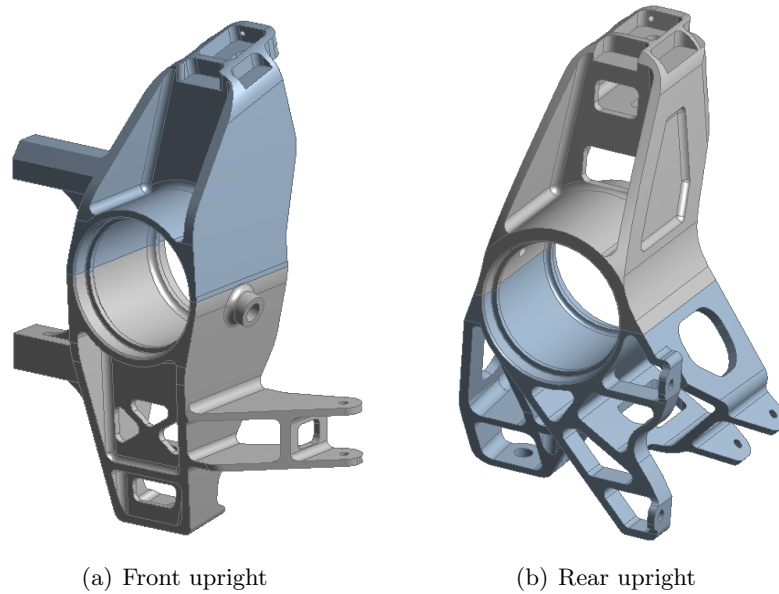


Figure 6.13: Imported models of uprights in Ansys Design Modeler

Firstly, I have imported models of the uprights into Ansys Design Modeler (the models of upright were kindly provided by Ing. Jakub Měsíček). Then, I have created mesh (use of linear tetrahedrons) which one can see in the Fig. 6.14(a). The boundary conditions are based on the assumption of evaluation of stiffness of the upright under circumstances of measuring of torsion stiffness.

The stiffness is the force divided by deformation caused by the force (see Eq. (6.1)). Therefore, I have fixed the upper part of the upright by Fixed support (all translations disabled) and applied displacement of 1 mm by Remote displacement function onto the cylindrical part of the upright. By the Displacement B (see Fig. 6.14(b)), I have fixed the upright in x and y axis because there has occurred deformations which do not occur in reality. The output from the simulation is the reaction force caused by the prescribed deformation. In this case (once the prescribed deformation is 1 mm), the value of the reaction force is right the value of the stiffness (the reaction force is divided by 1, resulting in the stiffness in [N/mm]). The simulation procedure is the same for both, front and rear uprights.

$$k = \frac{F}{\Delta L} [N/mm] \quad (6.1)$$

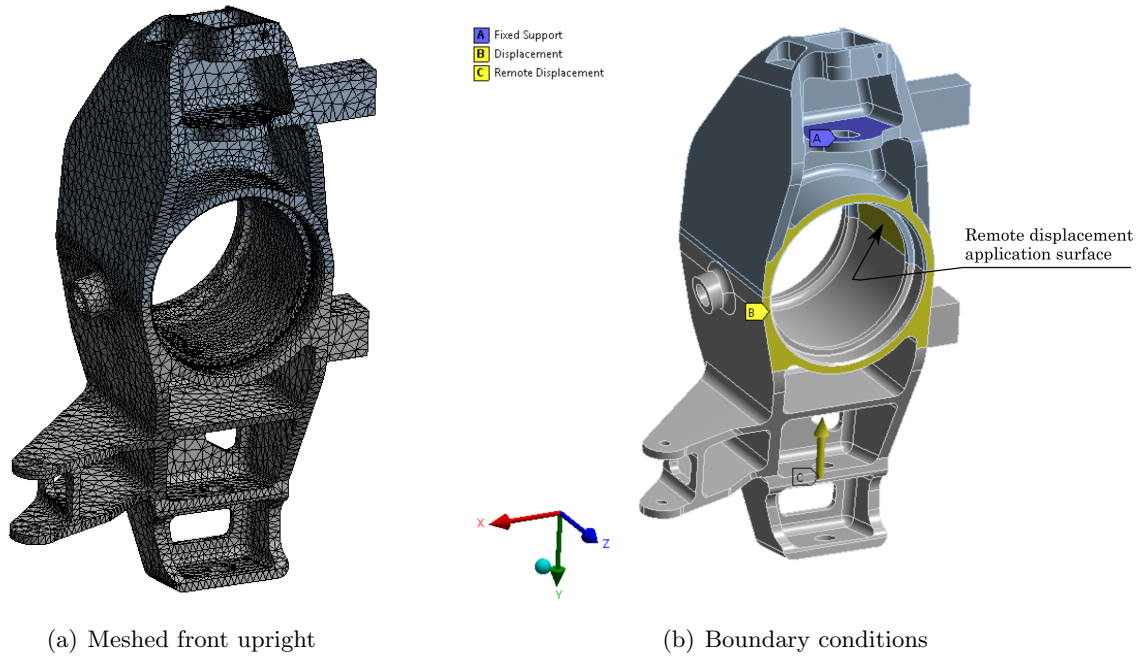


Figure 6.14: Imported models of uprights in Ansys Design Modeler

In the Tab. 6.2, one can see results of stiffness of the uprights.

Upright	Stiffness [N/mm]
Front	468324
Rear	373371

Table 6.2: Stiffness of uprights

Then, from Hooke's law Eq. (6.2), I have derived a formula to determine the length of the edge of the cross-section.

$$\sigma = E \cdot \varepsilon \quad (6.2)$$

where  $E$  is Young's modulus and  $\varepsilon$  is strain.

I have could perform a substitution (for case of tension or compression), thus:

$$\frac{F}{A} = E \cdot \frac{\Delta L}{L_0} \quad (6.3)$$

where  $F$  is force,  $A$  is area of cross-section,  $\Delta L$  is change of length of of the component and  $L_0$  is original length of the component.

Owing to square cross-section and the formula for stiffness (6.1), I have could perform a substitution again and after simplification I have got the final formula:

$$a = \sqrt{\frac{k \cdot L_0}{E}} [mm] \quad (6.4)$$

where  $a$  is the length of the edge of the cross-section.



Therefore, I have could determine the value of  $a$  for front and rear upright respectively:

$$a_F = \sqrt{\frac{k_F \cdot L_F}{E}} = \sqrt{\frac{468324 \cdot 222}{72000}} = 38mm \quad (6.5)$$

where  $k_F$  is stiffness of the front upright and  $L_F$  is length of the front upright (distance between suspension points of the A-arms)

and

$$a_R = \sqrt{\frac{k_R \cdot L_R}{E}} = \sqrt{\frac{373371 \cdot 210}{72000}} = 33mm \quad (6.6)$$

where  $k_R$  is stiffness of the rear upright and  $L_R$  is length of the rear upright (distance between suspension points of the A-arms).

The result, one can see in Fig. 6.15 below.

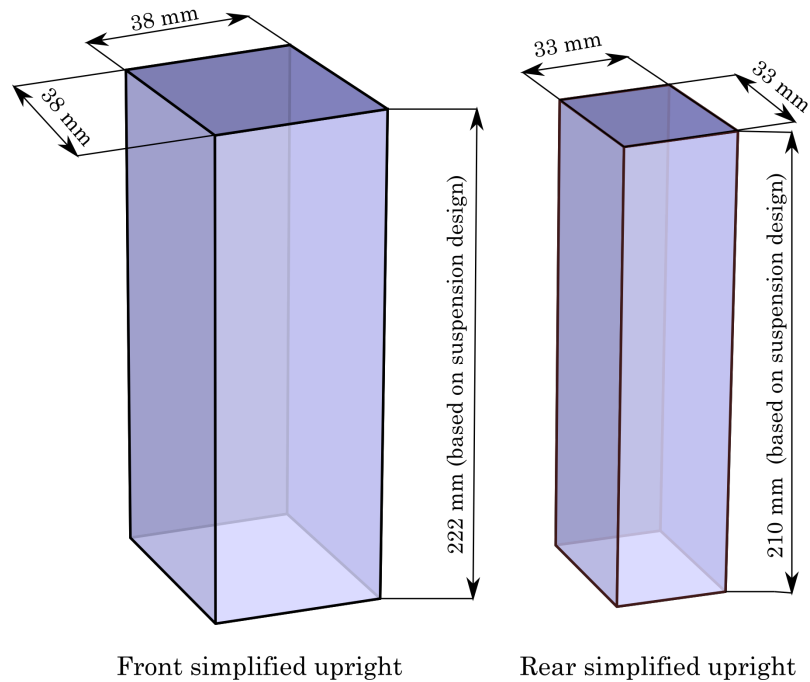


Figure 6.15: Design of the simplified uprights

## C Influence of Young’s Modulus of Carbon–Fibre Material on Torsional Stiffness

A-arms of suspension are made of carbon-fibre tubes. Carbon-fibre tubes are of composite material (carbon-fibre and matrix). Such a material is anisotropic. That means, the material’s properties are different in each direction (19). For purposes of this thesis, I have utilized a compression test of carbon-fibre tube to determine its Young’s modulus (see Appendix F). In this section, I have introduced the influence of the change of the Young’s modulus of the carbon-fibre tubes on torsion stiffness of the frame. Such examination would be useful for purposes of finding the inaccuracies out in the simulation model with respect to experiment.

I have used a procedure where I have reduced the Young’s modulus of the carbon-fibre tube five times by 10 percent and watched whether there is any change of results (torsion stiffness). The examination, I have performed with linear simulation model with ARB system and evaluated acc. to procedure discussed in chapter 4. Below in Figs. 6.16, 6.17, 6.18, 6.19, 6.20, follow evaluation tables of each step of reduction of the Young’s modulus of the carbon-fibre tubes (the default value of Young’s modulus of the carbon-fibre tubes was 12280 MPa).

The graph in Fig. 6.21 shows the relation between change of torsion stiffness at individual reduction steps (with respect to torsion stiffness for default value of Young’s modulus of carbon-fibre tubes) and change of the Young’s modulus . The results are also compared in the Tab. 6.3.

Young’s modulus [MPa]	Reduction [%]	Torsion stiffness [Nm/deg]	Difference [%]
12280	0	753	—
11052	10	745.5	1
9824	20	737.9	2
8596	30	731.4	2.9
7368	40	714.8	5
6140	50	711.2	5.6

Table 6.3: Evaluated influence of reduction

Young’s modulus reduced by 10% - 11 052 Mpa									
STEP	MASS[KG]	Torque[Nm]	FORCE[N]	u1[mm]	u2[mm]	step	Alpha12[deg]	C[Nm/deg]	
0	0.0	0	0.0	0.0	0.0	0	0.000000	N/A	
1	5.0	51.5	49.1	0.2	0.2	1	0.067407	764.1	
2	14.7	151.4	144.2	0.7	0.6	2	0.219071	691.2	
3	19.9	205.0	195.2	0.9	0.7	3	0.269625	760.2	
4	25.1	258.5	246.2	1.1	0.9	4	0.337030	767.1	
5	30.1	310.0	295.3	1.3	1.1	5	0.404434	766.6	
6	35.0	360.5	343.4	1.6	1.3	6	0.488687	737.7	
7	40.0	412.0	392.4	1.8	1.5	7	0.556089	740.9	
8	45.0	463.5	441.5	2.0	1.7	8	0.623488	743.4	
9	50.6	521.2	496.4	2.3	1.9	9	0.707735	736.4	
10	56.2	578.9	551.3	2.5	2.1	10	0.775131	746.8	
<b>Overall torsional stiffness -C [Nm/deg]</b>								<b>745.5</b>	

Figure 6.16: Evaluation table for 10% reduction

Young's modulus reduced by 20% - 9824 Mpa								
STEP	MASS[KG]	Torque[Nm]	FORCE[N]	u1[mm]	u2[mm]	step	Alpha12[deg]	C[Nm/deg]
0	0.0	0	0.0	0.0	0.0	0	0	N/A
1	5.0	51.5	49.1	0.2	0.2	1	0.067407	764.1
2	14.7	151.4	144.2	0.7	0.6	2	0.219071	691.2
3	19.9	205.0	195.2	0.9	0.8	3	0.286477	715.5
4	25.1	258.5	246.2	1.1	0.9	4	0.337030	767.1
5	30.1	310.0	295.3	1.4	1.1	5	0.421285	736.0
6	35.0	360.5	343.4	1.6	1.3	6	0.488687	737.7
7	40.0	412.0	392.4	1.8	1.5	7	0.556089	740.9
8	45.0	463.5	441.5	2.0	1.7	8	0.623488	743.4
9	50.6	521.2	496.4	2.3	1.9	9	0.707735	736.4
10	56.2	578.9	551.3	2.5	2.1	10	0.775131	746.8
<b>Overall torsional stiffness -C [Nm/deg]</b>								<b>737.9</b>

Figure 6.17: Evaluation table for 20% reduction

Young's modulus reduced by 30% - 8596 Mpa								
STEP	MASS[KG]	Torque[Nm]	FORCE[N]	u1[mm]	u2[mm]	step	Alpha12[deg]	C[Nm/deg]
0	0.0	0	0.0	0.0	0.0	0	0	N/A
1	5.0	51.5	49.1	0.2	0.2	1	0.067407	764.1
2	14.7	151.4	144.2	0.7	0.6	2	0.219071	691.2
3	19.9	205.0	195.2	0.9	0.8	3	0.286477	715.5
4	25.1	258.5	246.2	1.1	1.0	4	0.353881	730.6
5	30.1	310.0	295.3	1.4	1.2	5	0.438136	707.6
6	35.0	360.5	343.4	1.6	1.3	6	0.488687	737.7
7	40.0	412.0	392.4	1.8	1.5	7	0.556089	740.9
8	45.0	463.5	441.5	2.0	1.7	8	0.623488	743.4
9	50.6	521.2	496.4	2.3	1.9	9	0.707735	736.4
10	56.2	578.9	551.3	2.5	2.1	10	0.775131	746.8
<b>Overall torsional stiffness -C [Nm/deg]</b>								<b>731.4</b>

Figure 6.18: Evaluation table for 30% reduction

Young's modulus reduced by 40% - 7368 Mpa								
STEP	MASS[KG]	Torque[Nm]	FORCE[N]	u1[mm]	u2[mm]	step	Alpha12[deg]	C[Nm/deg]
0	0.0	0	0.0	0.0	0.0	0	0	N/A
1	5.0	51.5	49.1	0.2	0.2	1	0.067407	764.1
2	14.7	151.4	144.2	0.7	0.6	2	0.219071	691.2
3	19.9	205.0	195.2	0.9	0.8	3	0.286477	715.5
4	25.1	258.5	246.2	1.2	1.0	4	0.370732	697.4
5	30.1	310.0	295.3	1.4	1.2	5	0.438136	707.6
6	35.0	360.5	343.4	1.6	1.4	6	0.505538	713.1
7	40.0	412.0	392.4	1.8	1.6	7	0.572939	719.1
8	45.0	463.5	441.5	2.1	1.8	8	0.657187	705.3
9	50.6	521.2	496.4	2.3	2.0	9	0.724584	719.3
10	56.2	578.9	551.3	2.6	2.2	10	0.808828	715.7
<b>Overall torsional stiffness -C [Nm/deg]</b>								<b>714.8</b>

Figure 6.19: Evaluation table for 40% reduction

Young's modulus reduced by 50% -6140 Mpa									
STEP	MASS[KG]	Torque[Nm]	FORCE[N]	u1[mm]	u2[mm]		step	Alpha12[deg]	C[Nm/deg]
0	0.0	0	0.0	0.0	0.0		0	0	N/A
1	5.0	51.5	49.1	0.2	0.2		1	0.067407	764.1
2	14.7	151.4	144.2	0.7	0.6		2	0.219071	691.2
3	19.9	205.0	195.2	0.9	0.8		3	0.286477	715.5
4	25.1	258.5	246.2	1.2	1.0		4	0.370732	697.4
5	30.1	310.0	295.3	1.4	1.2		5	0.438136	707.6
6	35.0	360.5	343.4	1.6	1.4		6	0.505538	713.1
7	40.0	412.0	392.4	1.9	1.6		7	0.589789	698.6
8	45.0	463.5	441.5	2.1	1.8		8	0.657187	705.3
9	50.6	521.2	496.4	2.4	2.0		9	0.741433	703.0
10	56.2	578.9	551.3	2.6	2.2		10	0.808828	715.7
								<b>Overall torsional stiffness -C [Nm/deg]</b>	<b>711.2</b>

Figure 6.20: Evaluation table for 50% reduction

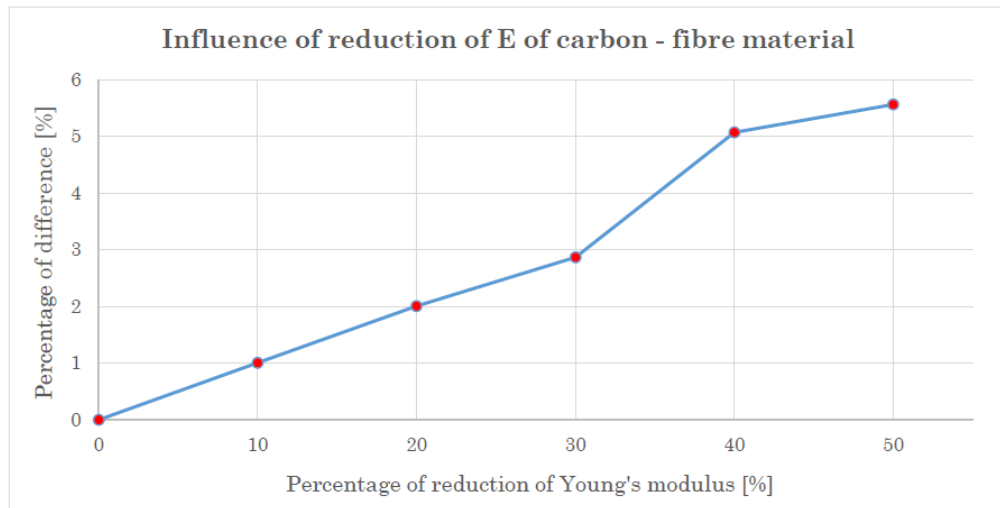


Figure 6.21: Progress of influence of reduction of Young's modulus

## D Data from Measurement

			First measurement												
STEP	MASS[KG]	FORCE[N]	ADDING MASS						RELEASING MASS						
			1	2	3	4	5	6	1	2	3	4	5	6	
0	0.0	0.0	0.0	0.0	0.0	0.0	0.0	0.0	0.0	0.0	0.0	0.0	0.0	0.0	0.0
1	5.0	49.1	0.3	0.2	0.2	0.2	0.1	0.1	0.1	0.3	0.2	0.3	0.2	0.2	0.1
2	14.7	144.2	0.8	0.5	0.7	0.4	0.3	0.2	0.2	0.8	0.5	0.7	0.5	0.4	0.2
3	19.9	195.2	1.0	0.7	0.9	0.6	0.4	0.3	0.3	1.1	0.7	0.9	0.7	0.4	0.3
4	25.1	246.2	1.4	0.9	1.1	0.8	0.4	0.5	0.4	1.4	0.9	1.2	0.9	0.4	0.6
5	30.1	295.3	1.7	1.0	1.4	1.0	0.4	0.7	0.5	1.7	1.1	1.4	1.1	0.4	0.7
6	35.0	343.4	1.9	1.2	1.6	1.2	0.5	0.8	0.6	1.9	1.3	1.6	1.3	0.4	0.8
7	40.0	392.4	2.2	1.4	1.8	1.4	0.5	0.9	0.7	2.1	1.5	1.9	1.5	0.5	1.0
8	45.0	441.5	2.4	1.6	2.0	1.5	0.6	1.0	0.8	2.3	1.8	1.9	1.7	0.6	1.0
9	50.6	496.4	2.5	2.0	2.1	1.9	0.6	1.1	0.9	2.5	2.0	2.1	1.9	0.6	1.1
10	56.2	551.3	2.8	2.2	2.3	2.1	0.7	1.2	1.0	2.8	2.2	2.3	2.1	0.7	1.2

(a) First measurement

			Second measurement												
STEP	MASS[KG]	FORCE[N]	ADDING MASS						RELEASING MASS						
			1	2	3	4	5	6	1	2	3	4	5	6	
0	0.0	0.0	0.0	0.0	0.0	0.0	0.0	0.0	0.0	0.0	0.0	0.0	0.0	0.0	0.0
1	5.0	49.1	0.3	0.2	0.3	0.1	0.1	0.1	0.1	0.3	0.2	0.3	0.2	0.1	0.0
2	14.7	144.2	0.8	0.5	0.7	0.4	0.3	0.2	0.2	0.8	0.5	0.7	0.4	0.3	0.2
3	19.9	195.2	1.0	0.6	0.9	0.6	0.4	0.3	0.3	1.1	0.7	1.0	0.6	0.4	0.3
4	25.1	246.2	1.5	0.8	1.2	0.8	0.4	0.5	0.4	1.5	0.9	1.2	0.9	0.3	0.6
5	30.1	295.3	1.7	1.0	1.4	1.0	0.4	0.7	0.5	1.7	1.0	1.5	1.0	0.4	0.7
6	35.0	343.4	1.9	1.2	1.6	1.1	0.4	0.8	0.6	1.9	1.2	1.6	1.2	0.4	0.8
7	40.0	392.4	2.2	1.4	1.8	1.3	0.5	0.9	0.7	2.1	1.4	1.8	1.4	0.5	0.9
8	45.0	441.5	2.3	1.6	2.0	1.6	0.5	1.0	0.8	2.3	1.7	1.9	1.6	0.5	1.0
9	50.6	496.4	2.5	1.9	2.1	1.8	0.6	1.1	0.9	2.5	1.9	2.1	1.8	0.6	1.1
10	56.2	551.3	2.8	2.2	2.3	2.0	0.7	1.2	1.0	2.8	2.2	2.3	2.0	0.7	1.2

(b) Second measurement

			Third measurement												
STEP	MASS[KG]	FORCE[N]	ADDING MASS						RELEASING MASS						
			1	2	3	4	5	6	1	2	3	4	5	6	
0	0.0	0.0	0.0	0.0	0.0	0.0	0.0	0.0	0.0	0.0	0.0	0.0	0.0	0.0	0.0
1	5.0	49.1	0.3	0.2	0.3	0.1	0.1	0.1	0.1	0.3	0.2	0.3	0.1	0.1	0.1
2	14.7	144.2	0.8	0.5	0.7	0.4	0.3	0.2	0.2	0.8	0.5	0.7	0.5	0.3	0.2
3	19.9	195.2	1.1	0.6	0.9	0.6	0.4	0.3	0.3	1.1	0.7	1.0	0.6	0.4	0.3
4	25.1	246.2	1.4	0.8	1.2	0.8	0.4	0.5	0.4	1.5	0.9	1.2	0.8	0.3	0.6
5	30.1	295.3	1.7	1.0	1.4	1.0	0.4	0.7	0.5	1.7	1.0	1.5	1.0	0.4	0.8
6	35.0	343.4	1.9	1.2	1.6	1.2	0.4	0.8	0.6	1.9	1.2	1.6	1.2	0.4	0.8
7	40.0	392.4	2.2	1.3	1.8	1.3	0.5	0.9	0.7	2.1	1.4	1.8	1.4	0.5	0.9
8	45.0	441.5	2.3	1.7	2.0	1.6	0.5	1.0	0.8	2.3	1.7	1.9	1.6	0.5	1.0
9	50.6	496.4	2.5	1.9	2.1	1.8	0.6	1.1	0.9	2.5	1.9	2.1	1.8	0.6	1.1
10	56.2	551.3	2.8	2.2	2.3	2.0	0.7	1.2	1.0	2.8	2.2	2.3	2.0	0.7	1.2

(c) Third measurement

Figure 6.22: Gathered data from measurement (values of displacement at 6 points of the frame [mm])

First measurement											
STEP	MASS[KG]	FORCE[N]	Torque[Nm]	ADDING MASS				RELEASING MASS			
				u1[mm]	u2[mm]	Alpha12[deg]	C[Nm/deg]	u1[mm]	u2[mm]	Alpha12[deg]	C[Nm/deg]
0	0.0	0.0	0.0	0.0	0.0	0	N/A	0.0	0.0	0	N/A
1	5.0	49.1	51.5	0.3	0.2	0.08425844	611.24	0.3	0.2	0.08425844	611.24
2	14.7	144.2	151.4	0.8	0.5	0.21907103	691.18	0.8	0.5	0.21907103	691.18
3	19.9	195.2	205.0	1.0	0.7	0.28647651	715.52	1.1	0.7	0.30332776	675.77
4	25.1	246.2	258.5	1.4	0.9	0.38758318	667.06	1.4	0.9	0.38758318	667.06
5	30.1	295.3	310.0	1.7	1.0	0.45498633	681.44	1.7	1.1	0.47183693	657.10
6	35.0	343.4	360.5	1.9	1.2	0.52238822	690.13	1.9	1.3	0.53923847	668.57
7	40.0	392.4	412.0	2.2	1.4	0.60663853	679.19	2.1	1.5	0.60663853	679.19
8	45.0	441.5	463.5	2.4	1.6	0.67403690	687.68	2.3	1.8	0.69088621	670.91
9	50.6	496.4	521.2	2.5	2.0	0.75828222	687.35	2.5	2.0	0.75828222	687.35
10	56.2	551.3	578.9	2.8	2.2	0.84252426	687.09	2.8	2.2	0.84252426	687.09

(a) First measurement

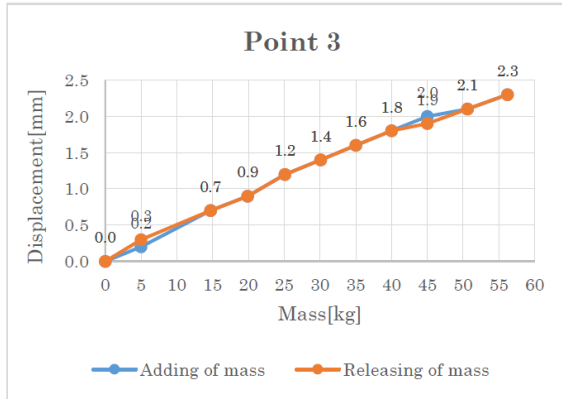
Second measurement											
STEP	MASS[KG]	FORCE[N]	Torque[Nm]	ADDING MASS				RELEASING MASS			
				u1[mm]	u2[mm]	Alpha12[deg]	C[Nm/deg]	u1[mm]	u2[mm]	Alpha12[deg]	C[Nm/deg]
0	0.0	0.0	0.0	0.0	0.0	0	N/A	0.0	0.0	0	N/A
1	5.0	49.1	51.5	0.3	0.2	0.08425844	611.24	0.3	0.2	0.08425844	611.24
2	14.7	144.2	151.4	0.8	0.5	0.21907103	691.18	0.8	0.5	0.21907103	691.18
3	19.9	195.2	205.0	1.0	0.6	0.26962521	760.24	1.1	0.7	0.30332776	675.77
4	25.1	246.2	258.5	1.5	0.8	0.38758318	667.06	1.5	0.9	0.40443408	639.27
5	30.1	295.3	310.0	1.7	1.0	0.45498633	681.44	1.7	1.0	0.45498633	681.44
6	35.0	343.4	360.5	1.9	1.2	0.52238822	690.13	1.9	1.2	0.52238822	690.13
7	40.0	392.4	412.0	2.2	1.4	0.60663853	679.19	2.1	1.4	0.58978866	698.59
8	45.0	441.5	463.5	2.3	1.6	0.65718747	705.31	2.3	1.7	0.67403690	687.68
9	50.6	496.4	521.2	2.5	1.9	0.74143341	702.97	2.5	1.9	0.74143341	702.97
10	56.2	551.3	578.9	2.8	2.2	0.84252426	687.09	2.8	2.2	0.84252426	687.09

(b) Second measurement

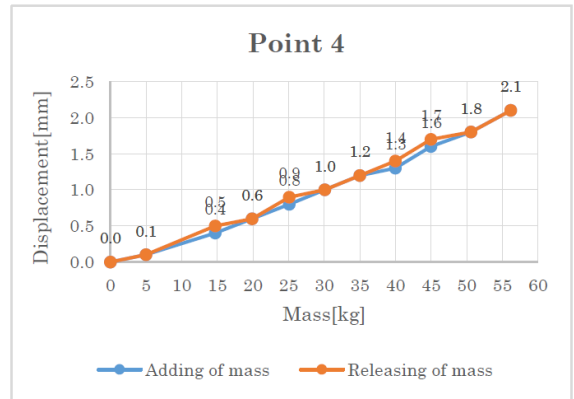
Third measurement											
STEP	MASS[KG]	FORCE[N]	Torque[Nm]	ADDING MASS				RELEASING MASS			
				u1[mm]	u2[mm]	Alpha12[deg]	C[Nm/deg]	u1[mm]	u2[mm]	Alpha12[deg]	C[Nm/deg]
0	0.0	0.0	0.0	0.0	0.0	0	N/A	0.0	0.0	0	N/A
1	5.0	49.1	51.5	0.3	0.2	0.08425844	611.24	0.3	0.2	0.08425844	611.24
2	14.7	144.2	151.4	0.8	0.5	0.21907103	691.18	0.8	0.5	0.21907103	691.18
3	19.9	195.2	205.0	1.1	0.6	0.28647651	715.52	1.1	0.7	0.30332776	675.77
4	25.1	246.2	258.5	1.4	0.8	0.37073222	697.38	1.5	0.9	0.40443408	639.27
5	30.1	295.3	310.0	1.7	1.0	0.45498633	681.44	1.7	1.0	0.45498633	681.44
6	35.0	343.4	360.5	1.9	1.2	0.52238822	690.13	1.9	1.2	0.52238822	690.13
7	40.0	392.4	412.0	2.2	1.3	0.58978866	698.59	2.1	1.4	0.58978866	698.59
8	45.0	441.5	463.5	2.3	1.7	0.67403690	687.68	2.3	1.7	0.67403690	687.68
9	50.6	496.4	521.2	2.5	1.9	0.74143341	702.97	2.5	1.9	0.74143341	702.97
10	56.2	551.3	578.9	2.8	2.2	0.84252426	687.09	2.8	2.2	0.84252426	687.09

(c) Third measurement

Figure 6.23: Evaluation tables for all measurements

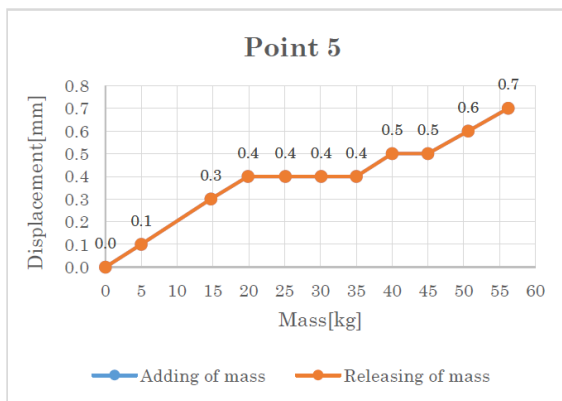


(a) Point 3

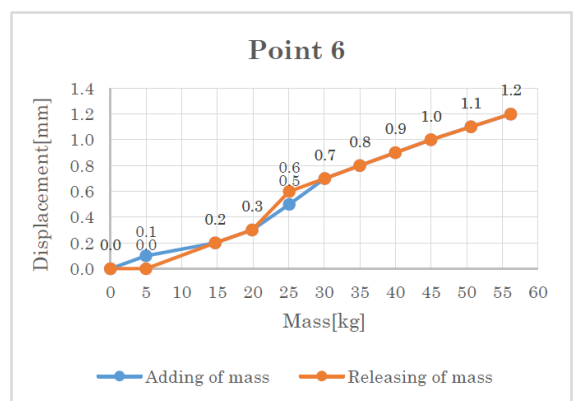


(b) Point 4

Figure 6.24: Averaged values of displacement at point 3 and point 4 with respect to applied mass



(a) Point 5



(b) Point 6

Figure 6.25: Averaged values of displacement at point 5 and point 6 with respect to applied mass

## E Evaluation Tables

Simulation (linear model with ARB system) for mesh size of 20 mm							
STEP	MASS[KG]	Torque[Nm]	FORCE[N]	u1[mm]	u2[mm]	Alpha12[deg]	C[Nm/deg]
0	0.0	0	0.0	0.0	0.0	0	N/A
1	5.0	51.5	49.1	0.2	0.2	0.067407	764.1
2	14.7	151.4	144.2	0.7	0.5	0.202220	748.8
3	19.9	205.0	195.2	0.9	0.7	0.269625	760.2
4	25.1	258.5	246.2	1.1	0.9	0.337030	767.1
5	30.1	310.0	295.3	1.3	1.1	0.404434	766.6
6	35.0	360.5	343.4	1.6	1.3	0.488687	737.7
7	40.0	412.0	392.4	1.8	1.5	0.556089	740.9
8	45.0	463.5	441.5	2.0	1.7	0.623488	743.4
9	50.6	521.2	496.4	2.2	1.9	0.690886	754.4
10	56.2	578.9	551.3	2.5	2.1	0.775131	746.8

**Overall torsional stiffness - mesh 20 mm [Nm/deg] 753.0**

(a) Mesh sizing of 20 mm per element

Simulation (linear model with ARB system) for mesh size of 10 mm							
STEP	MASS[KG]	Torque[Nm]	FORCE[N]	u1[mm]	u2[mm]	Alpha12[deg]	C[Nm/deg]
0	0.0	0	0.0	0.0	0.0	0	N/A
1	5.0	51.5	49.1	0.2	0.2	0.067407	764.1
2	14.7	151.4	144.2	0.7	0.5	0.202220	748.8
3	19.9	205.0	195.2	0.9	0.7	0.269625	760.2
4	25.1	258.5	246.2	1.1	0.9	0.337030	767.1
5	30.1	310.0	295.3	1.3	1.1	0.404434	766.6
6	35.0	360.5	343.4	1.6	1.3	0.488687	737.7
7	40.0	412.0	392.4	1.8	1.5	0.556089	740.9
8	45.0	463.5	441.5	2.0	1.7	0.623488	743.4
9	50.6	521.2	496.4	2.2	1.8	0.674037	773.3
10	56.2	578.9	551.3	2.5	2.1	0.775131	746.8

**Overall torsional stiffness -mesh 10 mm [Nm/deg] 754.9**

(b) Mesh sizing of 10 mm per element

Figure 6.26: Evaluation tables of mesh sizing comparison



Optimization simulation (linear model with ARB system)							
STEP	MASS[KG]	FORCE[N]	Torque[Nm]	u1[mm]	u2[mm]	Alpha12[deg]	C[Nm/deg]
0	0.0	0.0	0	0.0	0.0	0	N/A
1	5.0	49.1	51.50	0.2	0.1	0.050555	1018.7
2	14.7	144.2	151.42	0.5	0.4	0.151665	998.4
3	19.9	195.2	204.98	0.7	0.5	0.202220	1013.7
4	25.1	246.2	258.54	0.8	0.7	0.252774	1022.8
5	30.1	295.3	310.05	1.0	0.8	0.303328	1022.1
6	35.0	343.4	360.52	1.2	0.9	0.353881	1018.8
7	40.0	392.4	412.02	1.3	1.1	0.404434	1018.8
8	45.0	441.5	463.52	1.5	1.2	0.454986	1018.8
9	50.6	496.4	521.21	1.7	1.4	0.522388	997.7
10	56.2	551.3	578.89	1.9	1.5	0.572939	1010.4
<b>Overall torsional stiffness [Nm/deg]</b>							<b>1014.0</b>

Figure 6.27: Evaluation table of optimization

## F Carbon-Fibre Tube Material Testing

### Testing Procedure

The testing procedure, it was compression test therefore the specimen was compressed until broken. During the test, the applied force and deflection was measured directly by testing device.

Testing specimen (see Fig. 6.28) was a carbon-fibre tube of the same cross-section as that used for A-arms and Push/Pull rods, i.e. diameter of 20 mm with wall thickness of 2 mm and 200 mm long.



Figure 6.28: Testing specimen

Below in Fig. 6.29, one can see the specimen after compression test as it is broken near insert as presumed.



(a) Specimen immediately after test



(b) Closer look to the specimen's broken area

Figure 6.29: Specimen after testing procedure

## Results

In Fig. 6.30, there is a graph obtained from the testing device showing relation between force [N] and deflection [mm].

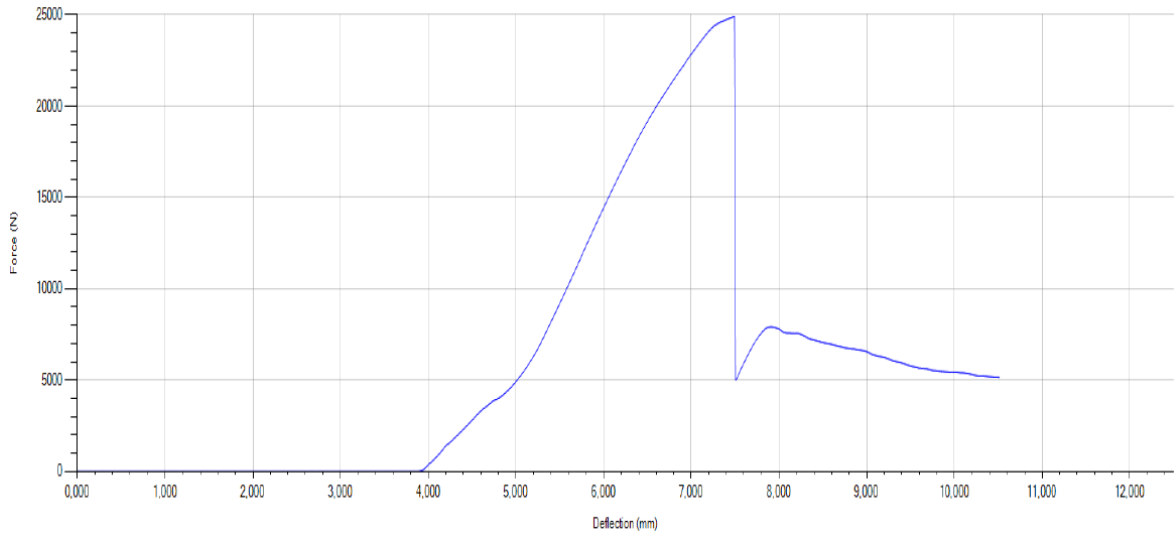


Figure 6.30: Resulting graph of force in relation to deflection

Since I have had just this graph, I have firstly determined the maximum force and deflection once the specimen is broken. Thus, force is 25 kN and deflection is (after subtraction of 3.9 mm from the beginning where is no deflection) 3.6 mm.

From Hooke's law, I have calculated the Young's modulus of the carbon-fibre tube as follows:

Firstly Hooke's law:

$$\sigma = E \cdot \varepsilon \quad (6.7)$$

where  $\sigma$  is stress,  $E$  is Young's modulus and  $\varepsilon$  is strain.

From that, I have could solve  $E$  as:

$$E = \frac{\sigma}{\varepsilon} \quad (6.8)$$

stress  $\sigma$ , I could express as:

$$\sigma = \frac{F}{A} \quad (6.9)$$

where  $F$  is force and  $A$  is cross-section area.

In my case, formula for tubular cross-section:

$$A = \frac{\pi}{4} \cdot (d_o^2 - d_i^2) \quad (6.10)$$

where  $d_o$  is outer diameter of the tube and  $d_i$  is inner diameter of the tube.

Then the strain, I could express as:

$$\varepsilon = \frac{\Delta L}{L_0} \quad (6.11)$$

where  $\Delta L$  is deformation of the specimen and  $L_0$  is original length of specimen.

Thus after substitution, I have got:

$$E = \frac{\frac{F}{\frac{\pi}{4} \cdot (d_o^2 - d_i^2)}}{\frac{\Delta L}{L_0}} = \frac{\frac{25000}{\frac{\pi}{4} \cdot (20^2 - 16^2)}}{\frac{3.6}{200}} = 12280 \text{MPa}. \quad (6.12)$$

## Conclusion

For simulations, I have used value of 12280 MPa for Young's modulus. Value 0.3 for Poisson's ratio, I have set as approximate according to (19). In Appendix C, I have proven that I can afford using of such values for material properties of carbon-fibre tube because of its minor influence on analysis results.